PhD - Thesis

A new digital twin for enzymatic hydrolysis processes applied to model-based process design

Christian Bernhard Appl

Student Number: 18163562

Research Degree: Biochemical Engineering

Principal Supervisor: Prof. Dr. Volker C. Hass

Subsidiary Supervisor: Prof. Dr. Frank Baganz

University College London (UCL)

Department of Biochemical Engineering

2023

Declaration

I, Christian Bernhard Appl, confirm that the work in this thesis is my own, except when indicated. The work presented in this thesis was carried out under the supervision of Prof. Dr. Frank Baganz and Prof. Dr. Volker C. Hass at the Department of Biochemical Engineering, University College London (UCL), between September 2018 and August 2023. This thesis has not been submitted, either in whole or in part, for another degree or another qualification at any other university.

Christian Bernhard Appl

25th of August 2023

Acknowledgement

I want to thank Frank Baganz and Volker C. Hass for allowing me to work on this research project and always supporting and believing in my abilities.

In addition, I would also like to thank Furtwangen University for providing me with the laboratories and equipment for my research. I like to sincerely thank Ursula Eschenhagen, Christian Fittkau, André Moser, Michael Menden and all former and part-time members of my working group at Furtwangen University. They always supported me in my work.

I would also like to express my special thanks to the students at Furtwangen University. During their bachelor's and master's theses, which I supervised, they gave me many important new insights and results.

Parts of this research were funded by the Federal Ministry of Education and Research (Germany) and conducted in a corporation with the Ingenieurbüro Dr.-Ing. Schoop GmbH (Hamburg, Germany), within the project "protP.S.I.", grant numbers: BMBF 031B0405C and 031B1080D.

This research would not have been possible without the Department of Biochemical Engineering, which provides me with a UCL Studentship for postgraduate work.

Finally, I would like to thank my parents, Susanne and Roland Appl, and my girlfriend, Linda Gras, for always supporting me and helping me through difficult times.

Abstract

Renewable raw materials containing starch and proteins are split into their main components using enzymatic hydrolysis processes. However, even small changes in temperature, pH or pressure may strongly affect the enzyme activity and stability. At the same time, natural fluctuations may lead to changes in the substrate composition. These mutually influencing factors place enormous demands on the design and control of enzymatic hydrolysis processes.

Individual enzymatic hydrolysis processes have already been modelled, but models for the hydrolysis of potato starch by α-amylase and glucoamylase and the proteolysis of organic sunflower seed meal by endopeptidase and exopeptidase in a stirred tank reactor, or even digital twins, are unavailable. Therefore, a new mechanistic model for the combined starch hydrolysis and proteolysis was developed.

Sigmoidal and double sigmoidal functions were implemented to map the temperature and pH-dependent enzyme activity. The model can simulate the enzymatic hydrolysis processes with an agreement of more than 90%. The new model was integrated into an existing digital twin of a 20 L stirred tank reactor to create a new stand-alone digital twin for enzymatic hydrolysis processes.

Applying the new digital twin core model, a model-based process design strategy based on the open-loop-feedback-optimal and model-based design of experiments strategies was established. By applying the new strategy, the amount of α-amylase and glucoamylase required for starch hydrolysis could be reduced by more than 30%. In addition, the required amount of endopeptidase and exopeptidase for proteolysis could be reduced by more than 50%. Compared to the classic design of experiments approach, the number of experiments required for process optimisation could be reduced by more than 50%.

The strategies resulting from this work can soon be used for the optimisation of the industrial organic nutrient media production from regenerative substrates for the cultivation of microorganisms such as *Saccharomyces cerevisiae*.

Impact Statement

This research combined model-based process design and control strategies with a new stand-alone digital twin for enzymatic hydrolysis processes in a stirred tank reactor (STR). This enabled enzymatic hydrolysis batch processes to be successfully optimised. The new strategies for model-based process optimisation can be used beneficially in the future both inside and outside academia.

The new strategies can be used directly in the industrial production of organic yeast products, where enzymatic hydrolysis processes are applied to produce nutrient media from organic, renewable raw materials. The global organic yeast market size was valued at about USD 364 million in 2020 and is expected to reach USD 599 million by 2025 (MarketsandMarkets, 2020). Factors such as increasing awareness among consumers about health and wellness, the growing need to replace monosodium glutamate (MSG) as an additive in food products, and increased demand for organic food products across the globe are driving the growth of the market (MarketsandMarkets, 2020). A large part of the total costs of producing nutrient media by enzymatic hydrolysis is caused by the enzymes used in the process. Improvements in enzymatic hydrolysis processes can reduce enzyme costs by more than 30%.

Due to the generic structure of the new stand-alone digital twin for enzymatic hydrolysis processes, the new strategies can be easily transferred to different enzymatic processes. This can accelerate the transfer from conventional chemical production of, e.g., chemicals, drugs or food to biotechnological organic production. The demand for organic products is becoming increasingly important and should be made even more available by reducing costs. Furthermore, the preconditions for transferring the strategies to microbial processes were provided.

Core findings of this research work have been published in “Springer - Advances in Biochemical Engineering/Biotechnology” (Digital Twins for Bioprocess Control Strategy Development and Realisation, DOI: 10.1007/10_2020_151; Mechanistic Mathematical Models as a Basis for Digital Twins, DOI: 10.1007/10_2020_152) and in “MDPI - Processes” (Development of a Digital Twin for Enzymatic Hydrolysis Processes, DOI: 10.3390/pr9101734). They also led to oral presentations at the 12th European Congress

of Chemical Engineering and 5th European of Applied Biotechnology, 2019 (Florence, Italy), at CHISA - 25th and 26th International Congress of Chemical and Process Engineering, 2021/2022 (Prague, Czech Republic) and at ESBES 13th European Symposium on Biochemical Engineering Sciences 2021 (Virtually).

Contents

Nomenclature

CDP	Cytidine diphosphate
CTP	Cytidine triphosphate
DLL	Dynamic-link library
DoE	Design of experiments
DS	Desirability score
DSig	Double sigmoidal
GUI	Graphic user interface
mDoE	Model-based design of experiments
MPC	Model predictive control
NMPC	Nonlinear model predictive control
ODE	Ordinary differential equation
OLFO	Open-loop-feedback-optimal
PBR	Packed bed flow tube reactor
P	Proportional
PI	Proportional-Integral
PID	Proportional-Integral-Derivative
Sig	Sigmoidal
STR	Stirred tank reactor
wRMSD	Weighted root-mean-square deviation

Figures

Tables

Motivation

Biochemical reactions must be catalysed to run at the pace needed to sustain life (Jaeger et al., 2018). These “life catalysts” are the enzymes. For each of the countless biochemical reactions of cell metabolism, a specific enzyme catalyses them (Jaeger et al., 2018). Due to the enormous variety of different enzymes, it is not presumptuous to claim that enzymes can also catalyse any chemical synthesis described so far (Illanes, 2008). Due to its versatility, the application range of enzymes in organic synthesis has expanded to an unprecedented level (Polaina and MacCabe, 2007).

Enzymatic hydrolysis processes, such as starch hydrolysis and proteolysis, play a vital role in producing organic nutrient media, as no toxic chemicals or other additives are needed (Jaeger et al., 2018; Tavano, 2013). Renewable raw materials (e.g., potato starch or sunflower seed meal) containing starch and proteins are split into their main components (e.g., glucose, free amino acids) using amylases and peptidases (Jaeger et al., 2018; Tavano, 2013). The nutrient media can subsequently be used for the cultivation of microorganisms. Due to the high costs of enzymes, the enzymatic production of organic nutrient media is often not yet competitive with the conventional production of nutrient media (Jaeger et al., 2018). Seasonal fluctuations in the quality of renewable raw materials (substrates) may also make it necessary to regularly adjust the process conditions and control strategies to achieve the optimal result. Optimisation of control strategies during production runs is usually exceedingly tricky or even impossible (Larroche et al., 2016; Zacher and Reuter, 2017). Interruptions of a production run and inadequate control lead to immense financial losses, which must be avoided (Zacher and Reuter, 2017). Using mathematical models or digital twins is a promising opportunity to optimise enzymatic hydrolysis processes. In combination with model-based control and process design strategies, it is possible to react to changes in the kinetics of the enzymatic process.

Furthermore, some enzymes show low activity and stability, which reduces their application potential. So far, the focus has been on counteracting the low activity and stability by enzyme immobilisation (Guisan, 2006) or working with low-temperature enzymes (Jaeger et al., 2018). However, other research has shown that also the use of high pressure could be beneficial. High pressure can significantly increase the activity and stability of some enzymes (Eisenmenger and Reyes-De-Corcuera, 2009).

1 State of the art and technology

This section covers the enzymatic hydrolysis processes of starch hydrolysis and proteolysis, the influence of high pressure on hydrolytic enzymes and reactor concepts for enzymatic hydrolysis processes.

In addition, the current state of the art and technology for designing and controlling enzymatic processes is examined. In this context, the focus is placed on model predictive control (MPC) and nonlinear model predictive control (NMPC), the open-loop-feedback-optimal (OLFO) strategy and the model-based design of experiments (mDoE). Furthermore, the status of digital twins in biochemical engineering and their use in developing process control and design strategies is discussed.

1.1 Enzymatic hydrolysis processes

Enzymatic hydrolysis is a process in which enzymes facilitate the cleavage of molecular bonds with the addition of the elements of water (Campbell and Reece, 2005). In more detail, this research examines the two-stage enzymatic hydrolysis processes of starch hydrolysis and proteolysis. These processes were chosen because they have already been well studied and are often carried out in STRs.

One of the focal points of research at Furtwangen University (working group of Prof. Dr. Volker C. Hass) is the optimisation of *Saccharomyces cerevisiae* (*S. cerevisiae*) cultivation processes. This has also resulted in cooperations with yeast manufacturers. During starch hydrolysis, starch is converted into glucose. In proteolysis, proteins are split into free amino acids. The products of starch hydrolysis and free amino acids can be used as the main components of many nutrient media used to cultivate microorganisms (e.g., *S. cerevisiae*). As a result of this work, the production of nutrient media for cultivating *S. cerevisiae* can already be optimised.

1.1.1 Enzymatic starch hydrolysis

In starch hydrolysis, starch is converted into glucose molecules using α- and glucoamylases (Bugg, 2012; Nebesny, 1989; Polaina and MacCabe, 2007). The enzyme α-amylase (α-1,4 glucan glucanohydrolase, EC. 3.2.1.1) catalyses the hydrolysis of 1,4-α-D-glucosidic linkages in polysaccharides containing three or more 1,4-α-linked D-glucose units

randomly (Buckow et al., 2007; Cordeiro et al., 2002). Starch is degraded to low molecular weight dextrin, limited by α-1,6 bonds in a way that α-amylase cannot hydrolyse (Buckow et al., 2007; Cordeiro et al., 2002). Glucoamylase (1,4-α-D-glucan glucohydrolase, EC 3.2.1.3) is a multi-domain exo-glycosidase that catalyses the hydrolysis of α-1,4 and α-1,6 glucosidic linkages of starch and related polysaccharides to release β-D-glucose from the non-reducing ends (Figure 1) (Bugg, 2012; Kumar and Satyanarayana, 2009).

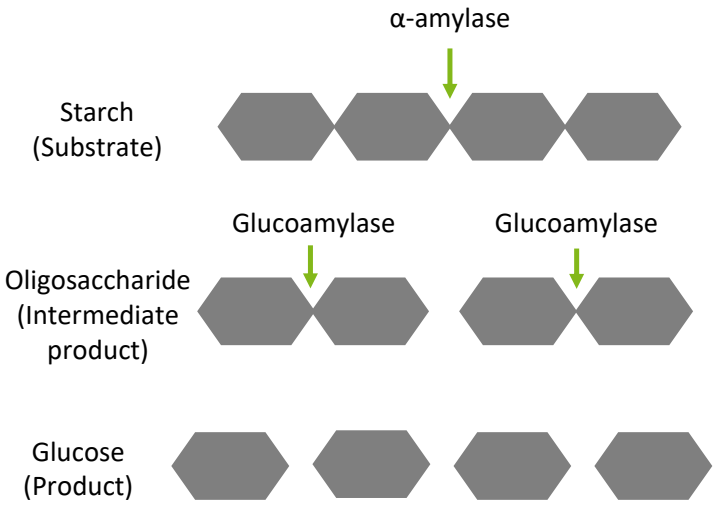

Figure 1: Simplified structure of two-step enzymatic starch hydrolysis. Green arrows indicate points of enzymatic cleavage.

The α-amylase splits the starch molecules (substrate) into the intermediate product (oligosaccharides). This intermediate product is converted into the desired product (glucose) by glucoamylase.

1.1.2 Enzymatic proteolysis

Peptidases catalyse the hydrolysis of peptide bonds. Peptide bond cleavage occurs by adding water molecules (Berg et al., 2018; Bugg, 2012). Based on the catalysed reaction, they are counted among the third main class of enzymes, the hydrolases (EC 3.4.) (Bugg, 2012). The catalytic centre of peptidase is structured as a catalytic triad. Depending on this triad or the catalytic mechanism, a classification is made into serine-, cysteine-, aspartate- and metallopeptidases (Berg et al., 2018). In addition, a classification can be made based on the position of the peptide bond cleavage into endo- and exopeptidases (Jaeger et al., 2018).

Endopeptidases enzymatically split peptide bonds within the protein. The exopeptidases, which can be further subdivided into carboxyl and aminopeptidases, split terminal peptide bonds of the amino acid sequence (Figure 2) (Rao et al., 1998).

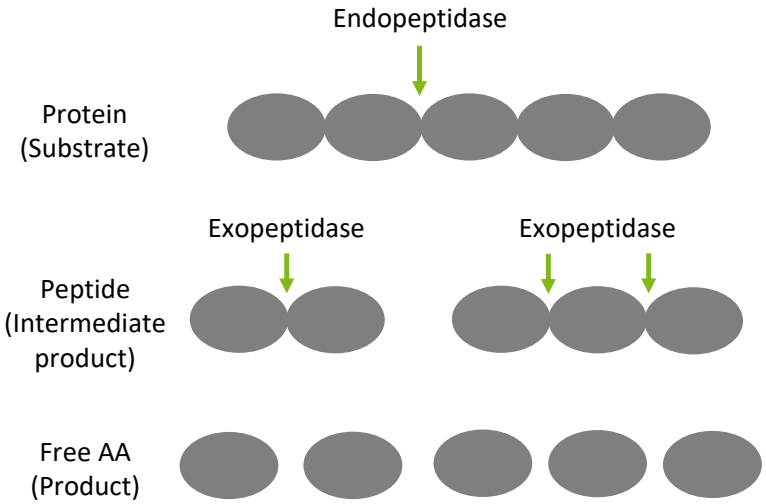

Figure 2: Simplified structure of two-step enzymatic proteolysis. Green arrows indicate points of enzymatic cleavage.

During proteolysis, the proteins (substrate) are split into di- and tripeptides (intermediate products) using endopeptidase. Then, the exopeptidase converts the intermediate into free amino acids (product).

Peptidases have a wide range of applications in industry. They are used, e.g., in detergents, cheese production and the leather industry (Rao et al., 1998). Peptidases are also suitable for producing nutrient media (Gupta et al., 2002; Rao et al., 1998). The advantages over chemical hydrolysis are more moderate conditions, less environmental pollution and easier process control (Tavano, 2013). From the point of view of sustainability, it is exciting to use renewable raw materials, such as potatoes (Kamnerdpetch et al., 2007) or soy (Jung et al., 2004), or waste products, such as salmon by-products (Gbogouri et al., 2004), as substrates.

1.2 Influence of high pressure on enzymes

While most current high-pressure applications are for inactivating deleterious enzymes (Figure 3), there is evidence that high pressure can induce stabilization and activation of some enzymes (Eisenmenger and Reyes-De-Corcuera, 2009). Various strategies have

been employed to enhance enzyme stability, including genetic engineering, immobilisation (Guisan, 2006) and operating in non-aqueous media. While each strategy has provided varying degrees of stability or activity enhancement, applying high pressure may be a complementary, synergistic, or additive enzyme enhancement technique (Eisenmenger and Reyes-De-Corcuera, 2009).

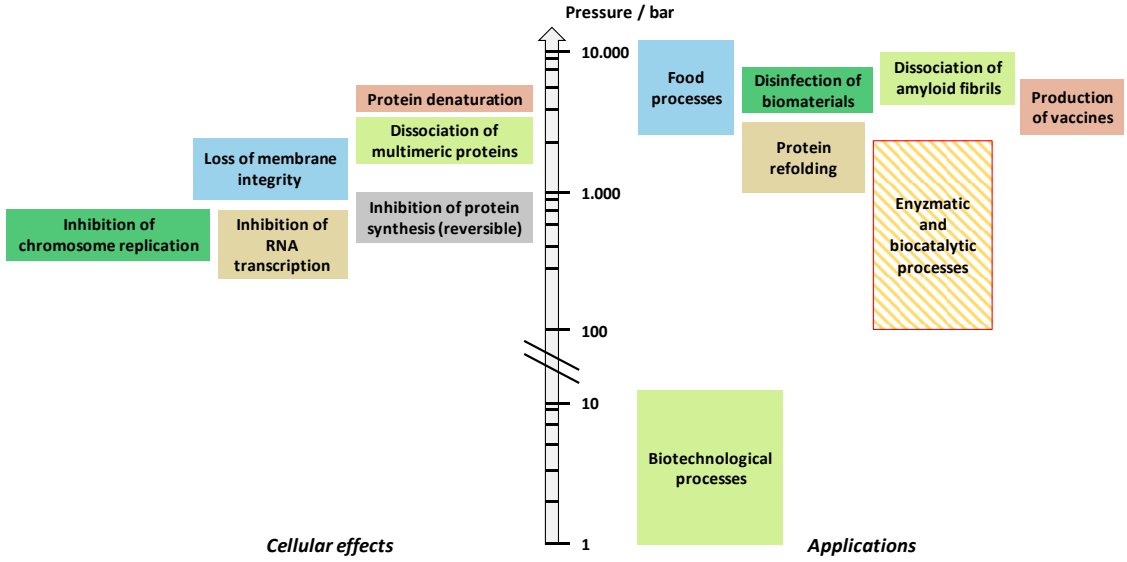

Figure 3: Effects of pressure on cells and enzymes (left) and applications where pressure is used (right). Based on Follonier et al. (2012).

According to Eisenmenger and Reyes-De-Corcuera (2009), the effects of high pressure are driven by direct changes in the reaction mechanism (reaction rates), changes in the structure of the enzyme and changes in the thermostability.

1.2.1 Changes in the reaction mechanism

The relation between pressure and volume change can explain the changes in reaction rates according to the Le Châtelier principle. The effect can be estimated using the Eyring and Magee (1942) equation (Equation 1), where p is the pressure, T is the absolute temperature, R is the ideal gas constant, $\Delta V^{\neq}$ is the activation volume that represents the dependence of the reaction rate with pressure, and k is the rate constant (Eisenmenger and Reyes-De-Corcuera, 2009).

$$\left(\frac{\delta ln\, k}{\delta p}\right)_T = -\frac{\Delta V^{\neq}}{RT} \quad (1)$$

After integration and rearrangement, Equation 1 can be rewritten as Equation 2, where k_0 is the rate constant at a reference pressure P_0.

$$\ln k_0 = -\frac{\Delta V^{\neq}}{RT} \cdot P + \ln k_{P_0} \tag{2}$$

Thus, each rate with a negative volume change is moved to a more compact state as the pressure rises, resulting in acceleration of the reaction and each reaction with a positive activation volume is slowed down (Eisenmenger and Reyes-De-Corcuera, 2009). Depending on the reaction or conformational changes of the enzyme, the activation volume can be positive, negative, or negligible. Typically, activation volumes range from – 70 cm^{-3} mol^{-1} to + 60 cm^{-3} mol^{-1}, with most having a magnitude of less than 30 cm^{-3} mol^{-1} (Adams and Kelly, 1992).

1.2.2 Changes in the enzyme configuration

Significant increases in pressure, temperature, or addition of a denaturing agent cause changes to the native enzyme (E_n) that are reversible (E_r), then irreversible (E_{ir}), and finally lead to the deactivation/denaturation (E_d) of the enzyme (Equation 3) (Eisenmenger and Reyes-De-Corcuera, 2009).

$$E_n \leftrightarrow E_r \rightarrow E_{ir} \rightarrow E_d \tag{3}$$

Moderately increasing pressure can produce a more active enzyme (E_{act}), as shown in Equation 4, which accounts for pressure-induced activation (Eisenmenger and Reyes-De-Corcuera, 2009).

$$E_n \leftrightarrow E_{act} \leftrightarrow E_r \rightarrow E_{ir} \rightarrow E_d \tag{4}$$

The rate constant is also affected by temperature and is generally expressed by the Arrhenius equation (Equation 5).

$$\ln k = -\frac{E_a}{R} \cdot \frac{1}{T} + \ln k_{T_0} \tag{5}$$

E_a is the activation energy, and k_{T_0} is the rate constant at a reference temperature (T_0). Both temperature and pressure can contribute to activation in a particular range, but they can also affect the reaction rate by inactivating the enzyme.

1.2.3 Changes in the thermostability

Advantages can also be taken from the increased thermostability of some enzymes under high pressure. High temperatures can enhance the reaction rate, while high pressure supports maintaining a functional structure (Eisenmenger and Reyes-De-Corcuera, 2009). However, temperature can also lead to the destabilisation of enzymes.

The pressure-temperature phase diagram of proteins exhibits an elliptic curve (Hawley, 1971; Suzuki, 1960), meaning that a pressure increase can stabilise or destabilise protein structures depending on the starting value and temperature (Figure 4).

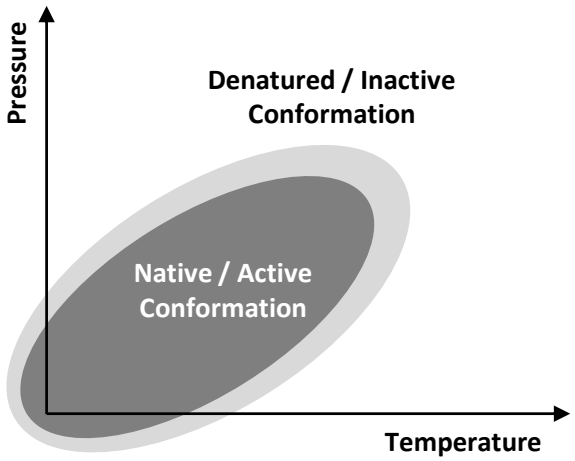

Figure 4: Pressure-temperature diagram representing the elliptical stability domain of proteins. The regions inside and outside of the ellipses correspond to native and denatured conformations. Based on Eisenmenger and Reyes-De-Corcuera (2009) and Follonier et al. (2012).

Pressure affects the activity and stability of enzymes in various ways. The enzymatic processes are usually characterised directly by specific experiments under high pressure.

Table 1 presents a selection of experimental results for the effect of high pressure and temperature on enzymes. The investigated enzymes, the examined conditions and the effects are shown (Eisenmenger and Reyes-De-Corcuera, 2009).

Table 1: Selection of pressure-dependent enzymes. Based on Eisenmenger and Reyes-De-Corcuera (2009).

Enzyme (Enzyme class)	Pressure tested (bar)	Temperature tested (°C)	Effects	Reference
Dehydrogenase (EC 1.1.1.1)	1 - 1500	28-101	Stabilised at 101 °C by application of 1300 bar.	Morita and Haight (1962)
Hydrogenase (EC 1.1.1.2)	6.5 - 8.5, 250 - 264	86	Activity at 86 °C, three times higher with increasing pressure up to 260 bar.	Miller et al. (1989)
Peroxidase (EC 1.11.1.)*	4000, 6000, 8000	18, 22	Activity increased by 13% after exposure to 4000 bar for 5 min.	Garcia-Palazon et al. (2004)
Lipoxygenase (EC 1.13.11.12)	1 - 6000	35 - 90	Activity increased to 120% with pressure up to 2000 bar at 55 °C compared to 1 bar.	Tedjo et al. (2000)
Polymerase (EC 2.7.7.7)	30, 450, 890	110 - 112.5	Half-lives increased from 6.9 min at 30 bar to 39 min at 890 bar.	Summit et al. (1998)
Lipase (EC 3.1.1.3)	1 - 500	50	Catalytic efficiency improved up to 100 bar and decreased above 100 bar.	Knez et al. (2007)
α-Amylase (EC 3.2.1.1)	1 - 8000	30 - 75	Activity increased by 25% at 1520 bar and 64 °C, compared to ambient pressure and 59 °C.	Buckow et al. (2007)
β-Amylase (EC 3.2.1.2)	1 - 7000	20 - 70	Activity increased by 15% at 1000 bar and 62 °C compared to optimum conditions at ambient pressure.	Heinz et al. (2005)
Glucoamylase (EC 3.2.1.3)	1 - 14000	40 - 90	The stable isoform was slow to inactivate up to 14000 bar at 50 °C.	(Buckow et al., 2005)
Invertase (EC 3.2.1.26)	1 - 3500	60	Half-life increased until the pressure reached 2000 bar.	Noel M.-O. et al. (2000)
Protease (EC 3.4.21-22)	1 - 2000	20 - 70	Increase of approx. 30% in the 20 °C-activity was reached after 2000 bar processing.	Tribst et al. (2012)
Aspartase (EC 4.3.1.1)	1 - 1000	45 - 56	Stabilised and activated at 45-56 °C by pressure up to 1000 bar.	Haight and Morita (1962)

The properties of the enzymes were studied directly under high-pressure conditions, or the enzymes were previously treated with high pressure. Then their altered characteristics were investigated under ambient pressure conditions. The changes in the enzyme configuration after high-pressure treatment can be permanent, depending on pressure, inlet temperature and enzyme storage conditions (Tribst et al., 2012).

Among the pressure-dependent enzymes are α-amylase, and glucoamylase, used in the starch hydrolysis process, for α-amylase from barley malt investigations have been carried out under combined pressure-temperature treatments in the range of 1 to 8000 bar and 30 to 75 °C. The activity increased by 25% after treatment at 1520 bar and 64 °C, compared to the native form of the enzyme (Buckow et al., 2007). For the stable isoform of a glucoamylase, pressure up to 14000 bar in a temperature range from 40-95 °C has been investigated. The stable isoform of a glucoamylase was inactivated more slowly at process conditions of 50 °C and 14000 bar compared to 50 °C and ambient pressure conditions. The stable isoform of a glucoamylase was slow to inactivate up to 14000 bar at 50 °C (Buckow et al., 2005). For the conversion of maltose to glucose at pH 4.5, the optimum was determined at 3180 bar and 84 °C for a 30-minute process. Compared to the maximum observed at ambient pressure (approx. 62 °C), glucose production was doubled (Buckow et al., 2005).

Furthermore, an increased activity of a commercial neutral protease from *Bacillus subtilis* after high-pressure treatment was observed by Tribst et al. (2012). No improvement in the activities at 55-70 °C was observed after high-pressure treatment, while an increase of approximately 30% in the activity at 20 °C was reached after 2000 bar processing. It suggests that high-pressure treatment modifies the protease configuration, changing enzyme performance (maximum activity condition), as the efficacy of the lock-and-key mechanism is strictly dependent on enzyme spatial structure (Tribst et al., 2012).

Treating enzymes with high pressure can lead to an improvement in enzyme activity and stability. However, these improvements vary from each enzyme to the other. In addition, improvements are only apparent at some temperatures, and no linear relationship can be observed. Therefore, it is difficult to accurately predict the specific activity and stability of the enzymes after high-pressure treatment.

1.3 Reactors for enzymatic processes

Several reactor concepts are available for enzymatic processes (Illanes, 2008) (Figure 5).

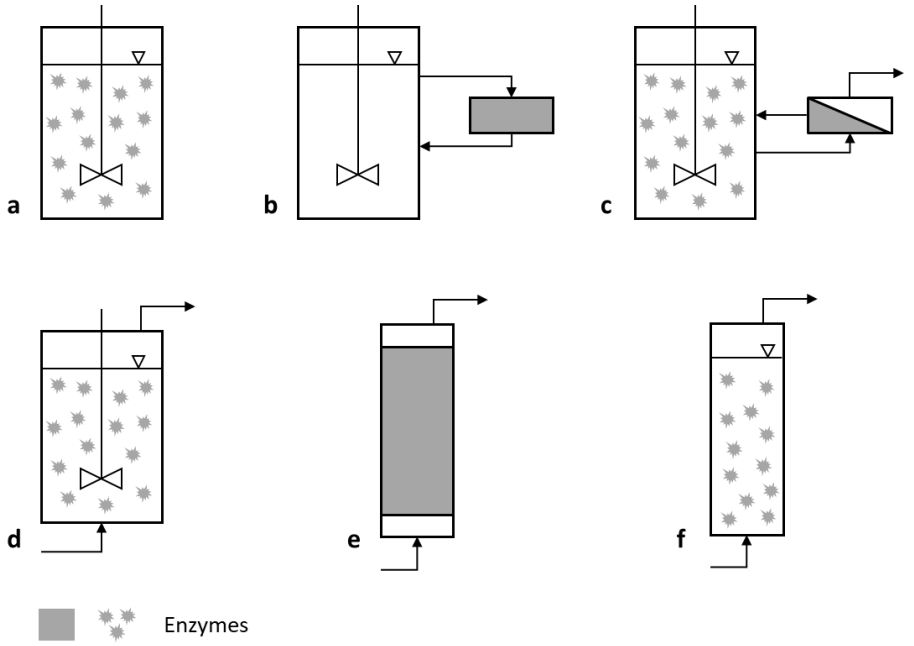

Figure 5: Reactor configurations for enzymatic processes: a: stirred tank batch reactor; b: recirculation batch reactor; c: stirred tank ultrafiltration reactor; d: continuous stirred tank reactor; e: continuous packed bed flow tube reactor; f: continuous fluidized bed reactor. Based on Illanes (2008).

One of the most straightforward reactor concepts is the stirred tank batch reactor (a), provided with mixing elements and systems for temperature control and pH control, where the substrate and soluble enzymes or immobilised enzymes are added directly to the reactor (Illanes, 2008; Krause and Merz, 2017; Nienow, 2014). Neither further substrate nor other enzymes are added (Illanes, 2008; Nienow, 2014). If there is an inflow to the reactor, it is called a stirred tank fed-batch reactor (Alford, 2006; Illanes, 2008; Nienow, 2014). If there is also an outflow, the system is called a continuous STR (d) (Illanes, 2008; Nienow, 2014). Further development of this reactor concept is the recirculation batch reactor (b). Recirculation batch reactors (b) provide the enzymes immobilised in a narrow bed through which the reaction medium is circulated (Illanes, 2008; Sudhakaran et al., 1992). This reactor configuration is appropriate when working with pH-sensitive enzymes because the enzymes only briefly contact the reaction medium and have no direct contact with the acid or base used for pH control in the main reactor (Illanes, 2008; Sudhakaran et al., 1992). The STR ultrafiltration (c) offers the advantage that a large throughput is possible even with small reactors (Illanes, 2008). A filter holds

the enzymes in the reactor system, and the broth is continuously drawn off (Illanes, 2008). The duration of the catalysis depends strongly on the enzyme stability since usually no enzymes are added afterwards (Illanes, 2008). Packed bed flow tube reactors (PBR) (e) are pretty simple to design and consist of solid catalyst particles being loaded and packed into a bed (Illanes, 2008). The medium flows through the bed and encounters the catalysts. In a fluidised bed reactor (f), a fluid (gas or liquid) is passed through a solid granular material (with immobilized catalysts) at high enough velocities to suspend the solid and cause it to behave as though it were a fluid (Allen et al., 1979; Illanes, 2008). Both fixed-bed and fluidized-bed reactors offer the advantage that high throughput is possible even with small reactor volumes (Illanes, 2008). The disadvantage of these reactor types is that the subsequent addition of enzymes is complex (Verhoff and Schlager, 1981). It is, therefore, necessary to maintain high stability of the enzymes.

1.4 Control and design of enzymatic processes

Depending on the enzymatic process and the selected type of reactor, particular control strategies are required. In general, controllers are divided according to continuous and discontinuous behaviour. Among the best-known continuous controllers are feedback controllers with proportional (P), proportional-integral (PI) and proportional-integral-derivative (PID) behaviour. Table 2 shows some control variables of enzymatic processes with their most used control strategies.

Table 2: Control strategies for control values occurring in enzymatic and biocatalytic processes.

Control variable	Control strategy	References
Temperature	**PI**, **MPC**, **NMPC**	Alford (2006), Fenila and Shastri (2016), Moradi et al. (2011), Bück et al. (2015)
Moisture	**NMPC**	Bück et al. (2015)
pH	**PI**	Alford (2006)
DO	**On-Off-Feedback control**, **PI**, **PID**, **Cascade Control**, **MPC**	Larroche et al. (2016), Alford (2006), Galvanauskas et al. (2013)
Concentration	**PI, Fuzzy control**, **MPC**, **NMPC**	Morales-Rodríguez et al. (2010), Alford (2006), Álvarez et al. (2006), Chang et al. (2016), Craven et al. (2014)

Simple control tasks can be solved using “standard control strategies”. For more demanding control tasks (such as concentration control), the use of model-based control strategies such as MPC or NMPC has been suggested (Larroche et al., 2016; Zacher and Reuter, 2017).

1.4.1 Model predictive control and nonlinear model predictive control

MPC does not operate based on the current state of the system. The control action is based on the calculated evolution of the system. For each sampling period, a mathematical optimisation system determines the controller actuation to be applied in the next time interval to minimise a cost function calculated with the predicted system error, stability, and other control criteria. The cost function requires a mathematical process model to predict its future behaviour (Larroche et al., 2016).

Figure 6 shows a block diagram which describes the working principle of MPC (Larroche et al., 2016). MPC strategies include a model update procedure that based on data from the controlled variable and the controller output, calculates updated parameters of a model describing the process. Then, the automated tuning procedure uses this updated model to calculate new parameters for the controller, which will be more adapted to the current process dynamics.

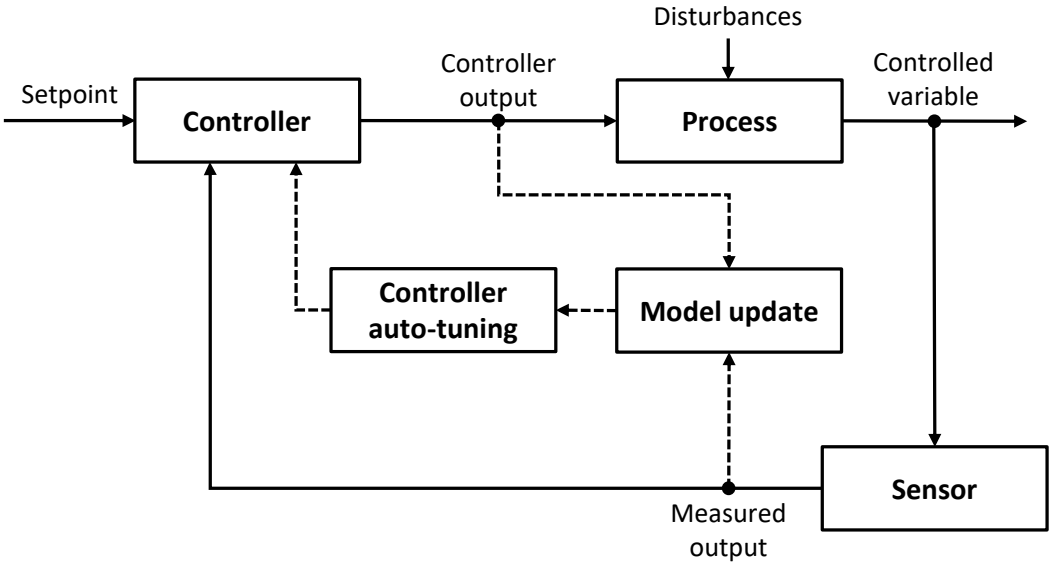

Figure 6: Working principle of MPC. Based on Larroche et al. (2016).

NMPC is a variant of MPC characterised using nonlinear system models. As with linear MPC, NMPC requires the iterative solution of optimal control problems on a finite prediction horizon (Allgöwer and Zheng, 2000; Biegler, 2021).

NMPC strategies have already been used to optimise enzymatic and biocatalytic processes.

Hodge et al. (2009) used NMPC for high-solids enzymatic cellulose hydrolysis in an STR. NMPC feeding profiles for experiments in STRs were calculated to maintain the insoluble solids concentration at a manageable level throughout the process. The STR experiments resulted in similar cellulose conversion rates as in batch shake flask reactors, where the temperature control problems are mitigated.

Fenila and Shastri (2016) used NMPC for temperature control in enzymatic hydrolysis of cellulose in an STR. Using NMPC resulted in an enzyme saving of 77.8% and a reduction in the processing time of 22.2%.

Bück et al. (2015) used NMPC to control temperature and moisture gradients along reactor length (solid-state fermentation). Using NMPC prevented locally critical process conditions requiring the bioreactor to be shut down.

1.4.2 Open-loop-feedback-optimal strategy

One special form of NMPC is the OLFO strategy (Luttmann et al., 1985; Witte et al., 1996). The OLFO controller consists of a mathematical process model, a model parameter identification part, and an optimisation part (Figure 7).

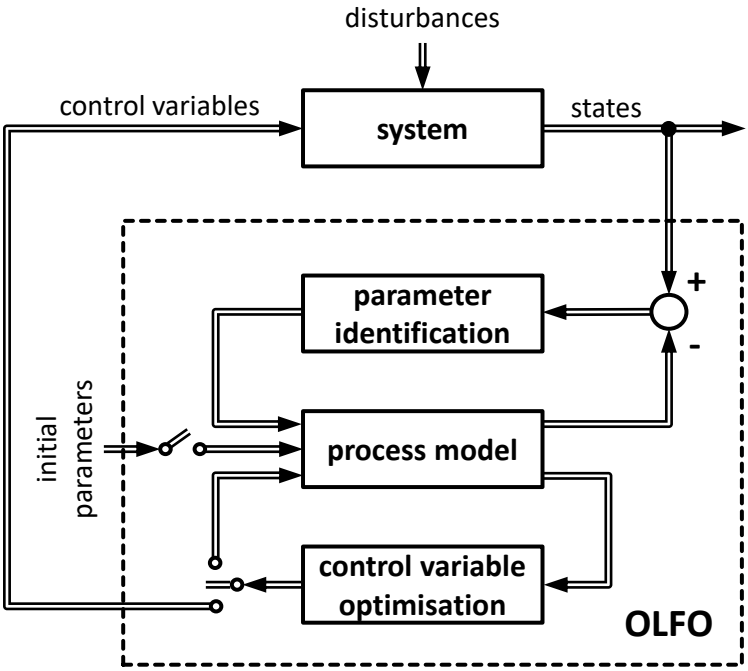

Figure 7: Structure of the open-loop-feedback-optimal strategy. Based on Luttmann et al. (1985) and Witte et al. (1996).

Model parameters are estimated frequently based on available online and offline data. The updated model parameters are passed on to the optimisation part, where process trajectories like substrate feeding profiles are calculated. Several optimisation criteria, such as maximised product concentrations, may be implemented in the controller. The OLFO strategy is superior to other process control strategies if the processes have not yet been optimised or if sophisticated process control formulas are not available. This is often the case at the beginning of a process development when relatively large quantities of a product must be made available for initial tests in a relatively short time. However, the industrial process has not been designed yet.

The OLFO control strategy has been investigated in a receding horizon (Appl et al., 2019; Li, 2015; Witte et al., 1996) and a moving horizon version (Frahm et al., 2002; Frahm et al., 2003a; Frahm et al., 2003b) for microbial bioprocesses.

1.4.3 Model-based design of experiments

Design-of-experiments (DoE) methods, which require many resource-consuming experiments, are often used to develop and optimise biotechnological processes (Glauche et al., 2017; Mandenius and Brundin, 2008). The design, especially narrowing the parameter boundaries, is complicated (Brunner et al., 2017; Manzon et al., 2020; Stosch and

Willis, 2017). Thus, there is a high risk that the experiments were selected falsely and delivered only inconclusive information, leading to higher costs and time delays (Möller et al., 2019; Moser et al., 2021; Stosch et al., 2016).

The mDoE concept (Kuchemüller et al., 2020; Möller et al., 2019) linked DoE strategies with mathematical process models. To make this concept usable for biotechnological processes, the "mDoE-toolbox" was developed (Moser et al., 2021). The mDoE concept allows for narrowing down the DoE design space and can thus reduce the number of necessary experiments (Gassenmeier et al., 2022; Kuchemüller et al., 2020; Möller et al., 2019; Möller and Pörtner, 2017; Moser et al., 2021).

1.5 Modelling of enzymatic processes

Enzymes play a central role in life, catalysing many chemical and biological processes occurring in nature (Illanes, 2008; Jaeger et al., 2018). Therefore, understanding how enzymes catalyse their reactions is essential, both from fundamental and practical perspectives, with application in a variety of areas, from more basic research that aims to understand how different events occur in the cell to the development of new treatments for diseases, and even in industrial biocatalytic applications (Illanes, 2008; Jaeger et al., 2018; Polaina and MacCabe, 2007).

Computational methods can be used to simulate various enzymatic reactions, bypassing some of the limitations of the experimental methods commonly used and providing an alternative strategy to complete the information obtained by the experimental methods (Narayanan et al., 2020; Polaina and MacCabe, 2007).

From a mathematical point of view, the art of modelling is based on a solid understanding of the biological process, a realistic mathematical representation of the relevant biological phenomena, the finding of solutions, preferably quantitative, and a biological interpretation of the mathematical results in the form of insights and predictions (Murray, 2004).

1.5.1 Modelling of enzymatic hydrolysis processes

The modelling of enzymatic hydrolysis processes has frequently been the subject of scientific investigations.

Beschkov et al. (1984) described a kinetic model for the hydrolysis and synthesis of maltose, isomaltose and maltotriose by glucoamylase. Simple first and second-order kinetics were implanted to map the kinetics of the glucoamylase. Beschkov et al. (1984) mentioned that the model adequately described the experimental results.

Lee et al. (1992) describe a mathematical model for the simultaneous saccharification and ethanol fermentation of sago starch using amyloglucosidase and *Zymomonas mobilis*. A series of Michaelis-Menten equations was used to realise the model. The model was parameterised using the results of simple experiments carried out at various substrate and enzyme concentrations. The authors mentioned that the simulated experimental results were in good agreement.

Beaubier et al. (2021) described an approach for modelling and optimising enzymatic proteolysis batch processes. In this research work, DoE methods were combined with second-order kinetic models. As a result, the model could reproduce the proteolysis process with over 80% agreement.

Models for combined starch hydrolysis and proteolysis in an STR are currently unknown.

1.6 Digital twin technology in biochemical engineering

In the early 2000s, the digital twin concept was first applied in mechanical engineering (El Saddik, 2018; Glaessgen and Stargel, 2012; Grieves, 2016). Various authors have already published definitions for “Digital Twin” (El Saddik, 2018; Glaessgen and Stargel, 2012; Grieves, 2016; He et al., 2019; Zobel-Roos et al., 2019). This research work is mainly based on the definition given by El Saddik (2018):

“Digital twins are (…) digital replications of living as well as non-living entities that enable data to be seamlessly transmitted between the physical and virtual worlds.”

(El Saddik, 2018)

Digital twins are digital representatives of material or immaterial objects or processes. Whether the counterpart already exists in the real world or will exist in the future is irrelevant. They consist of models of the represented object or process. They can also contain algorithms and services that describe or influence the properties or behaviour of the represented object or process. The coupling between the actual process and the

associated digital twin can take place directly during the running process (process accompanying) or cyclically after the execution of the actual process (El Saddik, 2018; Glaessgen and Stargel, 2012; Grieves, 2016; He et al., 2019; Zobel-Roos et al., 2019).

In many application areas, digital twins or “early stage” digital twins are becoming more important. Especially in “Industry 4.0”, digital twins are becoming increasingly valuable, and their application is being studied frequently (Liu et al., 2021; Tao et al., 2019; Vaccari et al., 2021). Digital twins also may represent the reactor macro-kinetics and the system's dynamics. They are thus ideally suited for systematically optimising dynamic processes (Appl et al., 2020; Narayanan et al., 2020).

In the early to mid-1980s, the first operator training simulators representing “early-stage” digital twins were used for operator training in the chemical, nuclear and energy industries. In the late 1980s and early 1990s, the implementation of operator training simulators in the chemical industry evolved from pioneering work to standardised practice (Patle et al., 2014). Today, digital twins are widely used in industries with high capital investment, complex processes and severe plant or operator failure consequences, such as the offshore oil and gas industry (Cameron et al., 2002; Dudley et al., 2008; Patle et al., 2014). Older educational facilities for training in the oil and gas industry were based on physical copies of the control room, which are expensive and no longer needed (Patle et al., 2014). Almost simultaneously with the first appearance of digital twins in the chemical industry, they were used as a tool for control strategy development (Patle et al., 2014). Initially, these were relatively simple control engineering tasks, but they became more complex with the advancing development of digital twins (Cameron et al., 2002; Patle et al., 2014).

Dudley et al. (2008) described a digital twin of a pebble bed modular reactor plant to design and test control strategies before using them on the actual plant. He et al. (2019) described using a digital twin for the Tennessee Eastman benchmark process. The effectiveness and performance of the digital twin in the design of control strategies were demonstrated in the presence of realistic fault scenarios. Three types of process faults, i.e., sensor faults, actuator faults and process disturbances, were investigated, and the corresponding fault size and temporal behaviour were discussed. All simulation studies

and numerical results indicated that the proposed configurations are valid for safe operations in case of a process fault. Zhang and Ji (2019) described using a digital twin for carbon emission reduction in intelligent manufacturing. Here, the digital twin predicts the carbon emissions of the plant.

One approach for the development of digital twins in biochemical engineering is the use of a shell structure (Blesgen and Hass, 2010; Hass et al., 2014; Kuntzsch, 2014; Moser et al., 2020), including a biokinetic, a physico-chemical, a reactor, a plant and periphery as well as a control and automation submodel (Figure 8).

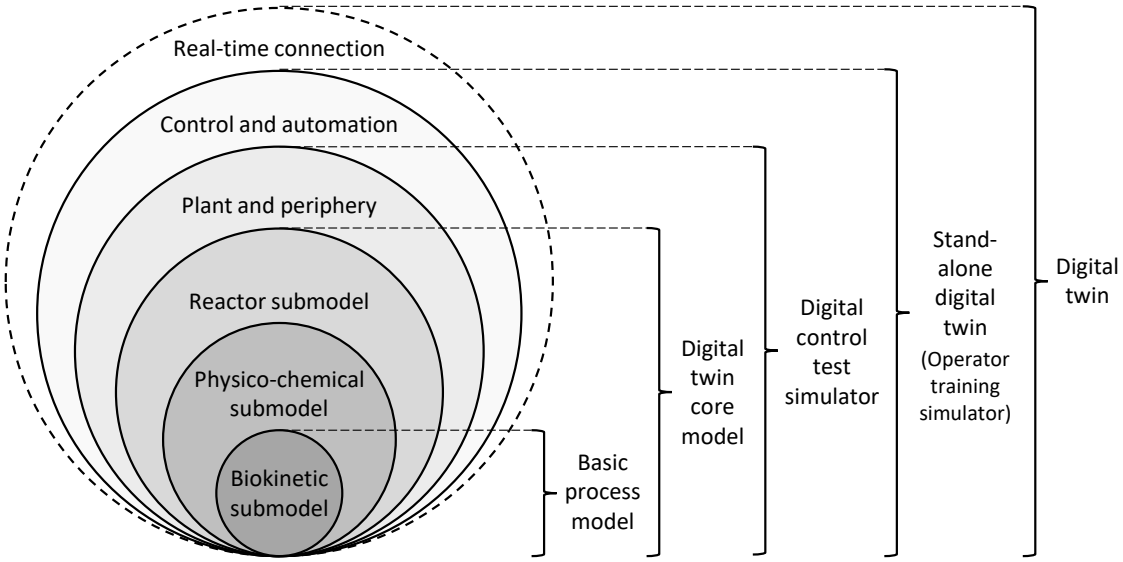

Figure 8: Shell structure of digital twins in biochemical engineering, with biokinetic, physico-chemical, reactor, plant and periphery and control and automation submodel. Based on Blesgen et al. (2010), Hass et al. (2014), Kuntzsch (2014) and Moser et al. (2020).

The core of a digital twin consists of a biokinetic submodel. The biokinetic submodel calculates all rates concerning the growth and product formation of microorganisms and mammalian cells, as well as enzymatic and biocatalytic reactions. The biokinetic submodel corresponds to the basic process model.

The second shell of the digital twin contains the physico-chemical submodel, which includes models for calculating broth temperature, pH, foam level and gas-phase concentrations. To further increase the flexibility of the digital twin, these physico-chemical models are independent of the biokinetic submodel. Only calculated values of rates and state variables are transferred between the submodels.

The biokinetic and physico-chemical submodels are embedded in the reactor submodel (e.g., STR model), resulting in the digital twin core model.

A digital control test simulator also features a plant and periphery submodel. This submodel describes the behaviour of the periphery connected to the reactor, e.g., pumps and pipes.

A stand-alone digital twin or operator training simulator also features a control and automation submodel. Control and automation strategies, e.g., temperature, pH or pressure, can be realised in this submodel. A stand-alone digital twin is adapted to the existing system as soon as deviations occur between the simulated and the actual behaviour of the existing system.

A complete digital twin is obtained if the stand-alone digital twin has an online connection to the existing system, which is constantly adapted to the actual process.

Compared to chemical processes, the application of digital twins or “early stage” digital twins, in biochemical engineering is still in its infancy. Thoroughness is required for modelling bioprocesses since a wide variety of parallel reactions occur simultaneously. Even small changes in critical process variables, such as pH or temperature, may immensely influence kinetics (Hass and Pörtner, 2011).

Pörtner et al. (2011) used a stand-alone digital twin to optimise process control strategies for mammalian cell cultivations. The developed stand-alone digital twin is a digital replica of the cultivation of mammalian cell lines in a small-scale STR. The stand-alone digital twin was used to simulate the impact of different glucose and glutamine feed rates on cell density and antibody concentration during the fed-batch cultivation of a mammalian cell line. Using the stand-alone digital twin, the cultivation process could be optimised in a considerably shorter time and with fewer experiments than process control optimisation on the actual process.

A contribution by Hass et al. (2014) presented the utilisation of an industrial biotechnology stand-alone digital twin. Control strategies developed using a new stand-alone digital twin of a bioethanol plant illustrated the potential for enhanced resource efficiency and reduced energy consumption. According to the authors, the potential savings in raw materials have a direct impact on the long-term profitability of the bioethanol plant and

enables a reduction of operating costs. Furthermore, using the stand-alone digital twin, the time course and dynamics of the entire plant could be analysed and subsequently optimised using new process control strategies. Performing such a study on an actual plant would have been overly complex and expensive, if not impossible.

1.6.1 Digital twin supported development of process control strategies

Digital twins can be used to design, test and optimise bioprocess design and control strategies. During process development or optimisation, digital twins can be used to determine suitable controller types and improve the overall process performance through appropriate process design.

If, for example, suitable controllers (e.g., for temperature, dissolved oxygen or product concentration) should be designed, the controller type can be selected based on simulations on the digital twin. An early step in controller selection should be defining appropriate control targets (Appl et al., 2020). When controlling the temperature of a bioreactor, such control targets are, e.g., a short rise time, a high control accuracy (essential for temperature- or pH-sensitive organisms or enzymes) or a low overshoot. For example, the conventional PID control can be compared to a more complex NMPC by applying them to a digital twin. If both control strategies yield equally good control results, PID control would be preferred because it is cheaper and easier to handle.

Once a control strategy can control the virtual process satisfactorily, the results are transferred to the actual process. The transfer of the developed control strategy from the digital twin to the actual process may be further simplified if the digital twin and the actual process are linked to the identical process control system (Appl et al., 2020).

To utilise a digital twin to develop both conventional (e.g., single loop PID control) and advanced control (e.g., multivariable controllers, MPC, NMPC), it must fulfil specific requirements that must be considered during the design process of the digital twin. Desirable characteristics of a functional digital twin include realistic simulation of the biological and physico-chemical processes, accurate representation of automation and control actions, as well as a GUI with a similar ‘look and feel’ to that of the actual plant (Hass, 2016).

2 Research aims and objectives

2.1 Research hypothesis

Mathematical process models and digital twins, in combination with model-based process design and control strategies according to the mDoE and OLFO principles, can improve and stabilise enzymatic hydrolysis processes like starch hydrolysis and proteolysis.

2.2 Aims and objectives

(1) Development of a new mathematical model for enzymatic hydrolysis processes (combined enzymatic starch hydrolysis and proteolysis).

(2) Development of a new stand-alone digital twin for enzymatic hydrolysis processes in an STR and application to model-based process design.

(3) Development and experimental validation of model-based process design strategies according to the mDoE and OLFO principles for enzymatic hydrolysis batch processes in an STR.

The structure of the PhD thesis is shown in Figure 9.

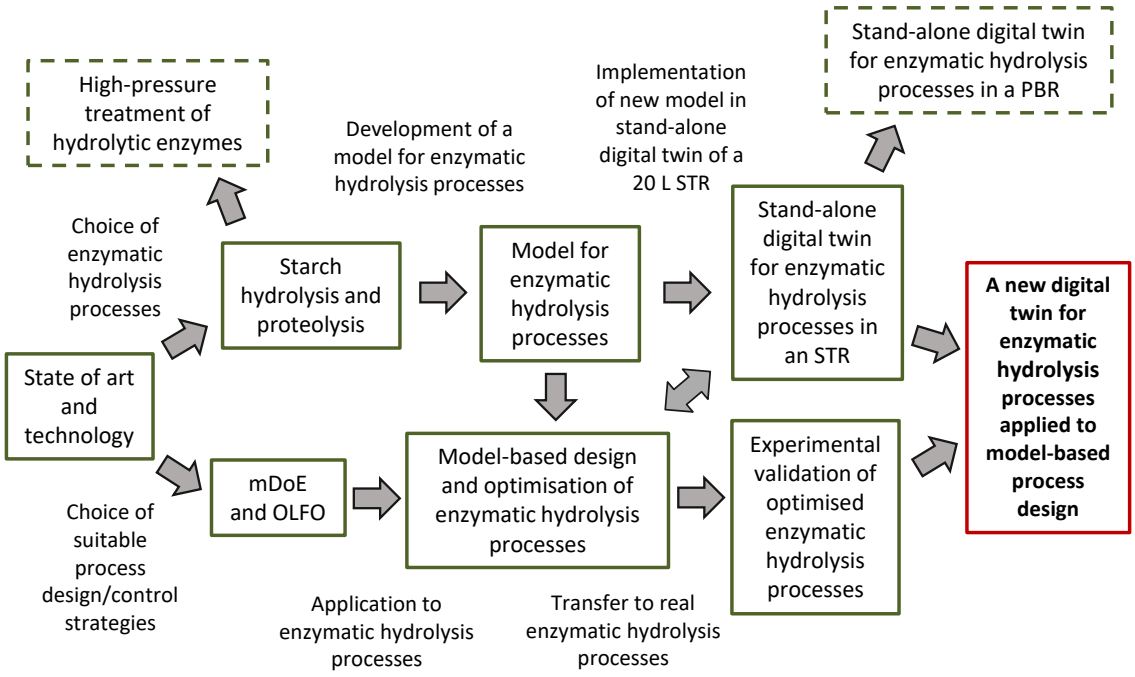

Figure 9: Structure of the PhD thesis.

3 Materials and methods

This section covers how the enzymatic hydrolysis processes were performed and describes the analytical methods used to evaluate the processes. Furthermore, the software and methods used for modelling, digital twin development and development of the process control and design strategies are covered. Table 3 summarises the materials and equipment used to conduct the enzymatic hydrolysis processes and analyse the samples.

Table 3: Materials used for the enzymatic hydrolysis experiments and analysis.

Description	**Specification**	**Producer**
Materials		
Casein	CAS No.: 9000-71-9	Carl Roth GmbH + Co. KG, Karlsruhe, Germany
Citric acid monohydrate (≥ 99%)	CAS No.: 7558-79-4	Merck KGaA, Darmstadt, Germany
D(+)-Glucose monohydrate	CAS No.: 77938-63-7	Carl Roth GmbH + Co. KG, Karlsruhe, Germany
EnerZyme® P7	Metalloendopeptidase (EC 3.4.24.4)	Erbslöh Geisenheim GmbH, Geisenheim, Germany
Enzytec™ Liquid D-Glucose	Enzymatic assay for D-Glucose in foodstuff and other sample materials. Art. No. E8140	R-Biopharm AG, Pfungstadt, Germany
Ethylene glycol (≥ 98%)	CAS No.: 107-21-1	Carl Roth GmbH + Co. KG, Karlsruhe, Germany
Flavourzyme®	Blend of endo- and exopeptidases	Novozymes A/S, Bagsværd, Denmark
Heliaflor® 45	Sunflower seed meal	All Organic Treasures GmbH, Wiggensbach, Germany
Hydrochloric acid fuming (37 %)	CAS No.: 7647-01-0	Carl Roth GmbH + Co. KG, Karlsruhe, Germany
Iodine (≥ 99.8%)	CAS No.: 7553-56-2	Honeywell Fluka, Morristown, New Jersey, USA
L-glutamic acid (≥ 98%)	CAS No.: 56-86-0	Honeywell Fluka, Morristown, New Jersey, USA
Ninhydrin (≥ 99%)	CAS No.: 485-47-2	Carl Roth GmbH + Co. KG, Karlsruhe, Germany
Potassium dihydrogen phosphate (≥ 99.5%)	CAS No.: 7778-77-0	Merck KGaA, Darmstadt, Germany
Potassium iodide (≥99,5%)	CAS No.: 7681-11-0	Carl Roth GmbH + Co. KG, Karlsruhe, Germany
Potassium hydroxide (≥85%)	CAS No. 1310-58-3	Carl Roth GmbH + Co. KG, Karlsruhe, Germany

di-Sodium hydrogen phosphate dihydrate (≥ 98%)	CAS No.: 10028-24-7	Merck KGaA, Darmstadt, Germany
Spirizyme® Ultra	Blend of α-amylases and glucoamylases	Novozymes A/S, Bagsværd, Denmark
Starch from potatoes	CAS No.: 9005-25-8	Carl Roth GmbH + Co. KG, Karlsruhe, Germany
Termamyl® SC	1,4-alpha-D-glucan glucanohydrolase (EC 3.2.1.1)	Novozymes A/S, Bagsværd, Denmark
Tin(II) chloride dihydrate (≥ 98%)	CAS No.: 10025-69-1	Carl Roth GmbH + Co. KG, Karlsruhe, Germany
TRIS PUFFERAN® (≥ 99.9%)	CAS No.: 77-86-1	Carl Roth GmbH + Co. KG, Karlsruhe, Germany
Equipment		
Bioreactor, STR	BioFlo 3000, V_{max} = 6 L	New Brunswick Scientific, Edison, New Jersey, USA
External pH/mV meter	FiveEasy	Mettler-Toledo, Columbus, Ohio, USA
External thermometer	testo® 110	Testo SE & Co. KGaA, Titisee-Neustadt, Germany
High-pressure homogeniser	HPH 2000/4-SH5	IKA®-Werke GmbH & CO. KG, Staufen, Germany
Magnetic stirrer	IKA® RH basic 2	IKA®-Werke GmbH & CO. KG, Staufen, Germany
UV-VIS Spectrophotometer	UVmini-1240	Shimadzu Europa GmbH, Duisburg, Germany
Water bath	WBT 12	Carl Roth GmbH + Co. KG, Karlsruhe, Germany

3.1 Enzymatic starch hydrolysis using amylases

Small-scale experiments were carried out in 15 mL test tubes to characterise the enzymes used in the starch hydrolysis process. The influence of temperature, pH and pressure on the activity of the enzymes was investigated. In addition, starch hydrolysis batch experiments were performed in an STR for model parameterisation and validation of the optimised process design.

The enzyme preparations Termamyl SC (Novozymes, Bagsværd, Denmark) and Spirizyme Ultra (Novozymes, Bagsværd, Denmark) were used for starch hydrolysis.

Termamyl SC is a liquid enzyme preparation containing an heat-stable α-amylase expressed in and produced by a genetically modified strain of *Bacillus* (Novozymes A/S, 2004). The systematic name for the enzyme is 1,4-alpha-D-glucan glucano-hydrolase (EC 3.2.1.1). Termamyl SC is an endo-amylase that hydrolyses 1,4-alpha-glucosidic linkages

in amylose and amylopectin (Novozymes A/S, 2004). The breakdown products are oligosaccharides of different chain lengths (Novozymes A/S, 2004).

Spirizyme Ultra is liquid enzyme preparation containing highly efficient, heat-stable and robust glucoamylase and an exceptional heat-stable α-amylase (Novozymes A/S, 2010). The glucoamylases hydrolyse both 1,4- and 1,6-alpha linkages to liberate glucose (Novozymes A/S, 2010).

3.1.1 Investigation of the temperature and pH-dependent activity of amylases

For the determination of the influence of temperature (0-99 °C) and pH (2.0-10.0) on the enzyme activity, 5 mL buffer (pH 2.0, 3.0 and 4.0 using phosphate citrate buffer, pH 5.0, 6.0, 7.0 and 8.0 using phosphate buffer, pH 9.0 and 10.0 using Tris-HCl buffer), containing 20 g L^{-1} potato starch (Carl Roth, Karlsruhe, Germany), 0.05 mg L^{-1} Termamyl SC (Novozymes, Bagsværd, Denmark) or 0.001 mg L^{-1} Spirizyme Ultra (Novozymes, Bagsværd, Denmark) was added to a 15 mL test tube (VWR, Darmstadt, Germany), mixed and placed in a water bath (T = 0, 21, 40, 50, 60, 70, 80, 99 °C). After 10 min, 90 µL of the sample was drawn, and the reaction was stopped by adding 600 µL of 5 M HCl and heating the sample for 5 min at 80 °C in a heating block (VWR).

To investigate the pH dependency, the temperature was set to 60 °C, and the pH value was varied from 2.0 to 10.0. To investigate the temperature dependency, the pH was set to 5.0, and the temperature was varied from 0-100 °C.

The samples were analysed for their starch concentration (Section 3.1.3). The concentration of converted starch was then calculated based on the initial starch concentration (20 g L^{-1}). The determined converted starch concentrations were finally standardised. A value of 1 was set for the highest converted starch concentration. The other results were scaled to the maximum result.

3.1.2 Starch hydrolysis batch experiments in a stirred tank reactor

Starch hydrolysis experiments were performed in a 6 L STR (BioFlo 3000, New Brunswick Scientific, Eppendorf, Hamburg, Germany) (Figure 10).

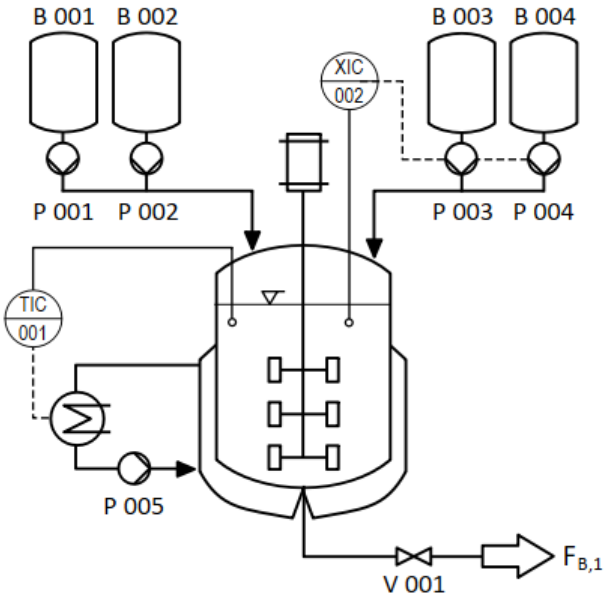

Label	Description
B 001	E1 (Termamyl SC)
B 002	E2 (Spirizyme Ultra)
B 003	Acid – 20% w/v HCl
B 004	Base – 20% w/v KOH
TIC 001	Temperature control
XIC 002	pH control

Figure 10: Batch enzymatic starch hydrolysis in a 6 L STR (BioFlo 3000, New Brunswick Scientific, Eppendorf, Hamburg, Germany).

3.0 L phosphate citrate buffer (pH = 4.15), with approx. 45 g L^{-1} potato starch (Carl Roth, Karlsruhe, Germany) was added to the reactor. The temperature was set to 60 °C, the stirrer speed (N_{Stirr}) to 300 rpm, and the pH was controlled at 4.15 using 20% w/v HCl and 20% w/v KOH. After the temperature in the reactor was achieved, the enzymes Termamyl SC (Novozymes, Bagsværd, Denmark) and Spirizyme Ultra (Novozymes, Bagsværd, Denmark) were added to the reactor. Every 5-15 min, 15 mL of sample was drawn from the reactor. Before the sample could be taken, 15 mL of dead sample volume was discarded. To analyse the starch concentration (Section 3.1.3), 360 µL of each sample was mixed with 2.4 mL 5 M HCl and heated for 5 min at 80 °C in a heating block (VWR, Darmstadt, Germany) to stop the reaction in the sample. The remaining samples were put on ice until they were used to determine the glucose concentration (Section 3.1.4).

3.1.3 Determination of starch concentration

The starch concentration of the samples was determined using the potassium iodide method (Illanes, 2008). In the first step, a potassium iodide solution was prepared, containing 20 g L^{-1} potassium iodide (Carl Roth, Karlsruhe, Germany) and 2 g L^{-1} iodine (Riedel-de Haën, Honeywell, Seelze, Germany), dissolved in H_2O. 50 µL of the potassium iodide solution was added to each mixture of sample and HCl (690 µL). After that, the

absorbance of each sample was measured in a UV-visible spectrophotometer (UVmini-1240, Shimadzu Europa GmbH, Duisburg, Germany) at a wavelength of 623 nm.

A calibration curve (Figure 11) was generated to calculate the starch concentration in the samples, using standards with a defined amount of potato starch (Carl Roth, Karlsruhe, Germany).

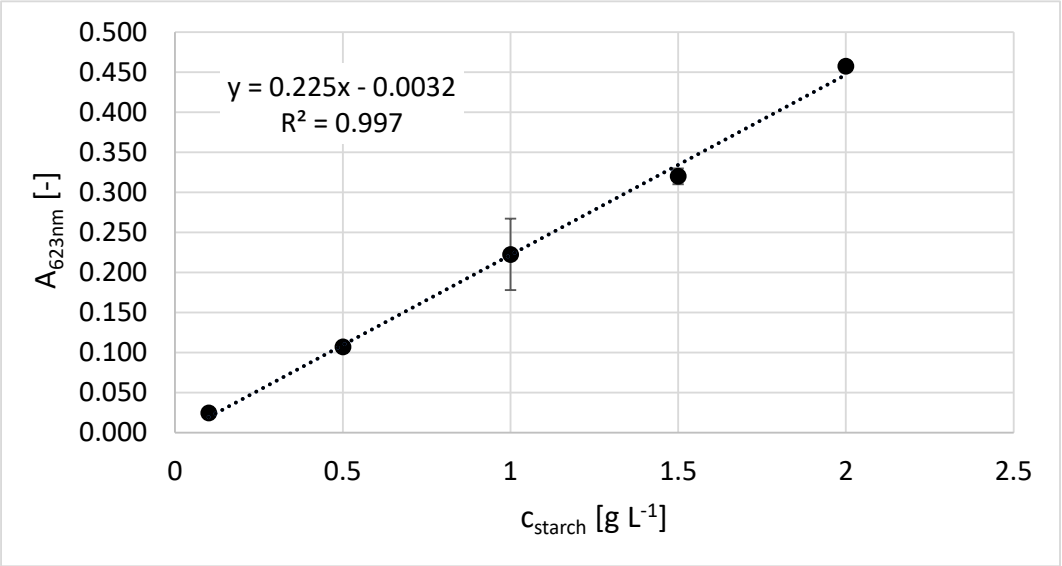

Figure 11: Calibration curve for determining the starch concentration using potato starch standards, with R^2 = 0.997. Error bars represent the mean value ± of one standard deviation resulting from a triple determination.

The starch concentration was calculated using the equation resulting from the calibration curve and the dilution factor (Equation 6).

$$c_{Starch}\ in\ g\ L^{-1} = \left(\frac{A_{623nm}}{0.225} - 0.0032\right) \cdot Dilution \qquad (6)$$

A sample containing 0.5 g L^{-1} potato starch (Carl Roth, Karlsruhe, Germany) was prepared and determined in triplicate for method validation. The method determined a starch concentration of 0.494 ± 0.033 g L^{-1}.

3.1.4 Determination of glucose concentration

The glucose concentration was determined using an enzymatic assay for D-glucose in foodstuff and other sample materials (Enzytec™ Liquid D-Glucose, R-Biopharm AG, Darmstadt, Germany) (R-Biopharm AG, 2022).

A sample containing 0.5 g L^{-1} glucose (Carl Roth, Karlsruhe, Germany) was prepared and determined in triplicate for method validation. The method determined a glucose concentration of 0.503 ± 0.004 g L^{-1}.

3.1.5 Determination of intermediate product concentration

The concentration of the intermediate products (*IP*) was calculated based on the measured starch (substrate, *S*) and glucose (product, *P*) concentrations (Equation 7).

$$IP_{Sample} = S_{t=0\ min} - S_{Sample} - P_{Sample} \quad (7)$$

The remaining starch concentration in the sample (S_{Sample}) and the glucose concentration (P_{Sample}) formed were subtracted from the starch concentration at the beginning of the experiment ($S_{t = 0\ min}$).

3.2 Enzymatic proteolysis using peptidases

Small-scale experiments were carried out in 2 mL test tubes to characterise the enzymes used in the proteolysis process. The influence of temperature, pH and pressure on the activity of the enzymes was investigated. In addition, proteolysis batch experiments were performed in a 6 L STR for model parameterisation and validation of the optimised process design.

The enzyme preparations EnerZyme P7 (Erbslöh, Geisenheim, Germany) and Flavourzyme (Novozymes, Bagsværd, Denmark) were used for proteolysis.

EnerZyme P7 is a concentrated liquid enzyme preparation containing a metalloendopeptidase (EC 3.4.24.4) from *Bacillus subtilis* for protein degradation in vegetable raw materials (ERBSLÖH Geisenheim GmbH). The activity range of the enzyme is between pH 5.0 and 10.0, with the optimum at pH 7.0 (ERBSLÖH Geisenheim GmbH). The temperature range is between 25-70 °C, with the optimum at 55 °C (ERBSLÖH Geisenheim GmbH).

Flavourzyme is a fungal peptidase complex produced by submerged fermentation of a selected strain of *Aspergillus oryzae,* which has not been genetically modified. It contains endopeptidase and exopeptidase activities (Merz et al., 2015; Novozymes, 2002).

The optimal pH for the enzyme complex ranges from 5.0 to 7.0. The optimal temperature for the enzyme complex is around 50 °C (Novozymes, 2002).

3.2.1 Investigation of the temperature and pH-dependent activity of peptidases

1 mL buffer (pH 4 using phosphate citrate buffer, pH 5.0, 5.5, 6.0, 6.5, 7.0, 7.5 and 8.0 using phosphate buffer, pH 9.0 and 9.5 using Tris-HCl buffer) with 2 g L^{-1} casein powder (Carl Roth, Karlsruhe, Germany), 0.2 mg L^{-1} EnerZyme P7 (Erbslöh, Geisenheim, Germany) or 0.2 mg L^{-1} Flavourzyme (Novozymes, Bagsværd, Denmark) was added to a 2 mL test tube (VWR, Darmstadt, Germany), mixed and placed in a water bath (T = 25, 30, 35, 40, 45, 50, 55, 60, 65 ad 70 °C). After a reaction time of 30 min, 0.1 mL of sample was drawn, and the reaction was stopped by heating the sample for 5 min at 95 °C in a heating block (VWR, Darmstadt, Germany). The samples were then analysed for the concentration of free amino acids (Section 3.2.3).

To investigate the pH dependency, the temperature was set to 50 °C, and the pH value was varied from 4.0 to 9.5. To investigate the temperature dependency, the pH was set to 7.0, and the temperature was varied from 25-70 °C.

The samples were analysed for their concentration of free amino acids (Section 3.2.3). The measured free amino acid concentrations were finally standardised. A value of 1.0 was set for the highest measured concentration of free amino acids. The other results were scaled to the maximum result.

3.2.2 Proteolysis batch experiments in a stirred tank reactor

The batch proteolysis experiments were performed in a 6 L STR (BioFlo 3000, New Brunswick Scientific, Eppendorf, Hamburg, Germany) (Figure 12).

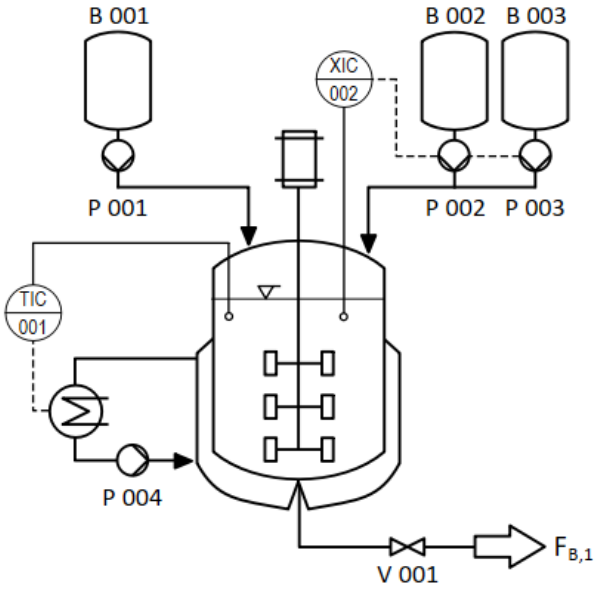

Label	Description
B 001	E2 (Flavourzyme)
B 002	Acid – 20% w/v HCl
B 003	Base – 20% w/v KOH
TIC 001	Temperature control
XIC 002	pH control

Figure 12: Batch enzymatic proteolysis in a 6 L STR (BioFlo 3000, New Brunswick Scientific, Eppendorf, Hamburg, Germany).

3 L phosphate buffer (pH = 7.5), with 30-50 g L^{-1} organic sunflower seed meal (All Organic Treasures, Wiggensbach, Germany), was added to the STR. The temperature was set to 50 °C, N_{Stirr} to 300 rpm, and the pH was controlled at 7.5 using 20% w/v HCl and 20% w/v KOH. Flavourzyme (Novozymes, Bagsværd, Denmark) was added to the reactor at a defined processing time. Every 5-15 min, 15 mL of sample was drawn from the reactor. Before the sample could be taken, 15 mL of dead sample volume was discarded. The reaction in the sample was stopped by heating 1 mL of the sample for 5 min at 95 °C in a heating block (VWR, Darmstadt, Germany). The samples were then analysed for the concentration of free amino acids (Section 3.2.3).

3.2.3 Determination of the free amino acid concentration

The free amino acid concentration was determined using the ninhydrin method (Anantharaman et al., 2017; Chutipongtanate et al., 2012; Kaspar et al., 2009).

For the preparation of the ninhydrin solution, two solutions were prepared and mixed in a ratio of 1:1. For the preparation of the first solution, 1.6 g L^{-1} tin chloride dihydrate (Carl Roth, Karlsruhe, Germany) was dissolved in citrate-phosphate buffer (pH = 5.2). To prepare the second solution, 40 g L^{-1} ninhydrin (Carl Roth, Karlsruhe, Germany) was dissolved in ethylene glycol (Carl Roth, Karlsruhe, Germany).

Then, 1 mL of the ninhydrin solution was added to 100 µL of the sample and incubated at 80 °C for 20 min in a water bath (WBT 12, Carl Roth, Karlsruhe, Germany). After that, 5 mL of isopropyl alcohol (Carl Roth, Karlsruhe, Germany) was added, and the absorbance of the mixture was measured in a UV-visible spectrophotometer (UVmini-1240, Shimadzu Europa GmbH, Duisburg, Germany) at a wavelength of 570 nm.

A calibration curve was determined (Figure 13) to calculate the concentration of free amino acids in the samples, using standards with a defined amount of L-glutamic acid (Honeywell Fluka, Morristown, New Jersey, USA).

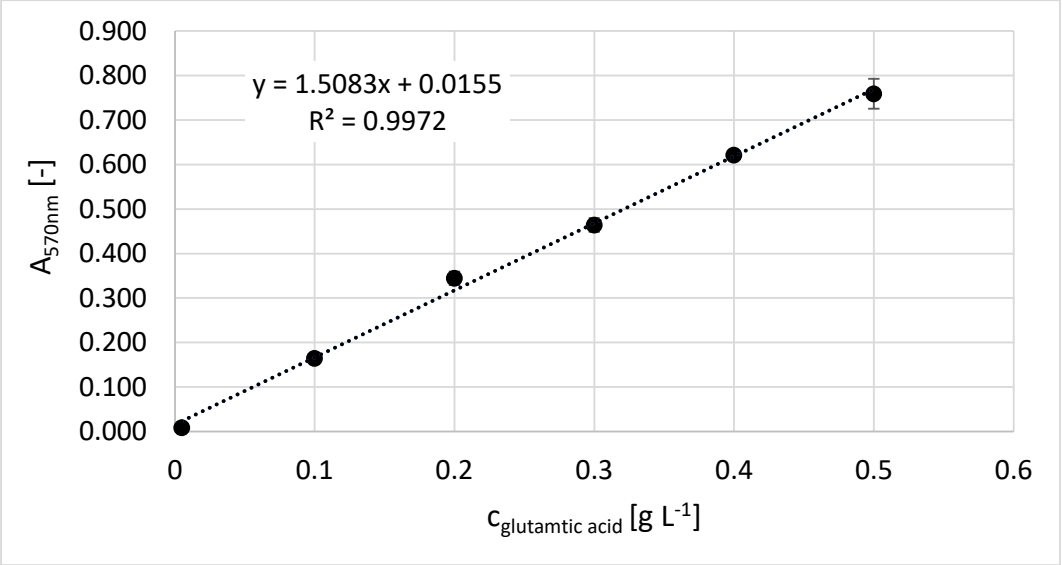

Figure 13: Calibration curve for determining the free amino acid concentration using L-glutamic acid standards, with R^2 = 0.9972. Error bars represent the mean value ± of one standard deviation resulting from a triple determination.

To calculate the total free amino acid concentration from the concentration of L-glutamic acid, the composition of amino acids in sunflower seed meal with 33.53% crude protein (Villamide and San Juan, 1998) was considered (Table 4).

Table 4: Amino acid composition of sunflower seed meal with 33.53% crude protein (Villamide and San Juan, 1998).

Amino acid	**Amount in 33.53% crude protein [%]**	**Molar mass [g mol^{-1}]**	**Share of molar mass in 33.53% crude protein [g mol^{-1}]**
Lysine	1.21	146.19	5.28
Methionine	0.76	149.21	3.38
Cystine	0.56	240.30	4.01
Methionine + cystine	1.32	194.76	7.67
Threonine	1.43	119.12	5.08
Isoleucine	1.36	131.17	5.32
Leucine	2.36	131.17	9.23
Valine	1.71	117.15	5.97
Histidine	0.85	155.15	3.93
Arginine	2.92	174.20	15.17
Glycine	2.11	75.07	4.72
Serine	1.57	105.09	4.92
Phenylalanine	1.65	165.19	8.13
Alanine	1.53	89.09	4.07
Tyrosine	0.86	181.19	4.65
Aspartic acid	3.29	133.10	13.06
Glutamic acid	6.60	147.13	28.96
Proline	1.44	115.13	4.94
Total	**33.53**	**2569.41**	**138.40**

The amino acids in sunflower seed meal with 33.53% crude protein have a combined molar mass of 138.40 g L^{-1}. Divided by the molar mass of L-glutamic acid (M = 147,13 g mol^{-1}), a value of 0.94 is obtained. The values resulting from the calibration curve are multiplied by 0.94 and the dilution factor to calculate the concentration of free amino acids (Equation 8).

$$c_{free\ amino\ acids}\ in\ g\ L^{-1} = \left(\frac{A_{570nm}}{1.5083} - 0.0155\right) \cdot Dilution \cdot 0.94 \qquad (8)$$

For method validation, a sample containing 0.300 g L^{-1} L-glutamic acid (Honeywell Fluka, Morristown, New Jersey, USA) was prepared and determined in triplicate. The method determined an L-glutamic acid concentration of 0.310 ± 0.015 g L^{-1}.

3.3 High-pressure treatment of hydrolytic enzymes

In the first step, the enzyme solutions were diluted with buffer and cooled to a temperature of approx. 10 °C. Then, the enzyme solutions were added to the reservoir of the high-pressure homogeniser (HPH 2000/4-SH5, IKA®-Werke GmbH & CO. KG, Staufen, Germany) (Figure 14).

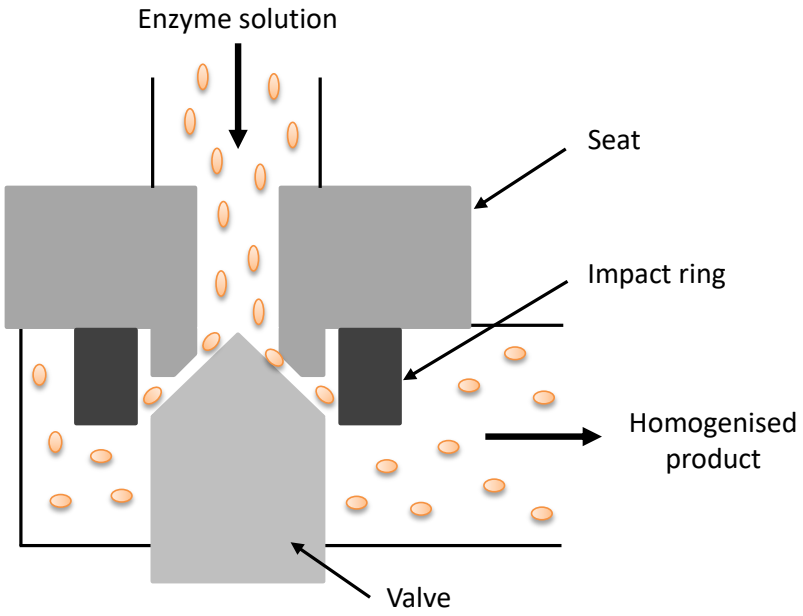

Figure 14: Treatment of enzyme solutions in a high-pressure homogeniser.

The flow rate of the high-pressure homogeniser was set to 3 L h^{-1}. The desired pressure (500, 1000, 1500 and 2000 bar) was set via a hand valve. Once the desired pressure was reached, 30 mL of the sample was drawn and put on ice.

Subsequently, the enzyme activity was determined and compared with the activity of the native untreated (native) enzyme solution.

3.3.1 High-pressure treatment of amylases

The influence of high pressure on the activity of the enzyme preparations Termamyl SC (Novozymes, Bagsværd, Denmark) and Spirizyme Ultra (Novozymes, Bagsværd, Denmark) was investigated. The enzyme preparations were diluted 1:1000 using phosphate-citrate buffer (pH = 5.0) and were then treated in a high-pressure homogeniser at 500, 1000, 1500 and 2000 bar.

To determine the enzyme activity after high-pressure treatment, 40 mL phosphate citrate buffer (pH = 5.0) containing 20 g L^{-1} potato starch (Carl Roth, Karlsruhe, Germany)

was added to a 50 mL test tube. Then 0.25 mL of 1:1000 diluted Termamyl SC (native or pressure treated at 500, 1000, 1500 and 2000 bar) or 1.0 mL of 1:1000 diluted Spirizyme Ultra (native or pressure treated at 500, 1000, 1500 and 2000 bar) was added. After adding the enzymes, the test tubes were placed in a water bath (T = 40, 60, 80 °C).

After 20 min, 0.36 mL of the sample was drawn from the test tubes with Termamyl SC, and the reaction in the sample was stopped by adding 2.40 mL of 5 M HCl and heating the sample for 5 min at 80 °C in a heating block (VWR). The samples were analysed for their starch concentration (Section 3.1.3). The concentration of converted starch was then determined based on the initial starch concentration (20 g L^{-1}). The converted starch concentration corresponds to the intermediate product's concentration (oligosaccharides).

From the test tubes where Spirizyme Ultra was used, 2 ml of sample were drawn after a processing time of 20 min and placed on ice. The samples were analysed for their glucose concentration (Section 3.1.4).

3.3.2 High-pressure treatment of peptidases

The influence of high-pressure treatment on the activity of the enzyme preparations EnerZyme P7 (Erbslöh, Geisenheim, Germany) and Flavourzyme (Novozymes, Bagsværd, Denmark) was investigated. The enzyme preparations were diluted 1:1000 using phosphate buffer (pH = 7.5) and were then treated in a high-pressure homogeniser at 500, 1000, 1500 and 2000 bar.

To determine the enzyme activity after high-pressure treatment, 0.8 mL phosphate buffer (pH = 7.5) containing 2.5 g L^{-1} casein (Carl Roth, Karlsruhe, Germany) was added to a 2 mL test tube. Then 0.2 mL of 1:1000 diluted EnerZyme P7 (native or pressure treated at 500, 1000, 1500 and 2000 bar) or 0.2 mL of 1:1000 diluted Flavourzyme (native or pressure treated at 500, 1000, 1500 and 2000 bar) was added. After adding the enzymes, the test tubes were placed in a water bath (T = 25, 50, 70 °C).

After a reaction time of 30 min, 0.1 mL of sample was drawn, and the reaction was stopped by heating the sample for 5 min at 95 °C in a heating block (VWR, Darmstadt, Germany). The samples were then analysed for the concentration of free amino acids (Section 3.2.3).

3.4 Modelling and simulation of enzymatic hydrolysis processes

The model for enzymatic hydrolysis processes was written using the software C-eStIM-2015 (Hass et al., 2005a; Kuhnen, 2008). The software includes different algorithms for solving ODE systems and identifying parameters (Witte et al., 1996). Parameters, initial values and time-dependently changing state variables (profiles) are provided in text files (control- and profile data file: *.xct, *.cfg). The calculation results are also provided in text files (simulation value: *.sim). The readily programmed submodel of a process (*.cpp) is then translated with a suitable compiler into an executable file (*.exe). At the call of the executable file, all initial values, parameters, profiles and the set-up of the solver are read from the parameter file. The calculation occurs with a static or dynamic step size depending on the solving algorithm. The executable program can be used to test and validate the described model. From the executable file, also so-called Dynamic Link Libraries (DLLs) can be created. These DLLs can be implemented into process control and simulation software like WinErs (Ingenieurbüro Dr.-Ing. Schoop GmbH, 2018).

The software R (R Core Team, 2014) was used to parameterise the developed model. R is a programming language for statistical computing and graphics supported by the R Core Team and the R Foundation for Statistical Computing (Giorgi et al., 2022). Users have created packages to augment the functions of the R language. In addition, R offers special Nelder-Mead packages.

Apart from C-eStIM and R, the software summarised in Table 5 was used.

Table 5: Software tools used for the development of control strategies and the process design of enzymatic hydrolysis processes.

Software	Version	Developer
C-eStIM-2015	2015	Florian Kuhnen, City University of Applied Sciences, Bremen, Germany
Gnuplot	5.2.6	Thomas Williams, Colin Kelley
Notepad++	8.5	Notepad++ Team
R	4.2.2	R Core Team and the R Foundation for Statistical Computing
RStudio	2022.07.1	RStudio
Visual Studio	2017 Community	Microsoft
Windows	10	Microsoft
WinErs Professional	7.4.C	Ingenieurbüro Dr.-Ing. Schoop GmbH, Hamburg, Germany
WinErs Simulation	7.6.D	Ingenieurbüro Dr.-Ing. Schoop GmbH, Hamburg, Germany

3.4.1 General modelling approach

The dynamic mechanistic mathematical model for the enzymatic hydrolysis processes was developed, applying the modelling cycle (Moser et al., 2020) shown in Figure 15.

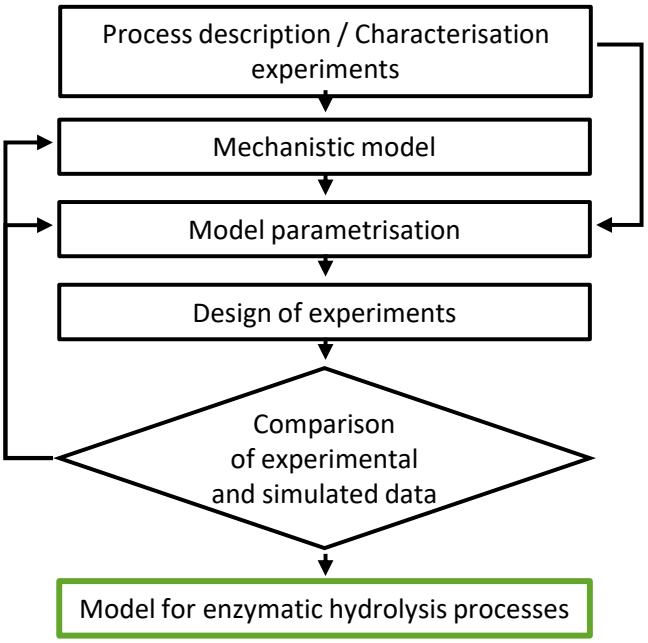

Figure 15: Structure of the modelling cycle.

In the first step, a dynamic mechanistic mathematical model representing the kinetics of the enzymatic hydrolysis processes (combined starch hydrolysis and proteolysis) derived from appropriate process descriptions and the knowledge gained from the small-scale characterisation experiments was developed.

In the next step, the model parameterisation was carried out based on the results from the characterisation experiments.

Then, experiments in an STR were planned with the first model version. After the experiments were carried out, the data simulated by the model and the experimental data were compared, and, if necessary, the model parameterisation was adjusted again.

3.4.2 Model parameterisation

The parameterisation of the C-eStIM model for enzymatic hydrolysis processes was realised using parts of the R (V4.2.2) version of the "mDoE-toolbox" (Moser et al., 2021). Therefore, the R packages "lme4", "ggplot2", "ggthemes", "nloptr", "RColorBrewer", "reshape2", "pracma", "truncnorm", "zoo", and "R.matlab" were needed.
The first step defines the number of experiments with associated experimental results. Then the C-eStIM model, with associated configuration files, is specified. Subsequently, the parameters to be adjusted are defined with lower and upper bounds. Afterwards, the simulated variables (e.g., substrate or product concentration) are specified, whose curves will be fitted to the experimental data. Finally, the maximum steps of the Nelder-Mead algorithm and the stop tolerance are set.

For parameterisation, the model parameters were adapted by minimizing the weighted root-mean-square deviation (*wRMSD*) between the simulated and the experimental values (Equation 9) using the Nelder-Mead algorithm (Brüning et al., 2017; Möller et al., 2020; Moser et al., 2021; Nelder and Mead, 1965).

$$wRMSD = \sqrt{\sum_{i=1}^{n} \frac{\left(y_{s,i} - y_{m,i}\right)^2}{n} \cdot k_{weighting}} \tag{9}$$

The *wRMSD* was calculated from the squared difference between the measured value y_m and the simulated value y_s, divided by the number of data points n in the data set and multiplied by a factor for weighting individual data points $k_{weighting}$.

To determine the accuracy of the fit after parameterisation, the coefficient of determination (R^2) was calculated by dividing the difference between experimental y_i and simulated data $y_{s,i}$ with the difference between the experimental data and their mean value $\bar{y}$ (Möller et al., 2019; Möller et al., 2020; Moser et al., 2021).

$$R^2 = 1 - \frac{\sum_{i=1}^{n}\left(y_i - y_{s,i}\right)^2}{\sum_{i=1}^{n}(y_i - \bar{y})^2} \tag{10}$$

In this research, an R^2 greater than 0.9 was considered a sufficiently accurate fit.

3.5 Development of the digital twin for enzymatic hydrolysis processes

For the development of a digital twin for enzymatic hydrolysis processes in an STR, the new mechanistic mathematical model of the enzymatic hydrolysis processes was implemented into an existing stand-alone digital twin of a 20 L STR developed by the working group of Prof. Dr. Volker C. Hass at Furtwangen University (Appl et al., 2021; Gerlach et al., 2013; Gerlach et al., 2015; Hass et al., 2005a, 2005b; Hass, 2005; Hass et al., 2012; Hass, 2016; Hirschmann et al., 2018; Hirschmann, 2021; Isimite et al., 2018). This stand-alone digital twin has been shown to simulate the cultivation of *S. cerevisiae*, the production of ethanol by *S. cerevisiae* and the whole-cell biocatalysis of ethyl-3-hydroxybutyrate (E3HB) from the substrate ethyl acetoacetate in a 20 L STR under aerobic and anaerobic conditions. The stand-alone digital twin consists of four submodels representing the biological and physical-chemical processes in the reactor and the interactions with associated equipment (plant and periphery). The submodels were written in the C++-based modelling and simulation environment C-eStIM (Hass et al., 2005a; Kuhnen, 2008). The C++ models were implemented in the modular process control, simulation and automation system WinErs (Ingenieurbüro Dr.-Ing. Schoop GmbH, 2018) using C-eStIM-DLL interfaces. In addition, the stand-alone digital twin is equipped with a control and automation submodel and a GUI, which were created directly in WinErs (Ingenieurbüro Dr.-Ing. Schoop GmbH, 2018).

3.6 Development of control and process design strategies

Using WinErs (Ingenieurbüro Dr.-Ing. Schoop GmbH, 2018), standard and multivariable controllers were implemented to the stand-alone digital twin for enzymatic hydrolysis processes in an STR.

Using R and the C-eStIM model for the enzymatic hydrolysis processes, a process design strategy according to the OLFO principle, as well as a script for the execution of a mDoE, was realised.

3.6.1 Standard and multivariable control

In the modular process control, simulation and automation system WinErs (Ingenieurbüro Dr.-Ing. Schoop GmbH, 2018), the realisation of control strategies is carried out using graphical block structures and functional plans. WinErs contains an extensive library with analogue and binary blocks (e.g., P, PI, PID, switches, relays). These blocks can be combined arbitrarily with each other or with other control algorithms.
Further automation functions are sequence control with functional plans (grafcet, batch-recipes), fuzzy-controllers with a graphical development environment, interface for own programmed algorithms (DLL-block) and user-defined blocks for differential equations, a function generator and a program generator.

The simulation modus in WinErs allows testing and optimising the implemented control strategies.

3.6.2 Open-loop-feedback-optimal strategy

The OLFO strategy was realised in R (V4.2.2), using parts of the “mDoE-toolbox” (Moser et al., 2021). The R-packages “lme4”, “ggplot2”, “ggthemes”, “nloptr”, “RColorBrewer”, “reshape2”, “truncnorm”, and “zoo” were needed.

Parameterisation part:

The parameterisation part corresponds to the R script described in Section 3.4.2.

Optimisation part:

The first step selects the C-eStIM model with corresponding configuration files (list of parameters, control files) used for optimisation. Then, the starting and end time of the

experiments is set. In addition, the optimisation variables (e.g., feed rates, temperature) with their lower and upper bound are chosen. Different profiles, such as constant or linear increasing, can be selected for the feed rates. Furthermore, it is determined at which time of the experiment the variables should take effect. After that, the Nelder-Mead algorithm used for the optimisation is configured. Therefore, the maximum steps and the stop tolerance are defined. Finally, the optimisation criterion (e.g., product concentration or cost function) is determined. The optimisation criterion can be minimised or maximised.

3.6.3 Model-based design of experiments

In this work, parts of the software tool “mDoE-toolbox” implemented in R (V4.2.2) were used, which makes the mDoE concept applicable to bioprocesses (Moser et al., 2021). Therefore, the R packages “lme4”, “ggplot2”, “ggthemes”, “nloptr”, “RColorBrewer”, “readxl”, “lhs”, “reshape2”, “pracma”, “plotly”, “truncnorm”, “zoo”, “rsm”, “R.matlab”, “matrixStats”, “openxlsx” and “corrplot” were needed.

The first step selects the C-eStIM model with corresponding configuration files (list of parameters, control files). Then, the DoE design space is set up with the number of different factors (e.g., feed rates) and the number of points in the experimental design. After that, the lower and upper bound of the DoE factors is defined. Different profiles, such as constant or linear increasing, can be selected for the feed rates. Furthermore, it is determined at which time of the experiment the variables should take effect. Finally, the DoE response (e.g., product concentration or cost function) is specified.

4 Model for enzymatic hydrolysis processes

In this section, a brief process description for enzymatic starch hydrolysis and proteolysis is given, and it is shown how the model equations were derived from this. In addition, data from experimental studies concerning the reaction rate dependency on temperature and pH values are shown. Furthermore, it is shown how treatment in a high-pressure homogenisation influences the activity of the enzymes used for the enzymatic hydrolysis processes. Finally, the results of experiments on enzymatic hydrolysis in an STR are presented, which were used for the parameterisation of the model.

4.1 Process description and model equations

The equations implemented in the model for the combined enzymatic starch hydrolysis and proteolysis have a similar structure and are indicated by suffixes *P1* (starch hydrolysis) and *P2* (proteolysis). For simplicity, the general equations are presented below without the suffixes. All model variables with their lower and upper bounds and parameters with their values can be found in Appendix B.

The structure of the model for enzymatic hydrolysis processes can be seen in Figure 16.

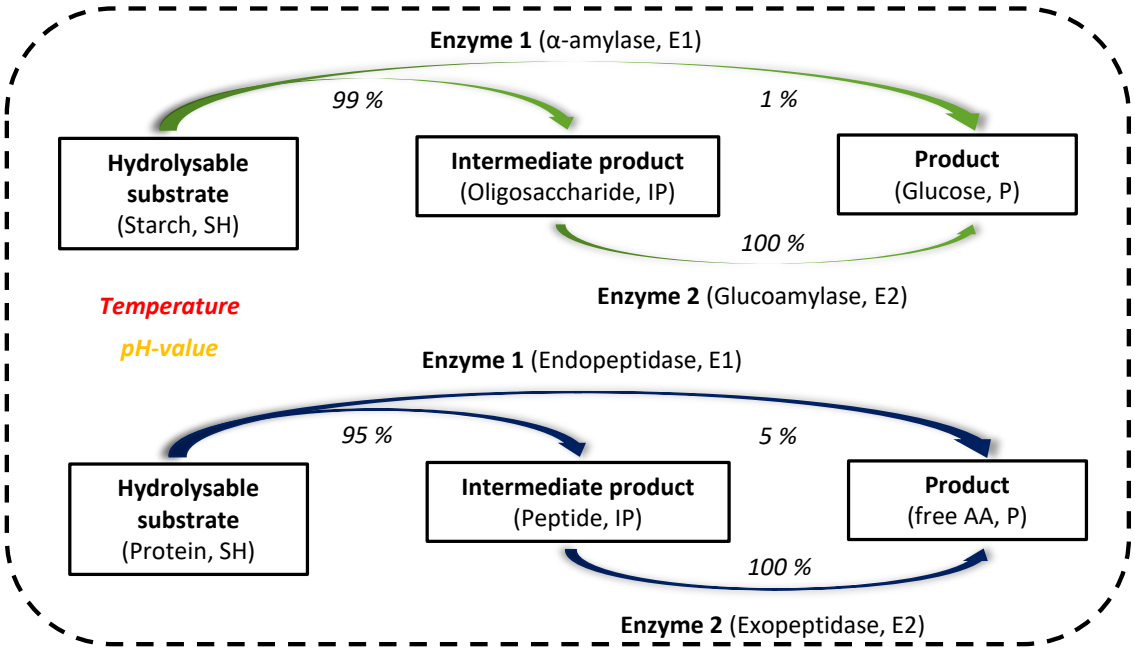

Figure 16: Structure of the model for enzymatic hydrolysis processes.

It is assumed that the substrates (*S*) for starch hydrolysis and proteolysis are composed of hydrolysable (*SH*) and non-hydrolysable components (*SN*). Therefore, the ratio must

be set via parameterisation before the simulation experiment depending on the type of substrate used.

During starch hydrolysis, 99% of the hydrolysable components of the starch (*SH*) are converted by α-amylase (*E1*) into oligosaccharides (*IP*) and 1% directly into glucose (*P*) (Buckow et al., 2005; Buckow et al., 2007; Nebesny, 1989). The oligosaccharides formed are then converted by glucoamylase (*E2*) to 100% glucose (*P*).

During proteolysis, 95% of the hydrolysable components of the protein (*SH*) are converted by endopeptidase (*E1*) into peptides (*IP*) and 5% directly into free amino acids (*P*) (Rao et al., 1998). The peptides (*IP*) formed are then converted by exopeptidase (*E2*) to 100% into free amino acids (*P*).

The reaction rates (*r*) can be calculated using Michaelis-Menten kinetics, with maximal reaction rates (r_{max}), Michaelis-Menten constants (K_M) and the concentration of the hydrolysable components of the starch (SH_1) (Equation 11).

$$r = \frac{r_{max} \cdot SH_1}{K_M + SH_1} \tag{11}$$

Michaelis-Menten kinetics were chosen because they have already been successfully applied by other research groups to model the enzymatic hydrolysis processes (Beaubier et al., 2021; Beschkov et al., 1984; Kusunoki et al., 1982; Lee et al., 1992). In addition, the relatively simple structure of the kinetics offers rapid adaptability, which supports the generic approach of the model.

For the degradation of the substrate through enzyme 1 (*E1*) and the degradation of the intermediate product through enzyme 2 (*E2*), Michaelis-Menten kinetics were implemented in the model (Equations 12 and 13).

$$r_{SIP,E1} = \frac{r_{max,SIP,E1} \cdot (f_{T,act,E1} \cdot f_{pH,act,E1}) \cdot SH_1}{K_{M,SIP,E1} + SH_1} \tag{12}$$

$$r_{IPP,E2} = \frac{r_{max,IPP,E2} \cdot (f_{T,act,E2} \cdot f_{pH,act,E2}) \cdot IP_1}{K_{M,IPP,E2} + IP_1} \tag{13}$$

The substrate to intermediate product degradation rate ($r_{SIP,E1}$) is the quotient of the maximum degradation rate ($r_{max,SIP,E1}$) multiplied by factors for the dependence on temperature ($f_{T,act,E1}$) and pH value ($f_{pH,act,E1}$) and the concentration of hydrolysable components of the substrate (SH_1) divided by the sum of the half-saturation constant ($K_{M,SIP,E1}$) and the concentration of hydrolysable components of the substrate (SH_1).

The reaction rate for intermediate product to product degradation ($r_{IPP,E2}$) is the quotient of the maximum degradation rate ($r_{max,IPP,E2}$) multiplied by factors for the dependence on temperature ($f_{T,act,E2}$) and pH value ($f_{pH,act,E2}$) and the concentration of intermediate product (IP_1) divided by the sum of the half-saturation constant ($K_{M,IPP,E2}$) and the concentration of the intermediate product (IP_1).

The rates for the build-up of intermediate product ($r_{IPS,E1}$) and product($r_{PS,E1}$) from substrate, as well as for the build-up of product from intermediate product ($r_{PIP,E2}$), are obtained by multiplying the degradation rates (Equations 12 and 13) by yield coefficients ($Y_{IPS,E1}$, $Y_{PIP,E2}$) (Equations 14-16).

$$r_{IPS,E1} = Y_{IPS,E1} \cdot r_{SIP,E1} \tag{14}$$

$$r_{PS,E1} = (1 - Y_{IPS,E1}) \cdot r_{SIP,E1} \tag{15}$$

$$r_{PIP,E2} = Y_{PIP,E2} \cdot r_{IPP,E2} \tag{16}$$

The yield coefficients ($Y_{IPS,E1}$, $Y_{PIP,E2}$) used in the model were based on assumptions derived from literature data (Buckow et al., 2005; Buckow et al., 2007; Nebesny, 1989; Rao et al., 1998).

The denaturation rates of the enzymes are calculated using Equations 17 and 18.

$$r_{den,E1} = r_{max,den,E1} \cdot f_{T,sta,E1} \cdot f_{pH,sta,E1} \tag{17}$$

$$r_{den,E2} = r_{max,den,E2} \cdot f_{T,sta,E2} \cdot f_{pH,sta,E2} \tag{18}$$

Therefore, the maximal denaturation rates $r_{max,den,E1}$ *and* $r_{max,den,E2}$ are multiplied by factors for the temperature ($f_{T,sta,E1}$, $f_{T,sta,E2}$) and pH ($f_{T,sta,E1}$, $f_{T,sta,E2}$) dependency on the stability of the enzymes.

Furthermore, a simplified model of an ideal STR was implemented into the model (Figure 17).

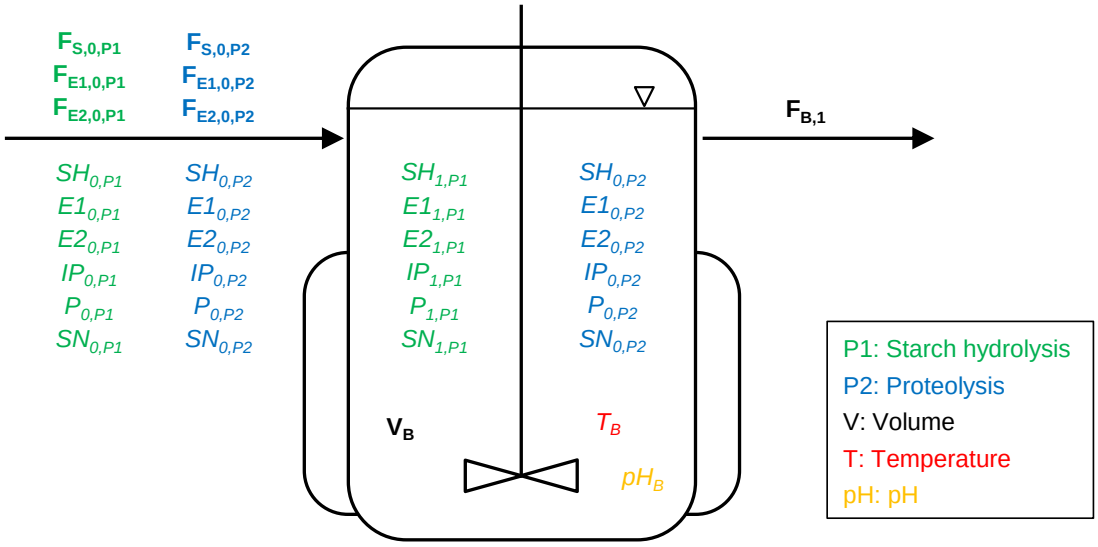

Figure 17: Simplified STR model of the model for enzymatic hydrolysis processes, with inflows, concentrations in the inflows, concentrations in the reactor and outflow of broth from the reactor ($F_{B,1}$).

Balance equations were introduced to map the concentration changes in the STR. The inflows to the reactor were summed up to F_{in} (Equation 19).

$$F_{in} = F_{S,0,P1} + F_{E1,0,P1} + F_{E2,0,P1} + F_{S,0,P2} + F_{E1,0,P2} + F_{E2,0,P2} \quad (19)$$

The differential equations in the model were created using the general dynamic mass balance (Equation 20).

$$accumulation = input - output + generation - consumption \quad (20)$$

The reactor model of the ideal STR consists of seven differential equations (Equations 21-27). The volume change (Equation 21) results from the difference between the inflow (F_{in}) and the outflow of broth ($F_{B,1}$).

$$\frac{dV_B}{dt} = F_{in} - F_{B,1} \quad (21)$$

The change in the concentration of hydrolysable components of the substrate results from the concentration of hydrolysable components (SH_0) in the inflow of substrate solution ($F_{S,0}$) minus a dilution term and the degradation by *E1* (Equation 22).

$$\frac{dSH_1}{dt} = \frac{F_{S,0} \cdot SH_0}{V_B} - \frac{SH_1 \cdot F_{in}}{V_B} - r_{SIP,E1} \cdot E1_1 \qquad (22)$$

The change in the concentration of the enzymes results from the concentration of the enzymes ($E1_0$, $E2_0$) in the inflows of enzyme solutions (F_{E1}, F_{E2}) minus a dilution term and the denaturation rates (Equations 23 and 24).

$$\frac{dE1_1}{dt} = (1 - f_{E2,F_{E1}}) \cdot \left(\frac{F_{E1,0} \cdot E1_0}{V_B}\right) + f_{E1,F_{E2}} \cdot \left(\frac{F_{E2,0} \cdot E2_0}{V_B}\right) - \frac{E1_1 \cdot F_{in}}{V_B} - r_{den,E1} \cdot E1_1 \qquad (23)$$

$$\frac{dE2_1}{dt} = (1 - f_{E1,F_{E2}}) \cdot \left(\frac{F_{E2,0} \cdot E2_0}{V_B}\right) + f_{E2,F_{E1}} \cdot \left(\frac{F_{E1,0} \cdot E1_0}{V_B}\right) - \frac{E2_1 \cdot F_{in}}{V_B} - r_{den,E2} \cdot E2_1 \qquad (24)$$

Since many enzyme preparations on the market contain both α- and glucoamylase as well as endo- and exopeptidases, factors ($f_{E2,FE1}$, $f_{E1,FE2}$) were introduced to determine the composition of *E1* and *E2* in the feeds.

The change in the concentration of the intermediate product results from the concentration of intermediate product (IP_0) in the inflow of substrate solution($F_{S,0}$) minus a dilution term and the degradation by *E2*, plus the formation through *E1* (Equation 25).

$$\frac{dIP_1}{dt} = \frac{F_{S,0} \cdot IP_0}{V_B} - \frac{IP_1 \cdot F_{in}}{V_B} + P_{IP} \cdot r_{IPS,E1} \cdot E1_1 - r_{IPP,E2} \cdot E2_1 \qquad (25)$$

The build-up rate of the intermediate product from substrate ($r_{IPS,E1}$) is multiplied by a proportionality factor (P_{IP}) which can represent the integration of water during hydrolysis.

The change in the concentration of the product results from the concentration of product (P_0) in the inflow of substrate solution ($F_{S,0}$) minus a dilution term, plus the formation by *E1* and *E2* (Equation 26).

$$\frac{dP_1}{dt} = \frac{F_{S,0} \cdot P_0}{V_B} - \frac{P_1 \cdot F_{in}}{V_B} + P_P \cdot r_{PIP,E2} \cdot E2_1 + r_{PS,E1} \cdot E1_1 \qquad (26)$$

The build-up rate of the intermediate product from substrate ($r_{PIP,E2}$) is multiplied by a proportionality factor (P_P), representing water integration during hydrolysis.

The change in the concentration of non-hydrolysable components of the substrate results from the concentration of non-hydrolysable components of substrate (SN_0) in the inflow of substrate solution ($F_{S,0}$) minus a dilution term (Equation 27).

$$\frac{dSN_1}{dt} = \frac{F_{S,0} \cdot SN_0}{V_B} - \frac{SN_1 \cdot F_{in}}{V_B} \tag{27}$$

In addition, the overall substrate concentration is given by Equation 28.

$$S_1 = SH_1 + SN_1 \tag{28}$$

The total substrate concentration (S_1) is the sum of the hydrolysable (SH_1) and non-hydrolysable components (SN_1) of the substrate.

4.2 Characterisation of the enzymes used for starch hydrolysis and proteolysis

The activity of the enzymes used for starch hydrolysis (Termamyl SC and Spirizyme Ultra) and proteolysis (EnerZyme P7 and Flavourzyme) was examined for its dependence on temperature, pH and high-pressure treatment up to 2000 bar.

All results of the experiments investigating the dependence of the enzyme activity on temperature and pH were normalised to values between 0 and 1 (Sections 3.1.1 and 3.2.1). A value of 1 corresponds to the temperature or pH value at which the highest product concentration was formed.

Furthermore, sigmoidal and double sigmoidal functions (Equation 29) (Brüning, 2016; Kuntzsch, 2014) were fitted manually to the experimental data. With an R^2 greater than 0.9, the fit was considered sufficiently good.

$$f_{Sig,DSig}(x) = \left(Y_{LS} + \frac{Y_{mid} - Y_{LS}}{1 + e^{-K_{LS} \cdot (x - r_{max,low})}}\right) \cdot \left(1 + \frac{\left(\frac{Y_{RS}}{Y_{mid}} - 1\right)}{1 + e^{-K_{RS} \cdot (x - r_{max,high})}}\right) \tag{29}$$

The value of a state variable is described by x. Y_{LS} is the value at low x, Y_{RS} is the value at high x, Y_{mid} is the value between $r_{max,low}$ and $r_{max,high}$, which are location parameters of

the low/high side of the function, K_{LS} determines the slope on the low side, and K_{RS} determines the slope on the high side of the function. By adjusting the parameters Y_{LS} and Y_{RS}, it is also possible to generate sigmoidal functions.

In the model, the factors ($f_{T,act,E1}$, $f_{T,act,E2}$, $f_{pH,act,E1}$, $f_{pH,act,E2}$) resulting from the sigmoidal and double sigmoidal functions for the temperature and pH-dependent enzyme activity are multiplied by the maximum reaction rates ($r_{max,SIP,E1}$, $r_{max,IPP,E2}$).

In addition, sigmoidal and double sigmoidal functions were implemented to describe the dependence of the enzyme stability on temperature and pH. In the model, the factors ($f_{T,sta,E1}$, $f_{T,sta,E2}$, $f_{pH,sta,E1}$, $f_{pH,sta,E2}$) resulting from the sigmoidal and double sigmoidal functions for the enzyme stability are multiplied by the maximum denaturation rates ($r_{max,den,E1}$, $r_{max,den,E2}$). The parameterisation of the sigmoidal and double sigmoidal functions for enzyme stability is based on assumptions derived from literature data (Beaubier et al., 2021; Buckow et al., 2005; Buckow et al., 2007; ERBSLÖH Geisenheim GmbH; Nebesny, 1989; Novozymes, 2002; Novozymes A/S, 2004, 2010). The temperature and pH-dependent enzyme stability was implemented as preparation for developing a stand-alone digital twin of enzymatic hydrolysis processes in a PBR. The processing time of enzymatic hydrolysis in a PBR is usually very long, and it is impossible to exchange the enzymes, which is why stability plays a significant role.

The complete set of parameters used to implement the sigmoidal and double sigmoidal functions in the model for enzymatic hydrolysis processes can be found in Appendix B.

4.2.1 Temperature and pH dependence of the starch hydrolysis enzymes

Figure 18 shows how temperature affects the activity of Termamyl SC (*E1, P1*) used in the starch hydrolysis process (*P1*). In addition, the sigmoidal functions representing the temperature-dependent activity and stability of the enzyme in the model are presented.

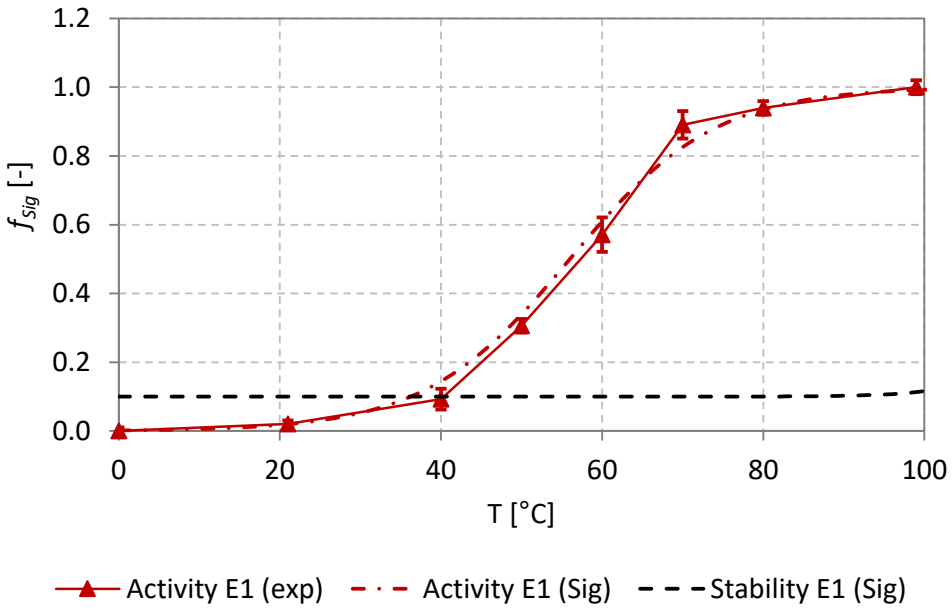

Figure 18: Experimentally (Activity E1 (exp)) determined temperature-dependent enzyme activity of Termamyl SC (E1), pH = 5.0, with fitted sigmoidal function for temperature-dependent enzyme activity (Activity E1 (Sig)), R^2 = 0.993 and assumed sigmoidal function for temperature-dependent enzyme stability (Stability E1 (Sig)). Error bars represent the mean value ± of one standard deviation resulting from a triple determination.

For Termamyl SC, almost no activity could be determined at temperatures below 20 °C. The activity of Termamyl SC increased at the highest rate between 40 and 70 °C. The maximal activity was reached at 100 °C. A temperature change from 100 to 50 °C leads to an approximate decrease in enzyme activity of 70% for Termamyl SC.

For Termamyl SC, the sigmoidal function for the temperature-dependent enzyme activity ($f_{T,act,E1,P1}$) could be fitted to the experimentally determined data with R^2 = 0.993.

From 0-90 °C, the sigmoidal function for the temperature-dependent enzyme stability of Termamyl SC ($f_{T,sta,E1,P1}$) remains at the minimum value of 0.1. Between 90-100 °C, a slight increase to a value of approx. 0.12 is indicated.

Figure 19 shows how temperature affects the activity of Spirizyme Ultra (*E2, P1*) used in the starch hydrolysis process (*P1*). Furthermore, the sigmoidal functions representing the temperature-dependent activity and stability of the enzyme in the model are presented.

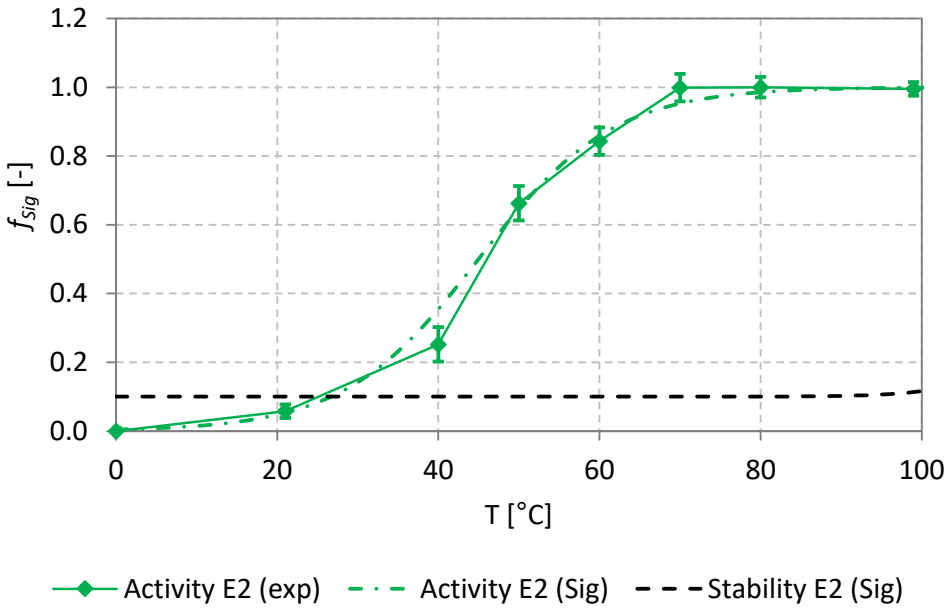

Figure 19: Experimentally (Activity E2 (exp)) determined temperature-dependent enzyme activity of Spirizyme Ultra (E2), pH = 5.0, with fitted sigmoidal function for temperature-dependent enzyme activity (Activity E2 (Sig)), R^2 = 0.990 and assumed sigmoidal function for temperature-dependent enzyme stability (Stability E2 (Sig). Error bars represent the mean value ± of one standard deviation resulting from a triple determination.

For Spirizyme Ultra, almost no activity could be determined at temperatures below 20 °C. The highest increase in activity for Spirizyme Ultra was found between 40 and 60 °C. The maximum activity was reached at 70 °C and above. A temperature change from 100 to 50 °C leads to an approximate decrease in enzyme activity of 35% for Spirizyme Ultra.

For Spirizyme Ultra, the sigmoidal function for the temperature-dependent enzyme activity ($f_{T,act,E2,P1}$) could be fitted to the experimentally determined data with R^2 = 0.990.

From 0-90 °C, the sigmoidal function for the temperature-dependent enzyme stability of Spirizyme Ultra ($f_{T,act,E2,P1}$) remains at the minimum value of 0.1. Between 90-100 °C, a slight increase to a value of approx. 0.12 is indicated.

Figure 20 shows how pH affects the Termamyl SC (E1) activity used in the starch hydrolysis process. Furthermore, double sigmoidal functions representing the pH-dependent activity and stability of the enzyme in the model are presented.

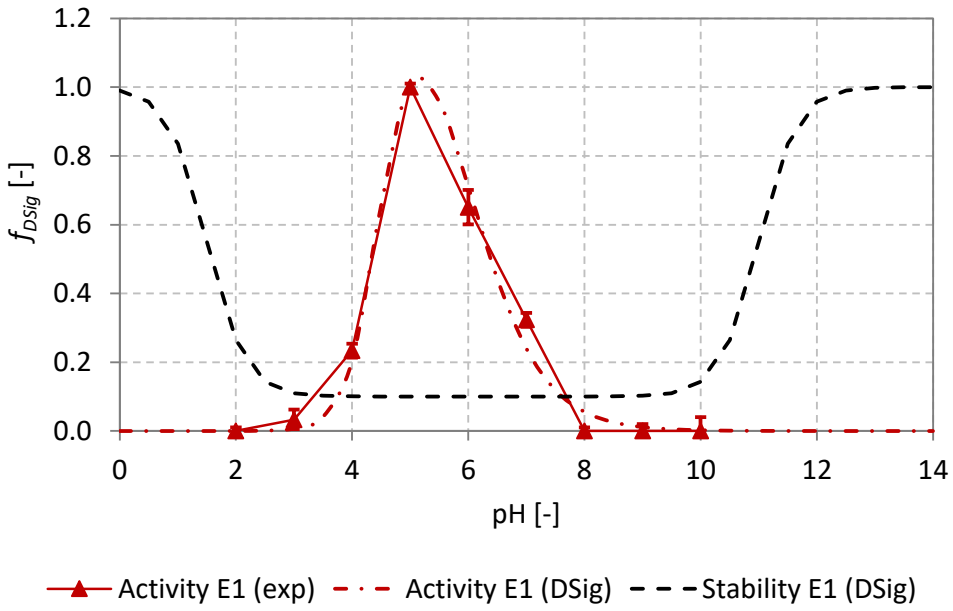

Figure 20: Experimentally (Activity E1 (exp)) determined pH-dependent enzyme activity of Termamyl SC (E1), T = 60°C, with fitted double sigmoidal function for pH-dependent enzyme activity (Activity E1 (DSig)), R^2 = 0.985 and assumed double sigmoidal function for pH-dependent enzyme stability (Stability E1 (DSig)). Error bars represent the mean value ± of one standard deviation resulting from a triple determination.

Termamyl SC shows almost no activity at pH values below 3 and above 8. The maximum activity was reached at a pH value of approx. 5.

The double sigmoidal function for the pH-dependent enzyme activity ($f_{pH,act,E1,P1}$) could be fitted to the experimentally determined data with R^2 = 0.985.

At a pH of 0, the double sigmoidal function for the pH-dependent enzyme stability of Termamyl SC ($f_{pH,sta,E1,P1}$) has a value of 1.0. At a pH of 3, $f_{pH,sta,E1,P1}$ drops to the minimum value of 0.1. At a pH of 9, $f_{pH,sta,E1,P1}$ rises to the maximum value of 1.0.

Figure 21 shows how pH affects the activity of Spirizyme Ultra (*E2*) used in the starch hydrolysis process. Furthermore, the double sigmoidal functions representing the pH-dependent activity and stability of the enzyme in the model are presented.

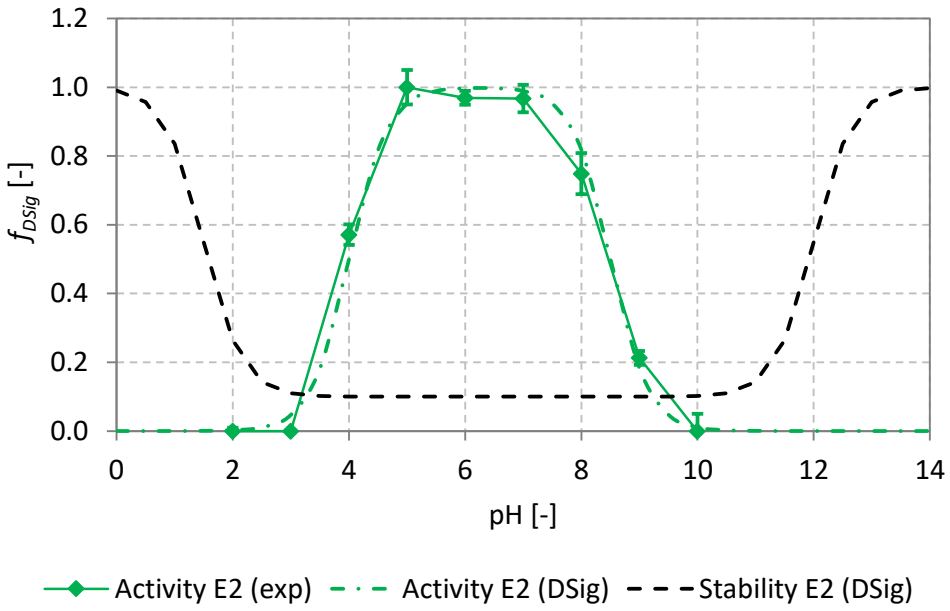

Figure 21: Experimentally (Activity E2 (exp)) determined pH-dependent enzyme activity of Spirizyme Ultra (E2), T = 60 °C, with fitted double sigmoidal function for pH-dependent enzyme activity (Activity E2 (DSig)), R^2 = 0.990 and assumed double sigmoidal function for pH-dependent enzyme stability (Stability E2 (DSig). Error bars represent the mean value ± of one standard deviation resulting from a triple determination.

For Spirizyme Ultra, almost no activity could be determined at pH values below 3 and above 10. The highest activity was found at pH values between 5 and 7.

The double sigmoidal function for the pH-dependent enzyme activity ($f_{pH,act,E2,P1}$) could be fitted to the experimentally determined data with R^2 = 0.990.

At a pH value of 0, the double sigmoidal function for the pH-dependent enzyme stability of Spirizyme Ultra ($f_{pH,sta,E2,P1}$) has a value of 1.0. At a pH of 3, $f_{pH,sta,E2,P1}$ drops to the minimum of 0.1. At a pH of 11, $f_{pH,sta,E2,P1}$ rises to the maximum value of 1.0.

4.2.2 Temperature and pH dependence of the proteolysis enzymes

Figure 22 shows how temperature affects the activity of EnerZyme P7 (*E1, P2*) and Flavourzyme (*E2, P2*) used in the proteolysis process (*P2*). Furthermore, sigmoidal and double sigmoidal functions representing the temperature-dependent activity and stability of the enzymes in the model for enzymatic hydrolysis processes are presented.

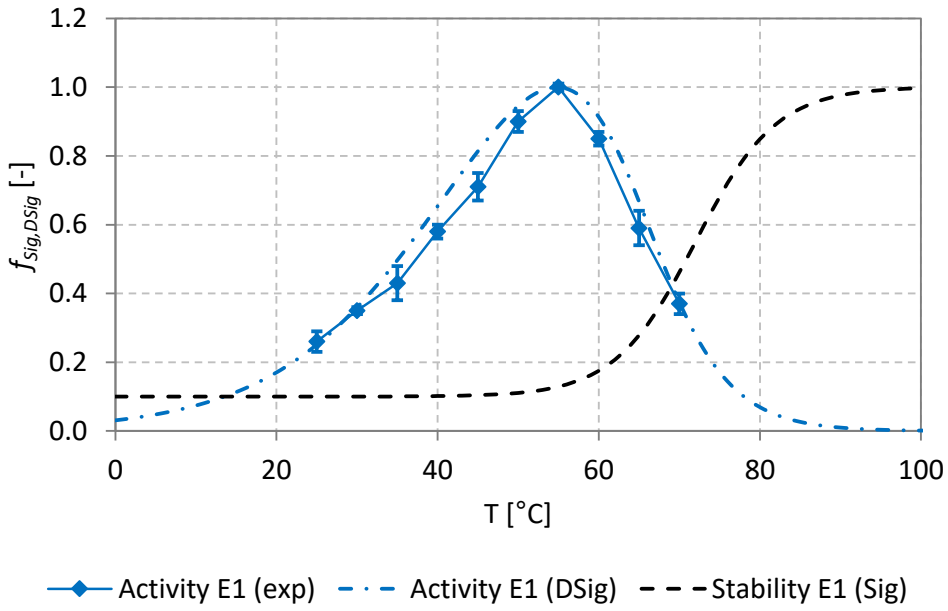

Figure 22: Experimentally (Activity E1 (exp)) determined temperature-dependent enzyme activity of EnerZyme P7 (E1), pH = 7.0, with fitted double sigmoidal function for temperature-dependent enzyme activity (Activity E1 (DSig)), R^2 = 0.944 and assumed sigmoidal function for temperature-dependent enzyme stability (Stability E1 (Sig). Error bars represent the mean value ± of one standard deviation resulting from a triple determination.

EnerZyme P7 showed the highest activity at a temperature of around 55 °C. Conversely, the enzyme activity decreases by over 50% at temperatures below 30 °C and above 70 °C.

The double sigmoidal function for the temperature-dependent enzyme activity ($f_{T,act,E1,P2}$) could be fitted to the experimentally determined data with R^2 = 0.944.

From 0-50°C, the sigmoidal function for the temperature-dependent enzyme stability of EnerZyme P7 ($f_{T,sta,E1,P2}$) remains at the minimum value of 0.1. Between 50-100 °C, $f_{T,sta,E1,P2}$ increases to a value of 1.0.

Figure 23 shows how temperature affects the activity of Flavourzyme (*E2, P2*) used in the proteolysis process (*P2*). Furthermore, sigmoidal and double sigmoidal functions representing the temperature-dependent activity and stability of the enzyme in the model are presented.

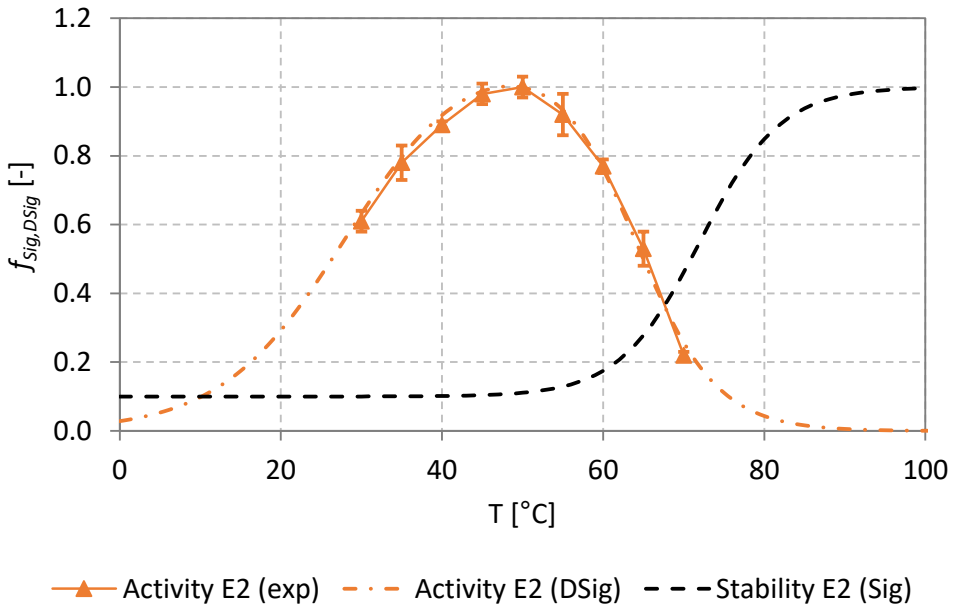

Figure 23: Experimentally (Activity E2 (exp)) determined temperature-dependent enzyme activity of Flavourzyme (E2), pH = 7.0, with fitted double sigmoidal function for temperature-dependent enzyme activity (Activity E2 (DSig)), R^2 = 0.992 and assumed sigmoidal function for temperature-dependent enzyme stability (Stability E2 (Sig). Error bars represent the mean value ± of one standard deviation resulting from a triple determination.

Flavourzyme showed the highest activity at a temperature of about 50 °C. Conversely, the enzyme activity decreases by over 50% at temperatures below 30 °C and above 70 °C.

The double sigmoidal function for the temperature-dependent enzyme activity ($f_{T,act,E2,P2}$) could be fitted to the experimentally determined data with R^2 = 0.992.

From 0-50°C, the sigmoidal function for the temperature-dependent enzyme stability of Flavourzyme ($f_{T,act,E2,P2}$) remains at the minimum value of 0.1. Between 50-100 °C, $f_{T,act,E2,P2}$ increases to a value of 1.0.

Figure 24 shows the experimentally determined pH dependency of EnerZyme P7 (*E1, P2*) used in the proteolysis process (*P2*). Furthermore, the double sigmoidal functions representing the pH-dependent activity and stability of the enzyme in the model are presented.

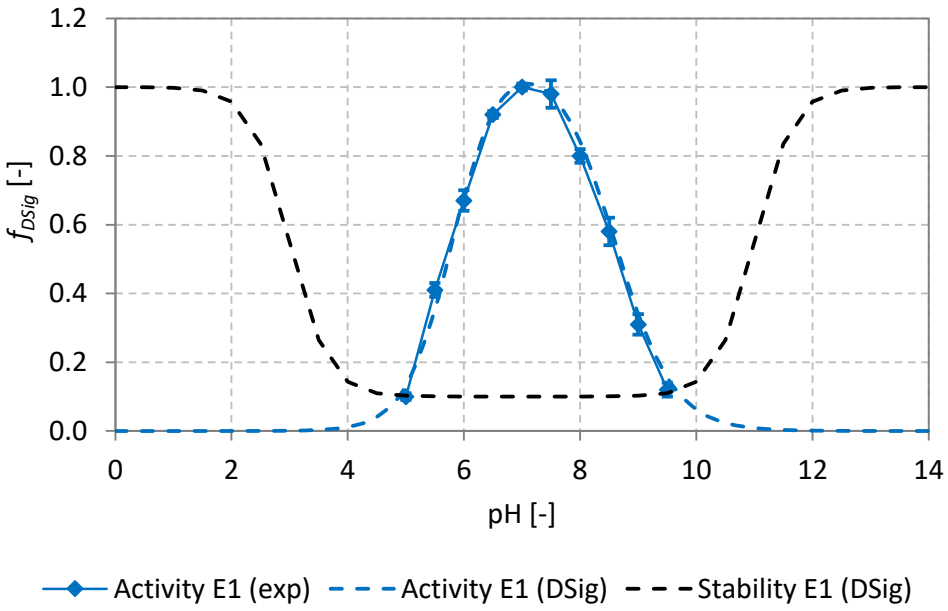

Figure 24: Experimentally (Activity E1 (exp)) determined pH-dependent enzyme activity of EnerZyme P7 (E1), T = 50 °C, with fitted double sigmoidal function for pH-dependent enzyme activity (Activity E1 (DSig)), R^2 = 0.991 and assumed double sigmoidal function for pH-dependent enzyme stability (Stability E1 (DSig)). Error bars represent the mean value ± of one standard deviation resulting from a triple determination.

For EnerZyme P7, only low activities could be determined at pH values below 5 and above 9. The highest activity was achieved at a pH value of approx. 7. The enzyme activity decreases by over 80% at a pH below 5 and above 9.

For EnerZyme P7, the double sigmoidal function for the pH-dependent enzyme activity ($f_{pH,act,E1,P2}$) could be fitted to the experimentally determined data with R^2 = 0.991.

At a pH value of 0, the double sigmoidal function for the pH-dependent enzyme stability of EnerZyme P7 ($f_{pH,sta,E1,P2}$) ranges at a value of 1.0. At a pH of 5, $f_{pH,sta,E1,P2}$ drops to the minimum of 0.1. At a pH of 9, $f_{pH,sta,E1,P2}$ rises to the maximum value of 1.0.

Figure 25 shows the experimentally determined pH dependency of Flavourzyme (*E2, P2*) used in the proteolysis process (*P2*). Furthermore, the double sigmoidal functions representing the pH-dependent activity and stability of the enzyme in the model are presented.

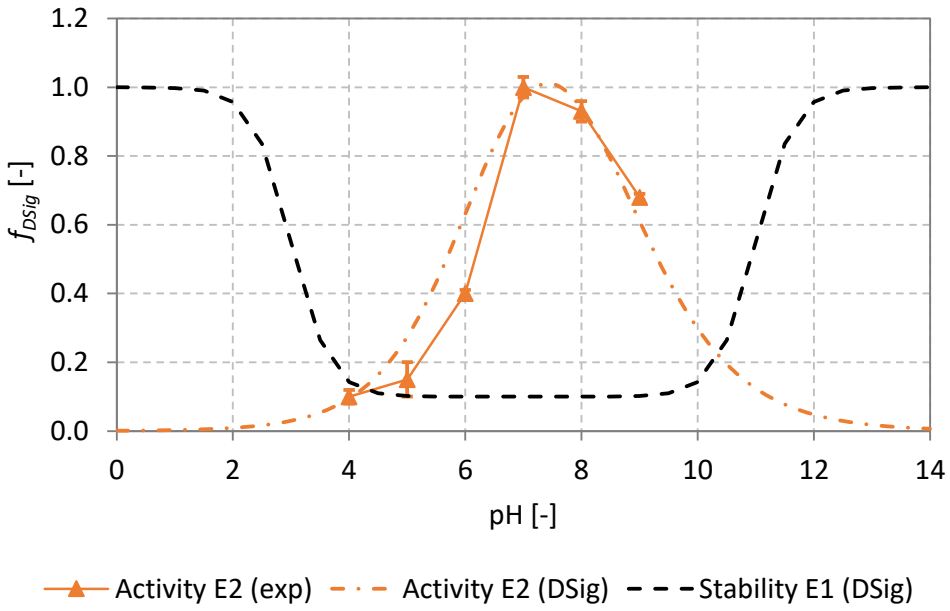

Figure 25: Experimentally (Activity E2 (exp)) determined pH-dependent enzyme activity of Flavourzyme (E2), T = 50 °C, with fitted double sigmoidal function for pH-dependent enzyme activity (Activity E2 (DSig)), R^2 = 0.901 and assumed double sigmoidal function for pH-dependent enzyme stability (Stability E2 (DSig)). Error bars represent the mean value ± of one standard deviation resulting from a triple determination.

For Flavourzyme, only low activities could be determined at pH values below 5 and above 9. The enzyme activity decreases by more than 80% at a pH below 5 and more than 30% above a pH of 9. Flavourzyme showed the highest activity at a pH value of approx. 7.

Flavourzyme's double sigmoidal function for the pH-dependent enzyme activity ($f_{pH,act,E2,P2}$) could be fitted to the experimentally determined data with R^2 = 0.901.

At a pH value of 0, the double sigmoidal function for the pH-dependent enzyme stability of Flavourzyme ($f_{pH,sta,E2,P1}$) has a value of 1.0. At a pH of 5, $f_{pH,sta,E2,P2}$ drops to the minimum of 0.1. At a pH of 9, $f_{pH,sta,E2,P2}$ rises to a maximum of 1.0.

4.2.3 Pressure dependence of the enzymes used for starch hydrolysis

The enzymes (Termamyl SC and Spirizyme Ultra) used in the starch hydrolysis process were treated at 1 to 2000 bar in a high-pressure homogeniser. Subsequently, the enzyme activity was examined under normal pressure conditions and compared with the enzyme activity of the untreated enzymes (Section 3.3).

Figure 27 shows the results of oligosaccharide formation from potato starch by untreated (native) and high-pressure homogenised (500, 1000, 1500 and 2000 bar) Termamyl SC at 40, 60 and 80 °C under normal pressure conditions.

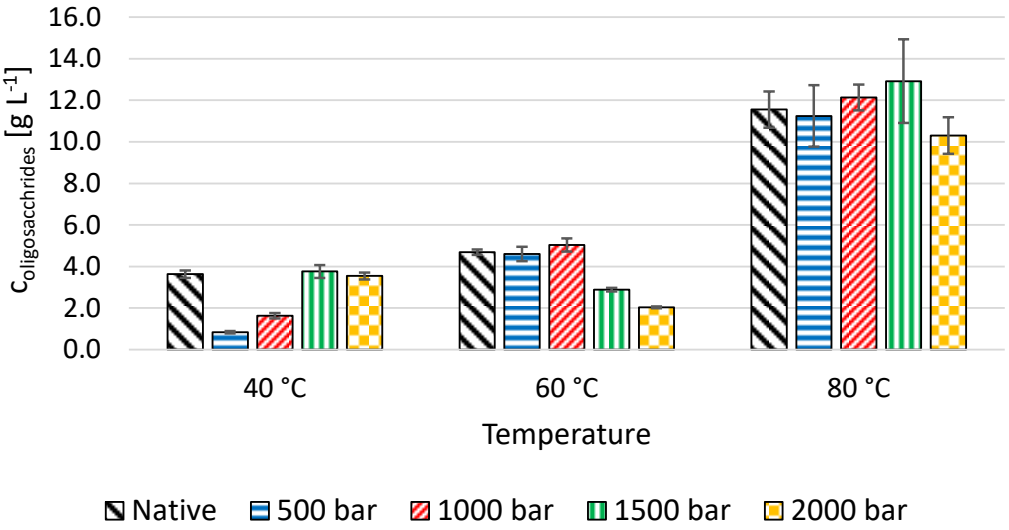

Figure 26: Oligosaccharide formation of untreated (native) and high-pressure homogenised (500, 1000, 1500, 2000 bar) Termamyl SC, V = 40.0 mL, $c_{substrate}$ = 20 g L^{-1}, c_{enzyme} = 6.25 µg L^{-1}, pH = 5.0, t = 20 min. Error bars represent the mean value ± of one standard deviation resulting from a quadruple determination.

At a reaction temperature of 40 °C, the native form of the enzyme produced an oligosaccharide concentration of 3.6 ± 0.2 g L^{-1}. The high-pressure homogenisation of the enzyme resulted in an oligosaccharide concentration of 0.8 ± 0.1 g L^{-1} at 500 bar, 1.6 ± 0.1 g L^{-1} at 1000 bar, 3.8 ± 0.3 g L^{-1} at 1500 bar, and 3.6 ± 0.2 g L^{-1} at 2000 bar.

At a reaction temperature of 60 °C, the native form of the enzyme produced an oligosaccharide concentration of 4.7 ± 0.1 g L^{-1}. The high-pressure homogenisation of the enzyme resulted in an oligosaccharide concentration of 4.6 ± 0.4 g L^{-1} at 500 bar, 5.0 ± 0.3 g L^{-1} at 1000 bar, 2.9 ± 0.1 g L^{-1} at 1500 bar, and 2.0 ± 0.1 g L^{-1} at 2000 bar.

At a reaction temperature of 80 °C, the native form of the enzyme produced an oligosaccharide concentration of 11.6 ± 0.9 g L^{-1}. The high-pressure homogenisation of the enzyme resulted in an oligosaccharide concentration of 11.2 ± 1.5 g L^{-1} at 500 bar, 12.1 ± 0.6 g L^{-1} at 1000 bar, 12.9 ± 2.0 g L^{-1} at 1500 bar, and 10.3 ± 0.9 g L^{-1} at 2000 bar.

Using the dependent samples t-test (Student, 1908), no significant increase in enzyme activity could be determined after high-pressure homogenisation compared to the native untreated form of Termamyl SC.

Figure 27 shows the results of glucose formation from starch using untreated (native) and high-pressure homogenised (500, 1000, 1500 and 2000 bar) Spirizyme Ultra at 40, 60 and 80 °C under normal pressure conditions.

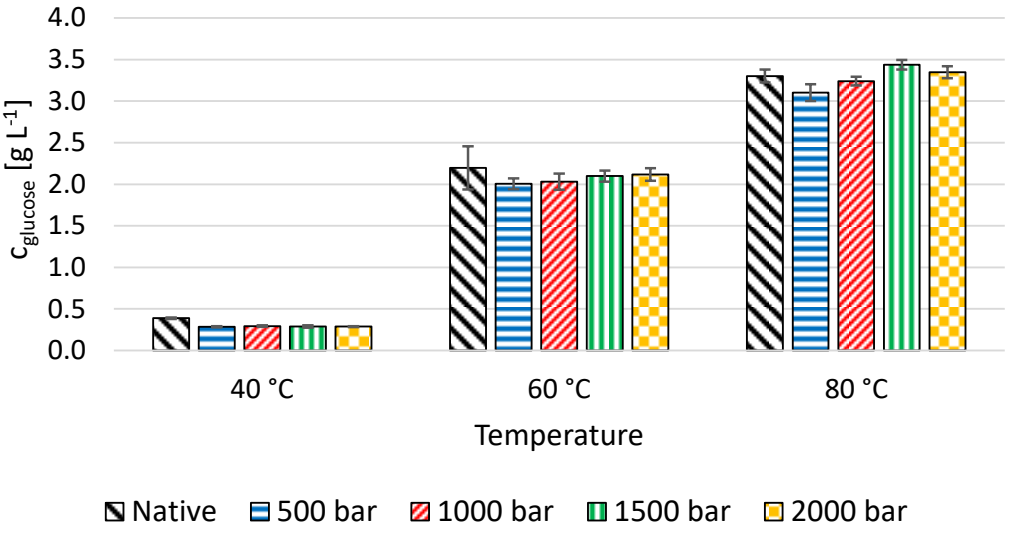

Figure 27: Glucose formation of untreated (native) and high-pressure homogenised (500, 1000, 1500, 2000 bar) Spirizyme Ultra, V = 40.0 mL, $c_{substrate}$ = 20.0 g L^{-1}, c_{enzyme} = 25.0 µg L^{-1}, pH = 5.0, t = 20 min. Error bars represent the mean value ± of one standard deviation resulting from a quadruple determination.

At a reaction temperature of 40 °C, the native form of the enzyme produced a glucose concentration of 0.4 ± 0.01 g L^{-1}. The high-pressure homogenisation of the enzyme resulted in a glucose concentration of 0.3 ± 0.01 g L^{-1} at 500 bar, 0.3 ± 0.01 g L^{-1} at 1000 bar, 0.3 ± 0.01 g L^{-1} at 1500 bar, and 0.3 ± 0.01 g L^{-1} at 2000 bar.

At a reaction temperature of 60 °C, the native form of the enzyme produced a glucose concentration of 2.2 ± 0.3 g L^{-1}. The high-pressure homogenisation of the enzyme resulted in a glucose concentration of 2.0 ± 0.1 g L^{-1} at 500 bar, 2.0 ± 0.1 g L^{-1} at 1000 bar, 2.1 ± 0.1 g L^{-1} at 1500 bar, and 2.1 ± 0.1 g L^{-1} at 2000 bar.

At a reaction temperature of 80 °C, the native form of the enzyme produced a glucose concentration of 3.3 ± 0.1 g L^{-1}. The high-pressure homogenisation of the enzyme resulted in a glucose concentration of 3.1 ± 0.1 g L^{-1} at 500 bar, 3.2 ± 0.1 g L^{-1} at 1000 bar, 3.4 ± 0.1 g L^{-1} at 1500 bar, and 3.4 ± 0.1 g L^{-1} at 2000 bar.

Using the dependent samples t-test (Student, 1908), no significant increase in enzyme activity could be determined after high-pressure homogenisation compared to the native untreated form of Spirizyme Ultra.

4.2.4 Pressure dependence of the enzymes used for proteolysis

The enzymes (EnerZyme P7 and Flavourzyme) used in the proteolysis process were treated at 1 to 2000 bar in a high-pressure homogeniser. Subsequently, the enzyme activity was examined under normal pressure conditions and compared with the enzyme activity of the untreated enzymes (Section 3.3).

Figure 29 shows the results of free amino acid formation from casein using untreated (native) and high-pressure homogenised (500, 1000, 1500 and 2000 bar) EnerZyme P7 at 25, 50 and 70 °C under normal pressure conditions.

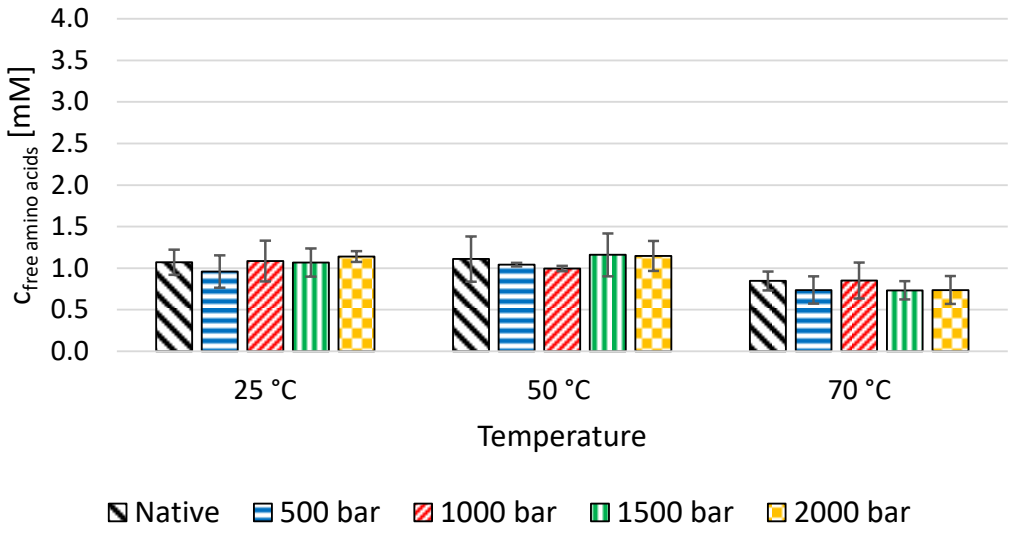

Figure 28: Free amino acid formation of untreated (native) and high-pressure homogenised (500, 1000, 1500, 2000 bar) EnerZyme P7, V = 1.0 mL, $c_{substrate}$ = 2.0 g L^{-1}, c_{enzyme} = 0.2 g L^{-1}, pH = 7.5, t = 30 min. Error bars represent the mean value ± of one standard deviation resulting from a triple determination.

At a reaction temperature of 25 °C, the native form of the enzyme produced a free amino acid concentration of 1.1 ± 0.2 mM. High-pressure homogenisation of the enzyme resulted in a free amino acid concentration of 1.0 ± 0.2 mM at 500 bar, 1.1 ± 0.2 mM at 1000 bar, 1.1 ± 0.2 mM at 1500 bar, and 1.1 ± 0.1 mM at 2000 bar.

At a reaction temperature of 50 °C, the native form of the enzyme produced a free amino acid concentration of 1.1 ± 0.3 mM. High-pressure homogenisation of the enzyme resulted in a free amino acid concentration of 1.0 ± 0.02 mM at 500 bar, 1.0 ± 0.03 mM at 1000 bar, 1.2 ± 0.3 mM at 1500 bar, and 1.2 ± 0.2 mM at 2000 bar.

At a reaction temperature of 70 °C, the native form of the enzyme produced a free amino acid concentration of 0.9 ± 0.1 mM. High-pressure homogenisation of the enzyme resulted in a free amino acid concentration of 0.7 ± 0.2 mM at 500 bar, 0.9 ± 0.2 mM at 1000 bar, 0.7 ± 0.1 mM at 1500 bar, and 0.7 ± 0.2 mM at 2000 bar.

Using the dependent samples t-test (Student, 1908), no significant increase in enzyme activity could be determined after high-pressure homogenisation compared to the native untreated form of EnerZyme P7.

Figure 29 shows the results of free amino acid formation from casein through untreated (native) and high-pressure homogenised (500, 1000, 1500 and 2000 bar) Flavourzyme at 25, 50 and 70 °C under normal pressure conditions.

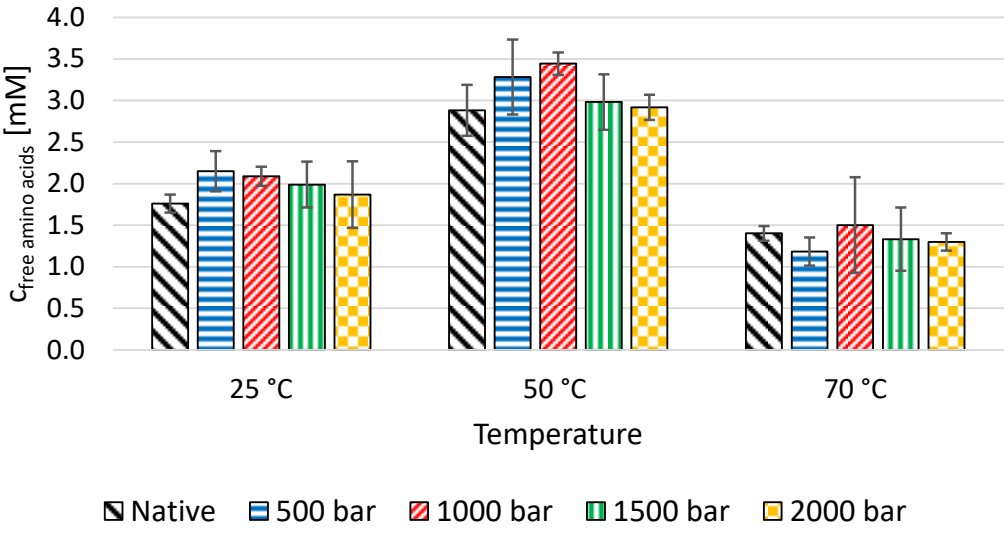

Figure 29: Free amino acid formation of untreated (native) and high-pressure homogenised (500, 1000, 1500, 2000 bar) Flavourzyme, V = 1.0 mL, $c_{substrate}$ = 2.0 g L^{-1}, c_{enzyme} = 0.2 g L^{-1},

pH = 7.5, t = 30 min. Error bars represent the mean value ± of one standard deviation resulting from a triple determination.

At a reaction temperature of 25 °C, the native form of the enzyme produced a free amino acid concentration of 1.8 ± 0.1 mM. High-pressure homogenisation of the enzyme resulted in a free amino acid concentration of 2.2 ± 0.2 mM at 500 bar, 2.1 ± 0.1 mM at 1000 bar, 2.0 ± 0.3 mM at 1500 bar, and 1.9 ± 0.4 mM at 2000 bar.

At a reaction temperature of 50 °C, the native form of the enzyme produced a free amino acid concentration of 2.9 ± 0.3 mM. High-pressure homogenisation of the enzyme resulted in a free amino acid concentration of 3.3 ± 0.5 mM at 500 bar, 3.4 ± 0.1 mM at 1000 bar, 3.0 ± 0.3 mM at 1500 bar, and 2.9 ± 0.2 mM at 2000 bar.

At a reaction temperature of 70 °C, the native form of the enzyme produced a free amino acid concentration of 1.4 ± 0.1 mM. High-pressure homogenisation of the enzyme resulted in a free amino acid concentration of 1.2 ± 0.2 mM at 500 bar, 1.5 ± 0.6 mM at 1000 bar, 1.3 ± 0.4 mM at 1500 bar, and 1.3 ± 0.1 mM at 2000 bar.

A dependent samples t-test (Student, 1908) was run to determine if high-pressure homogenisation increased the activity of Flavourzyme. The results showed that the production of free amino acids at 50 °C was significantly higher after high-pressure homogenisation at 1000 bar (3.4 ± 0.1 mM) compared to the native untreated form of the enzyme (2.9 ± 0.3 mM), ($t(3) = 3.2$, $p < .05$). The enzyme activity was increased by more than 19%.

No significant increase in enzyme activity was determined for the other pressures and temperatures investigated.

4.3 Parameterisation of the model for enzymatic hydrolysis processes

For the parameterisation of the model for enzymatic hydrolysis processes, batch experiments for starch hydrolysis and proteolysis in a 6 L STR were planned with the developed model (Sections 3.1.2 and 3.2.2). The parameterisation took place by minimising the difference between the data simulated by the model and the experimental data using the parameterisation tool described in Section 3.4.2.

4.3.1 Parameterisation of the starch hydrolysis model

For the parameterisation of the starch hydrolysis model (*P1*), two batch experiments were carried out in a 6 L STR. Potato starch was used as substrate. The enzyme preparations Termamyl SC (*E1, P1*) and Spirizyme Ultra (*E2, P1*) were used to convert the starch into glucose. The processing time was set to 180 min.

During the parameterisation, the model parameters were adjusted using the parameterisation tool described in Section 3.4.2. The parameterisation aimed to achieve agreement between the measured and simulated data with an R^2 greater than 0.9. All measured values of the two parameterisation experiments were weighted equally.

The parameter set Par_{Inital}, which resulted from the small-scale experiments, was used as starting values for parameterisation. During parameterisation, the maximum reaction rates (r_{max}) and the half-saturation constants (K_M) were adjusted according to Table 6.

Table 6: Parameters adjusted for the parameterisation of the starch hydrolysis model, with α-amylase (E1) and glucoamylase (E2).

Parameter	Description	Lower bound	Upper bound	Initial parameterisation (Par_{Inital})	Optimised parameterisation (Par_{Optim})
$r_{max,SIP,E1,P1}$	Maximum degradation rate of substrate to intermediate product.	0.1 s^{-1}	10.0 s^{-1}	4.23 s^{-1}	8.64 s^{-1}
$K_{M,SIP,E1,P1}$	Half-saturation constant for degradation of substrate to intermediate product.	1.0 g L^{-1}	30.0 g L^{-1}	5.72 g L^{-1}	25.60 g L^{-1}
$r_{max,IPP,E2,P1}$	Maximum degradation rate of intermediate product to product.	0.1 s^{-1}	10.0 s^{-1}	0.31 s^{-1}	0.82 s^{-1}
$K_{M,IPP,E2,P1}$	Half-saturation constant for degradation of intermediate product to product.	1.0 g L^{-1}	30.0 g L^{-1}	19.99 g L^{-1}	29.99 g L^{-1}

Figure 30 shows the simulated (set of parameters: Par_{Optim}) and experimental results of the first parameterisation starch hydrolysis batch experiment in a 6 L STR. After a processing time of 15 min, Termamyl SC was added to the reactor, followed by Spirizyme Ultra after a processing time of 60 min.

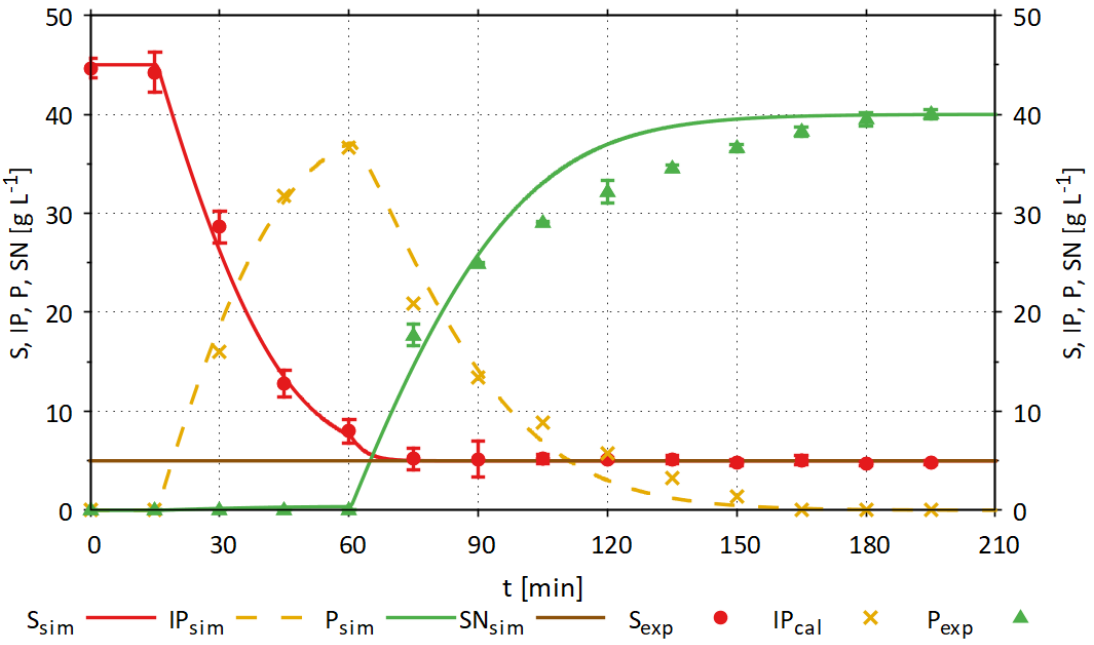

Figure 30: Comparison between simulation (index: sim) and experimental (index: exp) results of the first parameterisation starch hydrolysis batch experiment, with $R^2_{substrate}$ = 0.997 and $R^2_{product}$ = 0.980. V_{start} = 3.0 L, $c_{substrate,start}$ = 45 g L^{-1}, T = 60 °C, pH = 4.15 and N_{Stirr} = 300 rpm. Addition of 40 µL Termamyl SC (E1) after 15 min and 300 µL Spirizyme Ultra (E2) after 60 min. S: substrate (potato starch) concentration, IP: intermediate product concentration, P: product (glucose) concentration, SN: concentration of the non-hydrolysable components of the substrate. Error bars represent the mean value ± of one standard deviation resulting from a double determination. Set of parameters used for simulation: Par_{Optim}.

The measured substrate concentration started at a value of 44.65 g L^{-1}. After a processing time of approx. 75 min, the measured substrate concentration decreased to a value of approx. 5 g L^{-1}. After a processing time of 195 min, the measured substrate concentration reached the minimum value of 4.83 g L^{-1}. The measured product concentration started at a value of approx. 0 g L^{-1}. After adding *E1* and *E2* (t = 15 min), up to a processing time of 195 min, the measured product concentration increased to a maximum value of 40.01 g L^{-1}.

The substrate and product concentration curves simulated by the model reproduce the measured curves with $R^2_{substrate}$ = 0.997 and $R^2_{product}$ = 0.980.

In the first parameterisation experiment, *E1* and *E2* were added to the reactor with a time delay of 45 min. To ensure that the model can represent different process designs,

another experiment was carried out in which *E1* and *E2* were added to the reactor simultaneously. Figure 31 shows the simulated and experimental results of the second starch hydrolysis batch experiment in a 6 L STR.

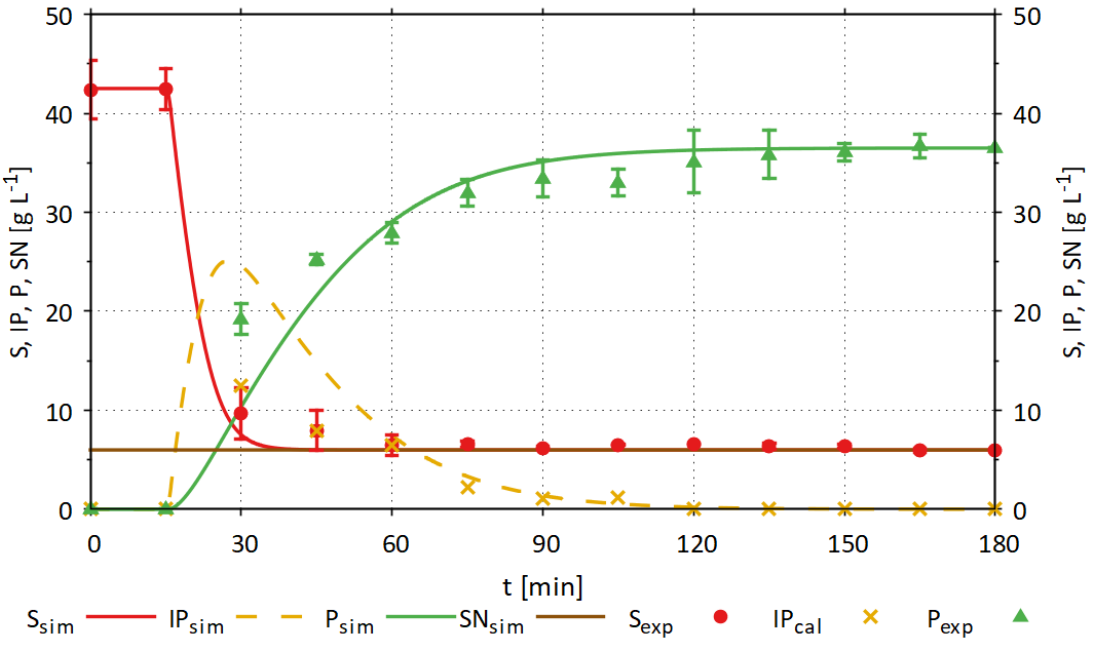

Figure 31: Comparison between simulation (index: sim) and experimental (index: exp) results of the second parameterisation starch hydrolysis batch experiment, with $R^2_{substrate}$ = 0.995 and $R^2_{product}$ = 0.947. V_{start} = 3.0 L, $c_{substrate,start}$ = 45 g L^{-1}, T = 60 °C, pH = 4.15 and N_{Stirr} = 300 rpm. Addition of 41 µL Termamyl SC and 305 µL Spirizyme Ultra after 15 min. S: substrate (potato starch) concentration, IP: intermediate product concentration, P: product (glucose) concentration, SN: concentration of the non-hydrolysable components of the substrate. Error bars represent the mean value ± of one standard deviation resulting from a double determination. Set of parameters used for simulation: Par_{Optim}.

The measured substrate concentration started at a value of 42.37 g L^{-1}. After a processing time of approx. 60 min, the measured substrate concentration decreased to a value of approx. 6 g L^{-1}. After a processing time of 180 min, the measured substrate concentration reached the minimum value of 5.98 g L^{-1}. The measured product concentration started at a value of approx. 0 g L^{-1}. After adding E1 and E2 (t = 15 min), up to a processing time of 180 min, the measured product concentration increased to a maximum value of 36.50 g L^{-1}.

The substrate and product concentration curves simulated by the model reproduce the measured values with $R^2_{substrate}$ = 0.995 and $R^2_{product}$ = 0.947.

4.3.2 Parameterisation of the proteolysis model

For the parameterisation of the proteolysis model, one batch experiment was carried out in a 6 L STR. Organic sunflower seed meal was used as substrate. The enzyme preparation Flavourzyme (*E1, P2* and *E2, P2*) was used to convert the protein (substrate) into free amino acids (product).

During the parameterisation, the model parameters were adjusted using the parameterisation tool described in Section 3.4.2. The parameterisation aimed to achieve agreement between the measured and simulated data with an R^2 greater than 0.9. All measured values of the two parameterisation experiments were weighted equally. The parameter set Par_{Inital}, which resulted from the small-scale experiments, was used as starting values for the parameterisation. All measured values of the parameterisation experiment were weighted equally. For the parameterisation of the proteolysis model, the maximum reaction rates (r_{max}) and the half-saturation constants (K_M) were adjusted according to Table 7.

Table 7: Parameters adjusted for the parameterisation of the proteolysis model, with endopeptidase (E1) and exopeptidase (E2).

Parameter	Description	Lower bound	Upper bound	Initial parameterisation (Par_{Inital})	Optimised parameterisation (Par_{Optim})
$r_{max,SIP,E1,P2}$	Maximum degradation rate of substrate to intermediate product.	0.1 s^{-1}	10.0 s^{-1}	0.25 s^{-1}	0.57 s^{-1}
$K_{M,SIP,E1,P2}$	Half-saturation constant for degradation of substrate to intermediate product.	1.0 g L^{-1}	30.0 g L^{-1}	5.29 g L^{-1}	22.55 g L^{-1}
$r_{max,IPP,E2,P2}$	Maximum degradation rate of intermediate product to product.	0.1 s^{-1}	10.0 s^{-1}	0.11 s^{-1}	0.67 s^{-1}
$K_{M,IPP,E2,P2}$	Half-saturation constant for degradation of intermediate product to product.	1.0 g L^{-1}	30.0 g L^{-1}	1.57 g L^{-1}	1.57 g L^{-1}

Figure 32 shows the results of the proteolysis batch experiment used for parameterisation and the corresponding results simulated by the model.

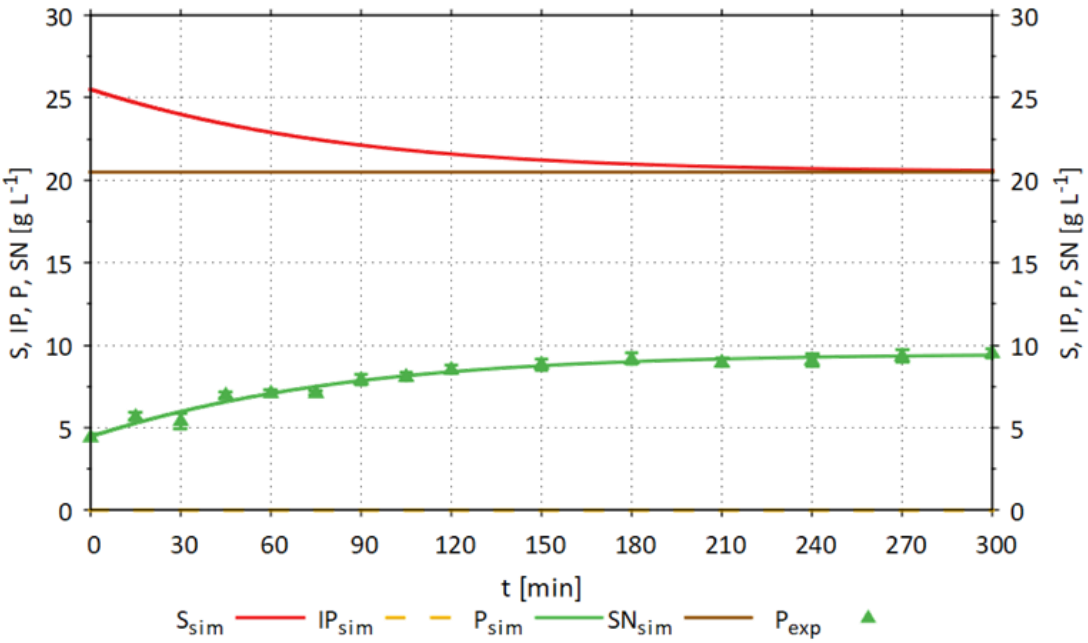

Figure 32: Comparison between simulation (index: sim) and experimental (index: exp) results of the parameterisation proteolysis batch experiment, with $R^2_{product}$ = 0.971. V = 3.0 L, $c_{substrate,start}$ = 30 g L^{-1}, T = 50 °C, pH = 7.5 and N_{stirr} = 300 rpm. Addition of 1.332 mL Flavourzyme (E1 and E2) after a processing time of 0 min. S: substrate (sunflower seed meal) concentration, IP: intermediate product concentration, P: product (free amino acid) concentration, SN: concentration of the non-hydrolysable components of the substrate. Error bars represent the mean value ± of one standard deviation resulting from a triple determination. Set of parameters used for simulation: Par_{Optim}.

The measured product concentration started at a value of 4.47 g L^{-1}. After a processing time of 300 min, the measured product concentration reached the maximum value of 9.52 g L^{-1}.

The curve of the product concentration simulated by the model reproduces the measured curve with $R^2_{product}$ = 0.971.

4.4 Discussion

Within the scope of this research work, a new mechanistic model for enzymatic hydrolysis processes (combined starch hydrolysis and proteolysis) was developed. The reaction rates could be calculated using Michaelis-Menten kinetics. By implementing double sigmoidal functions, the dependence of the enzyme activity on temperature and pH value can be mapped (Brüning, 2016; Kuntzsch, 2014). The double sigmoidal functions for representing the temperature and pH-dependent enzyme activity were manually adapted

to experimentally determined data. As a result, the agreement is always higher than 90%.

For the parameterisation of the model for enzymatic hydrolysis processes, two STR batch experiments were carried out for starch hydrolysis and one for proteolysis. Using a newly developed tool for model parameterisation, which was realised in R, the model could be adapted based on the experimental data. Only four parameters had to be estimated per enzymatic process for the parameterisation. As a result, the model can reproduce the experimentally generated data with an agreement of more than 90%.

Furthermore, the influence of high-pressure homogenisation on the activity of Termamyl SC (α-amylase), Spirizyme Ultra (α- and glucoamylase), EnerZyme P7 (endopeptidase) and Flavourzyme (endopeptidase and exopeptidase) was investigated. For Termamyl SC, an increase of approx. 7% in the 60 °C-activity was reached after high-pressure homogenisation at 1000 bar. An increase of approx. 5-12% in the 80 °C-activity was reached after high-pressure homogenisation at 1000-1500 bar. The increase in activity determined by Buckow et al. (2007) could not be detected for this α-amylase. For Spirizyme Ultra, an increase of approx. 1-4% in the 80 °C-activity was reached after high-pressure homogenisation at 1500-2000 bar. For EnerZyme P7, an increase of approx. 6% in the 25 °C-activity was reached after high-pressure homogenisation at 2000 bar. An increase of approx. 3-5% in the 50 °C-activity was reached after high-pressure homogenisation at 1500-2000 bar. For Flavourzyme, an increase of approx. 18-22% in the 25 °C-activity and approx. 13-20% in the 50 °C-activity was reached after high-pressure homogenisation at 500-1000 bar. Compared to Tribst et al. (2012), the highest increase of the 25 °C-activity could be achieved after treatment at 500-1000 bar and not at 2000 bar.

When investigating the enzyme activity after high-pressure treatment, the experimental results of all investigated enzyme preparations showed partially high standard deviations, which is why further investigations are necessary. A significantly higher enzyme activity could only be determined for high-pressure homogenisation of Flavourzyme at 1000 bar and 50 °C.

The design of most STRs only allows operation under normal pressure conditions, so the influence of pressure has not been included in the model.

5 Digital twins for enzymatic hydrolysis processes

To create the new stand-alone digital twin for enzymatic hydrolysis processes in an STR, the developed model for enzymatic hydrolysis was implemented into an existing stand-alone digital twin of a 20 L STR. Furthermore, a precursor of a stand-alone digital twin for enzymatic hydrolysis processes in a PBR was created using the stand-alone digital twin of an STR.

5.1 Development of a stand-alone digital twin for enzymatic hydrolysis processes in a stirred tank reactor

Once the C-eStIM model for enzymatic hydrolysis processes was able to represent starch hydrolysis and proteolysis satisfactorily, the model was implemented into the existing stand-alone digital twin of a 20 L STR (Section 3.5) developed by the working group of Prof. Dr. Volker C. Hass at Furtwangen University (Appl et al., 2021; Gerlach et al., 2013; Gerlach et al., 2015; Hass et al., 2005a, 2005b; Hass, 2005; Hass et al., 2012; Hass, 2016; Hirschmann et al., 2018; Hirschmann, 2021; Isimite et al., 2018).

For the implementation, the model equations of the C-eStIM model for enzymatic hydrolysis processes were included in the digital twin core model of the stand-alone digital twin, which was also realised in C-eStIM. Subsequently, the adapted C-eStIM-DLL interface of the digital twin core model was reimplemented in the WinErs project of the stand-alone digital twin.

The new stand-alone digital twin can represent the enzyme kinetics, as well as the complex behaviour of a 20 L STR (Biostat C, B. Braun Sartorius, Göttingen, Germany) with plant, periphery (e.g., pumps) and control (e.g., level, temperature, pH).

Integration into the stand-alone digital twin offers a wide range of possibilities:

- Mapping of the complex reactor behaviour (e.g., temperature and pH value).
- Mapping the complex behaviour of the plant and periphery (e.g., tanks, pumps and pipes).
- Implementation of measurement noise for the online measurement data.
- Design, test, and parameterise standard control (e.g., P, PI, PID) and model-based process design strategies (e.g., OLFO).

Furthermore, the GUI of the stand-alone digital twin was adapted (Figure 33). The GUI was designed to correspond to the process control system connected to the actual STR.

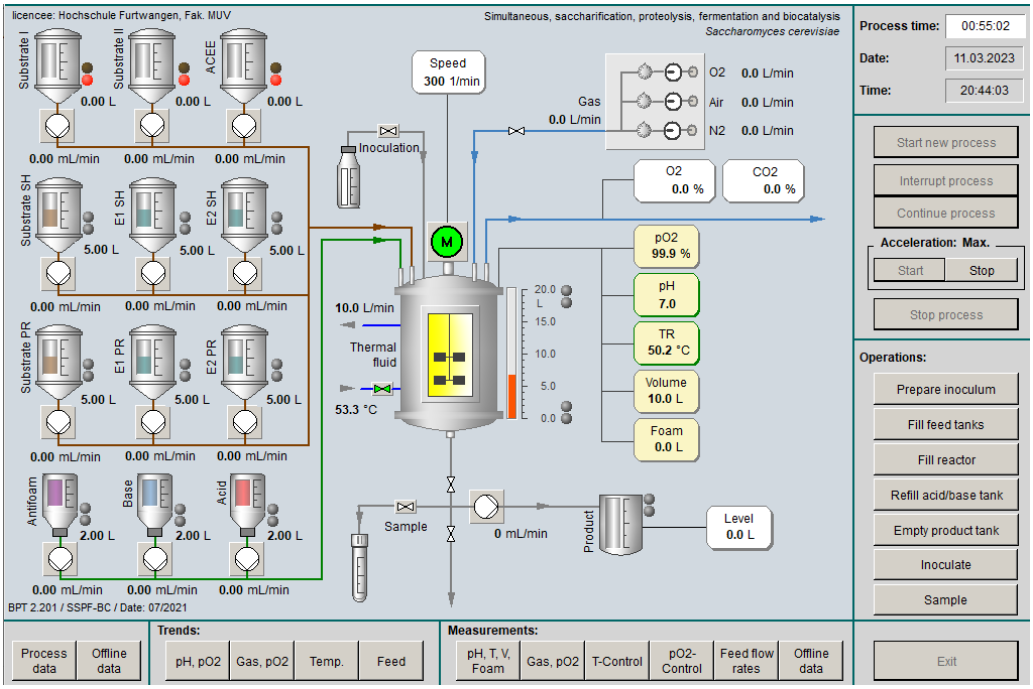

Figure 33: GUI of the stand-alone digital twin for simultaneous saccharification, proteolysis, fermentation and biocatalysis in a 20 L STR.

With the new stand-alone digital twin for the enzymatic hydrolysis processes, it is possible to accelerate the simulation of the enzymatic hydrolysis processes in a 20 L STR up to 100-fold. This makes it possible to simulate different process control strategies quickly and thus improve them. Furthermore, the parameterisation of the controllers implemented in the stand-alone digital twin can be adjusted via sub-windows of the GUI.

Since the process control system of the STRs available at Furtwangen University was also realised using WinErs, the process control strategies developed for the stand-alone digital twin can be easily applied to actual processes.

5.1.1 Implementation of standard and multivariable control strategies to the stand-alone digital twin for enzymatic hydrolysis processes in a stirred tank reactor

To enable the new stand-alone digital twin for enzymatic hydrolysis processes in an STR to reproduce not only the biokinetic processes but also the behaviour of the existing system with the standard control strategies available there, these standard control strategies were implemented to the digital twin and parameterised based on simulations.

For the implementation and optimisation of the standard control strategies to the stand-alone digital twin for enzymatic hydrolysis processes in an STR, the procedure shown in Figure 34 was established.

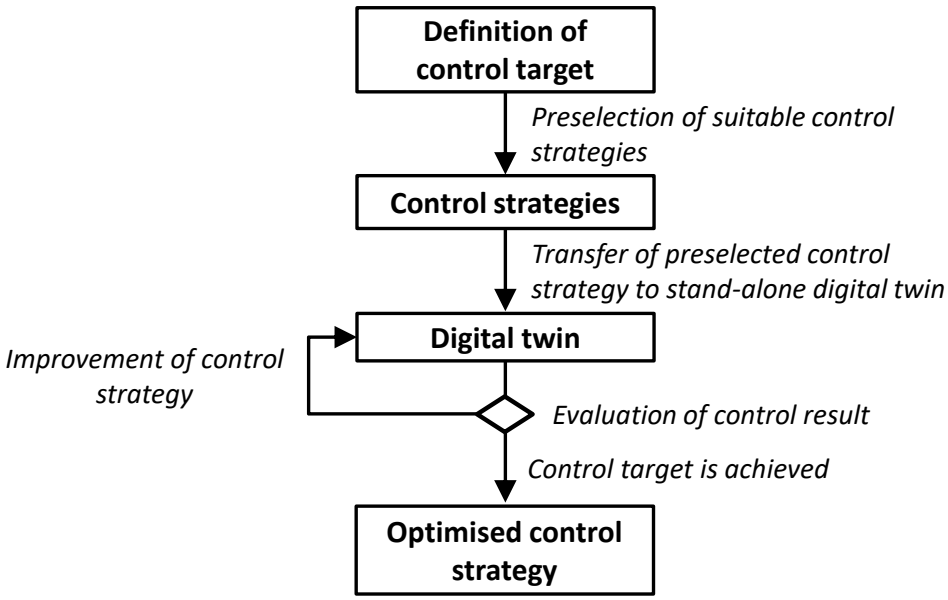

Figure 34: Development and optimisation of standard control strategies to the stand-alone digital twin for enzymatic hydrolysis processes in an STR.

In the first step, the desired control targets were defined, and the related system behaviour was characterised by using simulations. Then, suitable control strategies were selected for the associated control target. Subsequently, the selected process control strategies were implemented in the stand-alone digital twin. By simulating step responses and the controller behaviour in case of disturbances, the implemented controllers were tested, and the most suitable controller for the respective controlled variable was picked. Finally, the parameterisation of the selected controller was further optimised until the desired control target was achieved.

For a better representation of the actual STR and the equipped controls, standard multivariable controls for level, temperature, and pH have been implemented on the stand-alone digital twin for enzymatic hydrolysis processes in a 20 L STR (Figure 35).

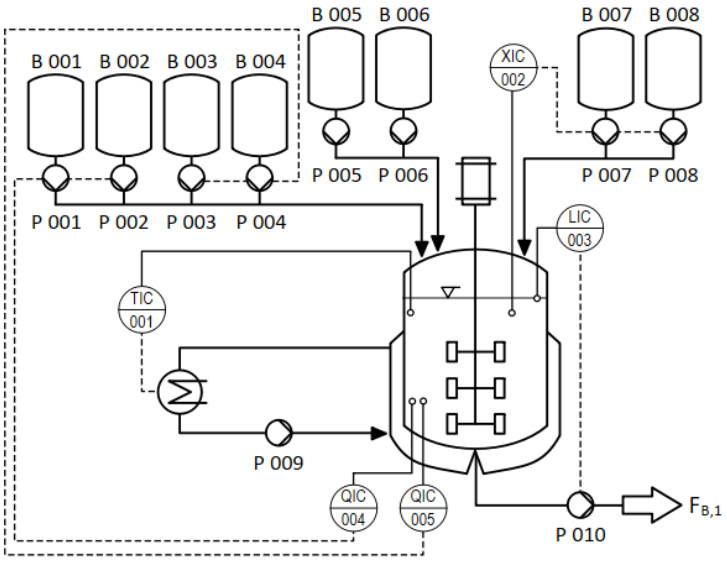

Label	Description
B 001	E1 (Termamyl SC) – P1
B 002	E2 (Spirizyme Ultra) – P1
B 003	E1 (EnerZyme P7) – P2
B 004	E2 (Flavourzyme) – P2
B 005	S (Potato starch) – P1
B 006	S (Sunflower protein) – P2
B 007	Acid – 20% w/v HCl
B 008	Base – 20% w/v KOH
TIC 001	Temperature control
XIC 002	pH control
LIC 003	Level control
QIC 004	Product conc. control – P1
QIC 005	Product conc. control – P2

Figure 35: P&ID flowchart of the stand-alone digital twin for enzymatic hydrolysis processes in an STR.

The volume level in the reactor is controlled via the outflow of broth from the reactor ($F_{B,1}$). The level control was implemented in the digital twin using a PI controller. The broth temperature in the reactor is controlled via the temperature of the heating fluid inflow to the reactor's heating jacket. The temperature control was implemented in the digital twin using a PI controller. Finally, the pH of the broth in the reactor is controlled via the inflow of acid (20% w/v HCl) and base (20% w/v KOH) to the reactor. The pH control was implemented in the digital twin using a PI controller.

Figure 36 shows the simulated results of the implemented PI temperature control with a setpoint change of 5 °C. The signal of $T_{B,m}$ was provided with measurement noise to make the behaviour of the stand-alone digital twin even more realistic.

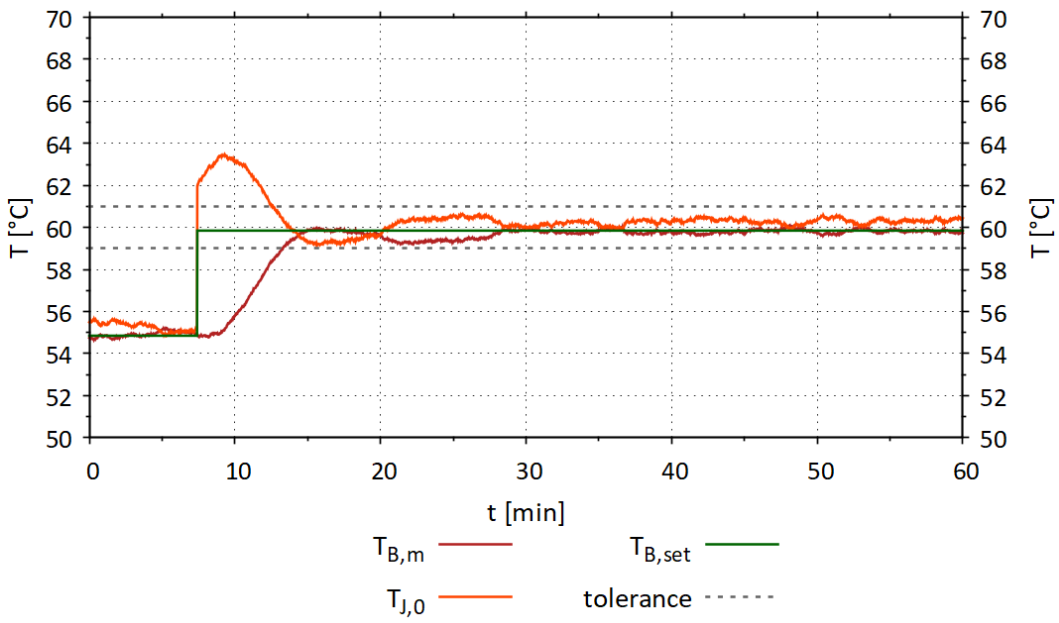

Figure 36: Simulation result of PI temperature control (Gain = 1.35, Ti = 420 s), with V_B = 10 L and inflow of heating fluid to the heating jacket $F_{J,0}$ = 40 L min^{-1}. $T_{B,m}$ = measured broth temperature in the reactor, $T_{B,set}$ = setpoint for the temperature of broth in the reactor, $T_{J,0}$ = temperature of the heating fluid in the inflow to the heating jacket.

To check the quality of the implemented PI temperature control, the setpoint for the temperature of the broth was increased from 55 °C to 60 °C. After a rise time of approx. 390 s, $T_{B,m}$ reached the setpoint for the first time. Since the tolerance range is not left afterwards, the rise time corresponds to the settling time. No overshoot of $T_{B,m}$ was observed.

Furthermore, standard controls for product concentration control (glucose and free amino acids) have been implemented in the stand-alone digital twin for enzymatic hydrolysis processes in an STR. For the realisation of these controls, it was assumed that there is an online signal for the product concentrations.

Figure 37 shows how the developed PID starch hydrolysis product concentration control responded to broth temperature changes (T_B). The product concentration is controlled by the inflows of the enzyme solutions (F_{E1} and F_{E2}).

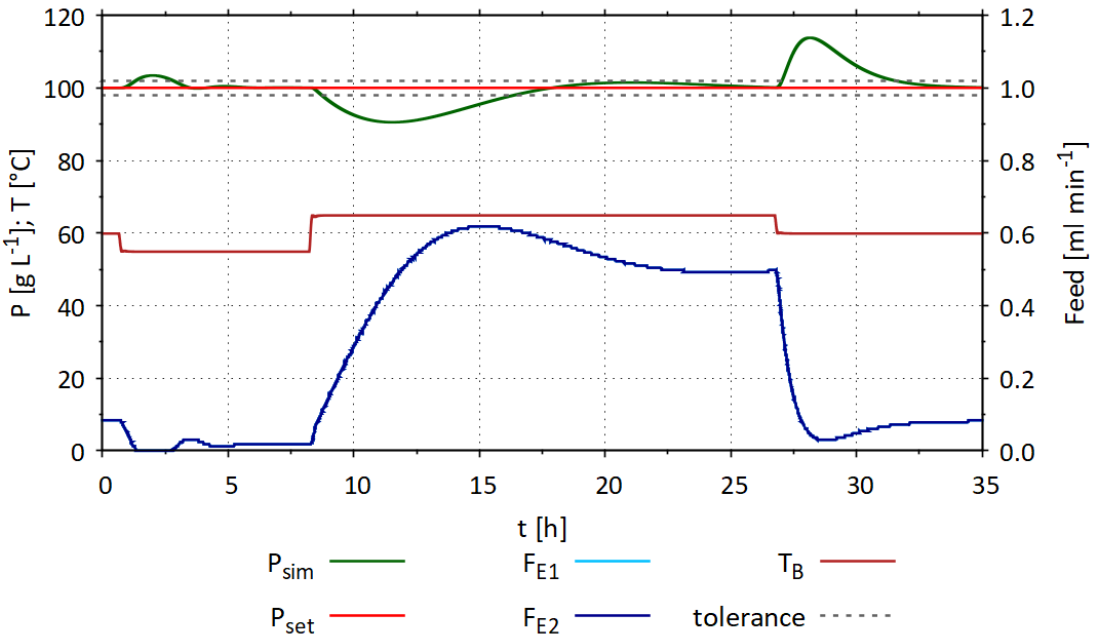

Figure 37: Simulation result of a continuous process in an STR, with PID starch hydrolysis product concentration control (Gain = 5 e^{-10}, T_i = 8000 s, T_d = 900 s) and V = 10 L. P_{sim} = measured product concentration, P_{set} = setpoint for the product concentration, F_{E1} = inflow of α-amylase solution to the reactor, F_{E2} = inflow of glucoamylase solution to the reactor.

The setpoint for the product concentration control was set to 100 g L^{-1}. A decrease in temperature after a processing time of 1 h led to a slight overshoot of the product concentration, which the controller could compensate for after a processing time of 5 h. After a processing time of 8 h, the temperature was increased from 55 to 65 °C, which caused the product concentration to drop below 90 g L^{-1}. It took the controller approx. 17 h to stabilise the product concentration at 100 g L^{-1} again. After a processing time of 27 h, the temperature was set to 60 °C again, which caused the product concentration to overshoot to over 110 g L^{-1}. After another 8 h, the product concentration stabilised at 100 g L^{-1}.

The scenario simulated using the stand-alone digital twin for enzymatic hydrolysis processes in an STR shows clearly how temperature and product concentration control affect each other. Especially in continuous processes with a high reactor volume, even small changes in the broth's temperature can significantly change the formation of the product. Developing a product concentration control on the existing system for this case is only possible with great effort. Therefore, the use of the digital twin can be beneficial here.

5.2 Precursor of a stand-alone digital twin for enzymatic hydrolysis processes in a packed bed flow tube reactor

Figure 38 shows the model structure of a stand-alone digital twin for enzymatic hydrolysis processes in a PBR. The stand-alone digital twin can map the enzymatic hydrolysis processes in a PBR with l_{PBR} = 0.03 m, d_{PBR} = 0.003 m and V_{PBR} = 0.212 mL. To reflect the conditions in the PBR, a cascade of ten modified STRs with l_{STR} = 0.003 m, d_{STR} = 0.003 m and V_{STR} = 0.0212 mL was created in the reactor submodel of the stand-alone digital twin.

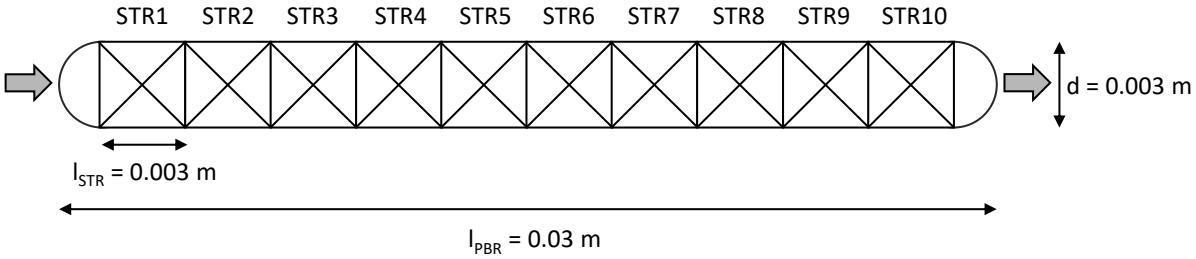

Figure 38: Reactor model structure of the stand-alone digital twin for enzymatic hydrolysis processes in a PBR (ten connected STRs) with immobilised enzymes.

It was assumed, that the enzymes are immobilised on a carrier substance retained in the individual STRs. The carrier substance was assumed to take up 75% of the volume in the PBR. This results in a $V_{PBR,free}$ = 0.053 mL. The ideally mixed substrate solution passes through the STRs. In addition, back mixing between the individual STRs can be simulated to approximate non-ideal flow behaviour. Each STR model uses the same biokinetic and physico-chemical submodel with only one set of parameters.

The developed strategy for mapping a PBR model by coupling several STR models was validated using a model representing the enzymatic regeneration of cytidine triphosphate (CTP) from cytidine diphosphate (CDP) in a PBR (Arndt, 2022). The PBR model was realised using partial differential equations and validated based on experimental data. The equations used in the model for the enzymatic regeneration of CTP from CDP in a PBR were transferred to the PBR model with coupled STR models. Subsequently, various process scenarios were simulated using the two models. Comparing the simulated results showed an agreement between the models of over 80%.

A scenario for the combined starch hydrolysis and proteolysis was simulated with the new stand-alone digital twin for enzymatic hydrolysis processes in a PBR. The PBR contained 30 g L^{-1} α-amylase, 20 g L^{-1} glucoamylase, 50 g L^{-1} endopeptidase and 50 g L^{-1} exopeptidase. The substrate solution (pH = 6) containing 50 g L^{-1} potato starch (90% hydrolysable) and 50 g L^{-1} sunflower seed meal (8.5 g L^{-1} hydrolysable, 34.0 g L^{-1} non-hydrolysable, 7.5 g L^{-1} product) continuously passed through the PBR. The temperature in the PBR was set to 60 °C.

Figure 39 shows the start-up phase of a continuous starch hydrolysis process in a PBR, simulated with the developed stand-alone digital twin.

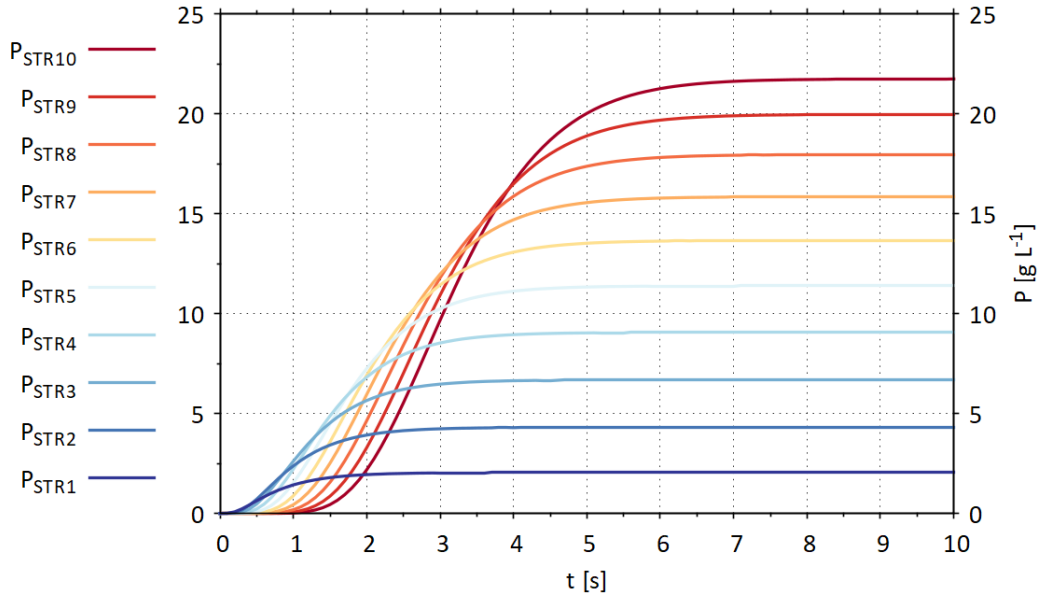

Figure 39: Simulation results of starch hydrolysis (P1) in ten connected STRs (STR_1-STR_{10}) representing a PBR (l = 0.03 m, d = 0.003 m), with T = 60 °C, pH = 6, $c_{E1,P1}$ = 30 g L^{-1}, $c_{E2,P1}$ = 20 g L^{-1}, inflow of substrate solution = 1 mL min^{-1} (50 g L^{-1} potato starch (90% hydrolysable), back mixing = 0.1 mL min^{-1} and outflow of 1 mL min^{-1}. P: product (glucose) concentration. Set of parameters used for simulation: Par_{Optim}.

After a processing time of approx. 4 s, almost stationary conditions with a product concentration of approx. 2 g L^{-1} are reached in STR_1. After a processing time of approx. 9 s, almost stationary conditions with a product concentration of approx. 22 g L^{-1} are reached in STR_{10}.

The product concentration increases over the length of the PBR from STR_1 with a product concentration of approx. 2.0 g L^{-1} to STR_{10} with a product concentration of approx. 22 g L^{-1}.

Figure 40 shows the start-up phase of a continuous proteolysis process in a PBR, simulated with the developed stand-alone digital twin.

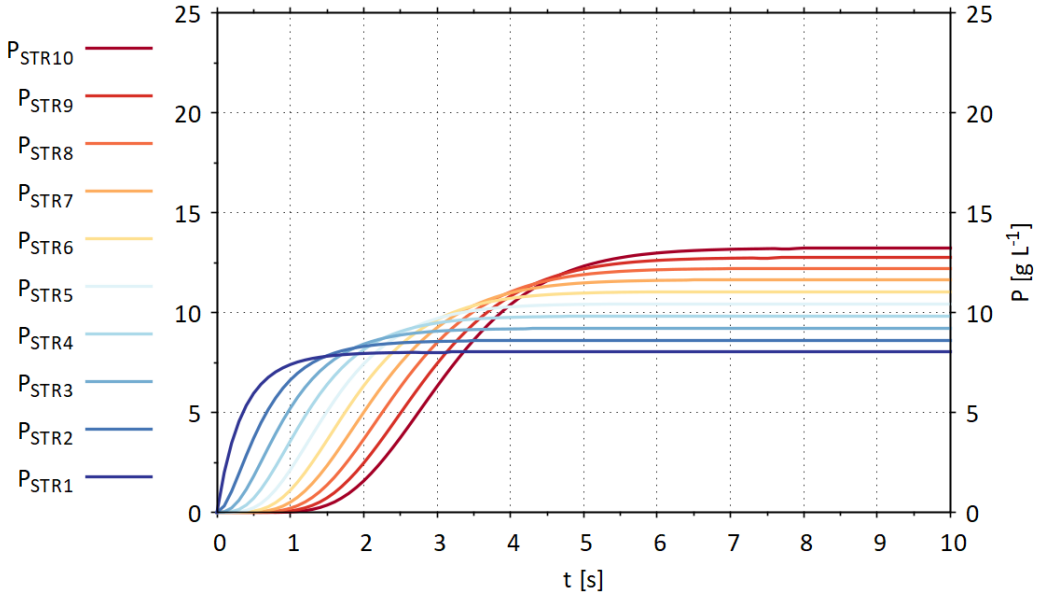

Figure 40: Simulation results of proteolysis (P2) in ten connected STRs representing a PBR (l = 0.03 m, d = 0.003 m), with T = 60 °C, pH = 6, c_{E1} = 50 g L^{-1}, c_{E2} = 50 g L^{-1}, inflow of substrate solution = 1 mL min^{-1} (50 g L^{-1} sunflower seed meal (8.5 g L^{-1} hydrolysable, 34.0 g L^{-1} non-hydrolysable, 7.5 g L^{-1} product)), back mixing = 0.1 mL min^{-1} and outflow of 1 mL min^{-1}. P: product (glucose) concentration. Set of parameters used for simulation: Par_{Optim}.

After a processing time of about 2 s, almost stationary conditions with a product concentration of approx. 8 g L^{-1} were reached in STR_1. After a processing time of about 9 s, almost stationary conditions with a product concentration of approx. 13 g L^{-1} were reached in STR_{10}. The product concentration increased over the length of the PBR from STR_1 with a product concentration of approx. 8 g L^{-1}, over STR_5 with a product concentration of approx. 11 g L^{-1} to STR_{10} with a product concentration of approx. 13 g L^{-1}.

5.3 Discussion

The developed model for enzymatic hydrolysis processes was implemented in the digital twin core model of a stand-alone digital twin (operator training simulator) of a 20 L STR. The new stand-alone digital twin can represent the enzyme kinetics, as well as the behaviour of a 20 L STR (e.g., temperature) with plant, periphery (e.g., pumps) and control (e.g., level, temperature, pH).

Standard controls for level, temperature and pH were implemented in the stand-alone digital twin for enzymatic hydrolysis processes and optimised based on simulations. As a result, the digital twin is now able to reproduce the control behaviour in a similar way to the existing system.

In addition, the stand-alone digital twin could be used to design precursors of PID product concentration controls for the enzymatic hydrolysis processes.

Furthermore, the digital twin core model of the new stand-alone digital twin for enzymatic hydrolysis processes in a 20 L STR was successfully integrated into a newly developed PBR reactor model. The now available precursor of a stand-alone digital twin can map enzymatic hydrolysis processes in a PBR with immobilised enzymes and can be used for model-based process optimisation. With the help of the stand-alone digital twin of a PBR, future experiments can be planned to determine the enzyme stability under different process conditions (temperature, pH). Decreased enzyme activity affects substrate conversion to product in starch hydrolysis and proteolysis. The enzyme denaturation constant can be identified by determining the substrate and product concentrations throughout the process.

The new stand-alone digital twins are an ideal tool for developing, testing and optimising process control and design strategies. Moreover, they are perfectly suitable for training in control engineering. The parameterisation of the implemented controllers can be changed directly via the GUI of the digital twin, and thus the resulting changes to the system can be observed. Such an investigation of the existing system is only possible with a high investment of resources and time.

6 Model-based design and optimisation of enzymatic hydrolysis processes

The processing time is relatively short in enzymatic batch processes due to the high reaction rates. An adjustment of the control strategy by the OLFO strategy on the running process is, therefore, challenging to implement. However, it is possible to use the OLFO strategy to design successive batch processes.

To use the OLFO strategy for the design of successive batch processes, the model is adapted based on the previous batch process, and the subsequent batch process is designed to achieve the best result. This becomes particularly interesting when there are large fluctuations in the quality of the substrates or enzymes. This is often the case, especially in processes using organic resources.

Starch hydrolysis and proteolysis were optimised separately since these processes are also conducted separately in reality. If the products from the enzymatic hydrolysis processes are to be used as a nutrient medium, e.g., for cultivating *S. cerevisiae*, they must be autoclaved in advance. Excessive heating of carbon (sugar) and nitrogen (free amino acids) sources can lead to the Maillard reaction, which causes the colour and properties of the nutrient medium to change (Hodge, 1953; Maillard, 1912).

The developed OLFO controller (Section 3.6.2) was applied to optimise enzymatic hydrolysis batch processes in an STR. In addition, parts of the "mDoE toolbox" (Section 3.6.3) were used to validate the result of the OLFO controller. OLFO and mDoE used the digital twin core model of the new stand-alone digital twin for enzymatic hydrolysis processes in an STR. For process optimisation, a desirability score (*DS)* was defined (Equation 30). The optimisation aimed to maximise *DS*.

$$DS = w_P \cdot P_1 - (w_S \cdot S_{Start} + w_{IP} \cdot IP_1 + w_{E1} \cdot E1_1 + w_{E2} \cdot E2_1) \qquad (30)$$

The *DS* describes the difference between the product generated (P_1), the substrate (S_{Start}), and the enzymes used for production. For the concentrations of the enzymes, the values at the end of the processing time were used since enzyme denaturation has hardly any effect on the enzyme concentrations at a processing time of less than 5 h. Furthermore, the final concentration of the intermediate product (IP_1) is subtracted. The concentrations in the *DS* can be weighted differently by specific weighting factors (*w*). For example, the price of the substrate, the product or the enzymes can be considered.

6.1 Model-based design and optimisation of a starch hydrolysis batch process in a stirred tank reactor

At the beginning of the process optimisation, the general conditions of the starch hydrolysis batch process were defined. The fixed settings for optimising the process were V_{Start} = 3.0 L, S_{Start} = 45 g L^{-1}, T = 60 °C, pH = 4.15, N_{Stirr} = 300 rpm and t = 180 min. Potato starch was used as substrate.

The control variables to be optimised were the addition of the enzymes Termamyl SC (F_{E1}) and Spirizyme Ultra (F_{E2}) after a processing time of 15 min. The limits for adding enzymes were set to 0.0-1.0 mL for F_{E1} and 0.1-0.4 mL for F_{E2}. The model-based process optimisation aimed at producing the maximum amount of product with the least possible use of enzymes.

To determine the DS_{SH} for starch hydrolysis optimisation, mDoEs were carried out and the response surfaces were analysed.

For $DS_{SH,1}$, the concentration $E1_1$ and $E1_2$ were weighted equally with a value of 1000 (Equation 31).

$$DS_{SH,1} = 50 \cdot P_1 - (20 \cdot 45 + 1 \cdot IP_1 + 1000 \cdot E1_1 + 1000 \cdot E2_1) \quad (31)$$

In the first mDoE, $DS_{SH,1}$ was calculated for 1000 equally distributed points in the DoE design space. For $DS_{SH,1}$, the mDoE resulted in the response surface shown in Figure 41.

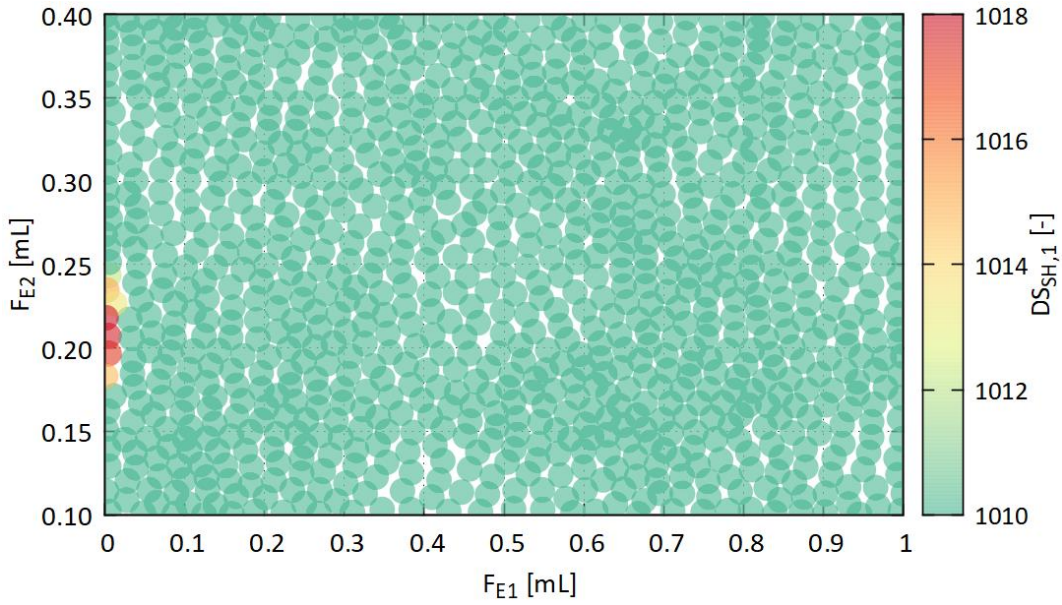

Figure 41: Results of the first mDoE performed for an enzymatic starch hydrolysis batch experiment. $DS_{SH,1}$ with w_{E1} = 1000 and w_{E2} = 1000. V_{start} = 3.0 L, $c_{substrate,start}$ = 45 g L^{-1}, T = 60 °C, pH = 4.15 and N_{Stirr} = 300 rpm. Addition of 0.0-1.0 mL Termamyl SC (F_{E1}) and 0.1-0.4 mL Spirizyme Ultra (F_{E2}) after a processing time of 15 min. Set of parameters used for simulation: Par_{Optim}.

Weighting $E1_1$ and $E2_1$ with a value of 1000 results in the optimum of $DS_{SH,1}$ for F_{E1} = 0.000-0.010 mL and F_{E2} = 0.190-0.220 mL. F_{E2} (Spirizyme Ultra) also contains approx. 30% of $E1_1$. If $E1_1$ is weighted too high, adding F_{E1} is not profitable, as seen in the response surface of the mDoE. For this reason, the weighting of $E1_1$ was reduced from 1000 to 1.

For $DS_{SH,2}$, the concentration $E1_1$ was weighted at 1 and $E2_1$ with 1000 (Equation 32).

$$DS_{SH,2} = 50 \cdot P_1 - (20 \cdot 45 + 1 \cdot IP_1 + 1 \cdot E1_1 + 1000 \cdot E2_1) \quad (32)$$

In the second mDoE, $DS_{SH,2}$ was calculated for 1000 equally distributed points in the DoE design space. For $DS_{SH,2}$, the mDoE resulted in the response surface shown in Figure 42.

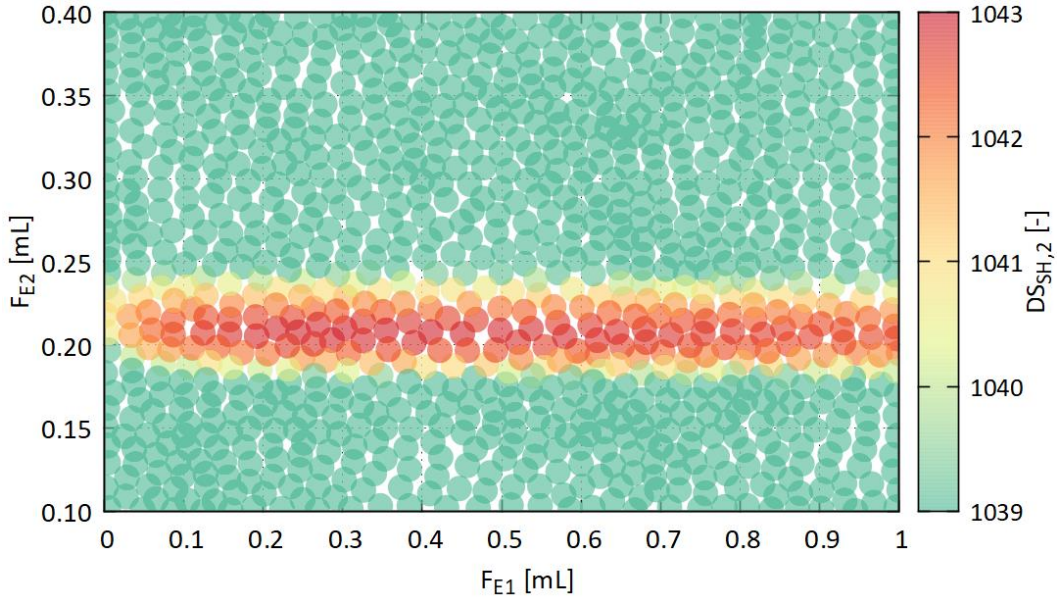

Figure 42: Results of the second mDoE performed for an enzymatic starch hydrolysis batch experiment. $DS_{SH,2}$ with w_{E1} = 1 and w_{E2} = 1000. V_{start} = 3.0 L, $c_{substrate,start}$ = 45 g L^{-1}, T = 60 °C, pH = 4.15 and N_{Stirr} = 300 rpm. Addition of 0.0-1.0 mL Termamyl SC (F_{E1}) and 0.1-0.4 mL Spirizyme Ultra (F_{E2}) after a processing time of 15 min. Set of parameters used for simulation: Par_{Optim}.

Weighting $E1_1$ with a value of 1 leads to a very long-drawn-out optimum for F_{E1} between 0.020 and 1.000 mL. Due to the low weighting, F_{E1} thus has little effect on $DS_{SH,2}$. Therefore, the only decisive factor here was F_{E2} in the range of 0.220 to 0.230 mL. For this reason, the weighting of $E1_1$ was increased from 1 to 10.

For $DS_{SH,3}$, the concentration $E1_1$ was weighted with a value of 10 and $E2_1$ with 1000 (Equation 33).

$$DS_{SH,3} = 50 \cdot P_1 - (20 \cdot 45 + 1 \cdot IP_1 + 10 \cdot E1_1 + 1000 \cdot E2_1) \quad (33)$$

In the third mDoE, $DS_{SH,3}$ was calculated for 1000 equally distributed points in the DoE design space. For $DS_{SH,3}$, the mDoE resulted in the response surface shown in Figure 43.

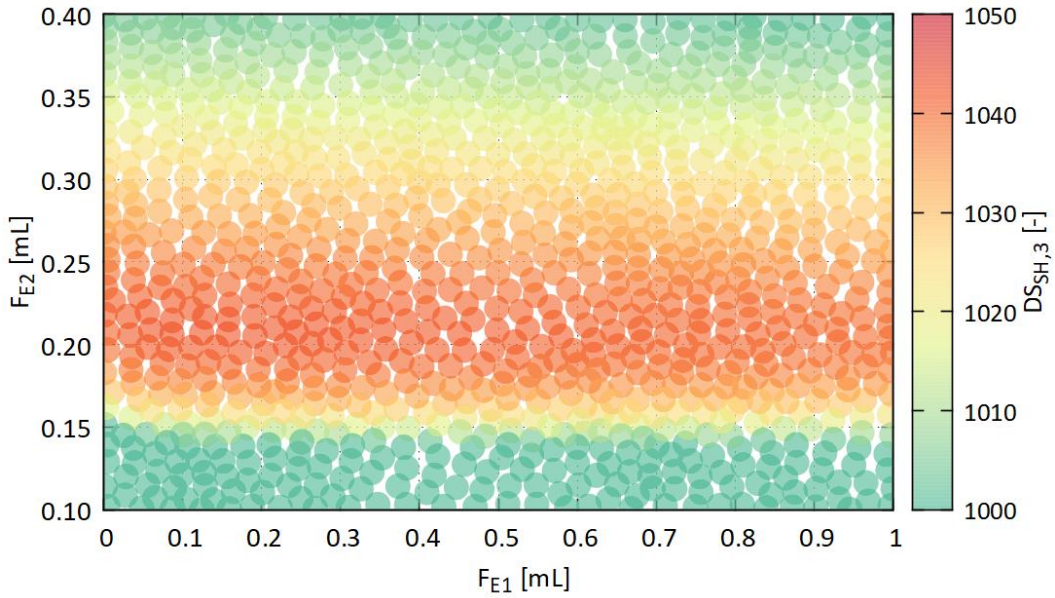

Figure 43: Results of the third mDoE performed for an enzymatic starch hydrolysis batch experiment. $DS_{SH,3}$ with w_{E1} = 10 and w_{E2} = 1000. V_{start} = 3.0 L, $c_{substrate,start}$ = 45 g L^{-1}, T = 60 °C, pH = 4.15 and N_{Stirr} = 300 rpm. Addition of 0.0-1.0 mL Termamyl SC (F_{E1}) and 0.1-0.4 mL Spirizyme Ultra (F_{E2}) after a processing time of 15 min. Set of parameters used for simulation: Par_{Optim}.

To highlight the points of optimal conditions, the resolution of $DS_{SH,3}$ was changed from 1000-1050 to 1038-1042 (Figure 44).

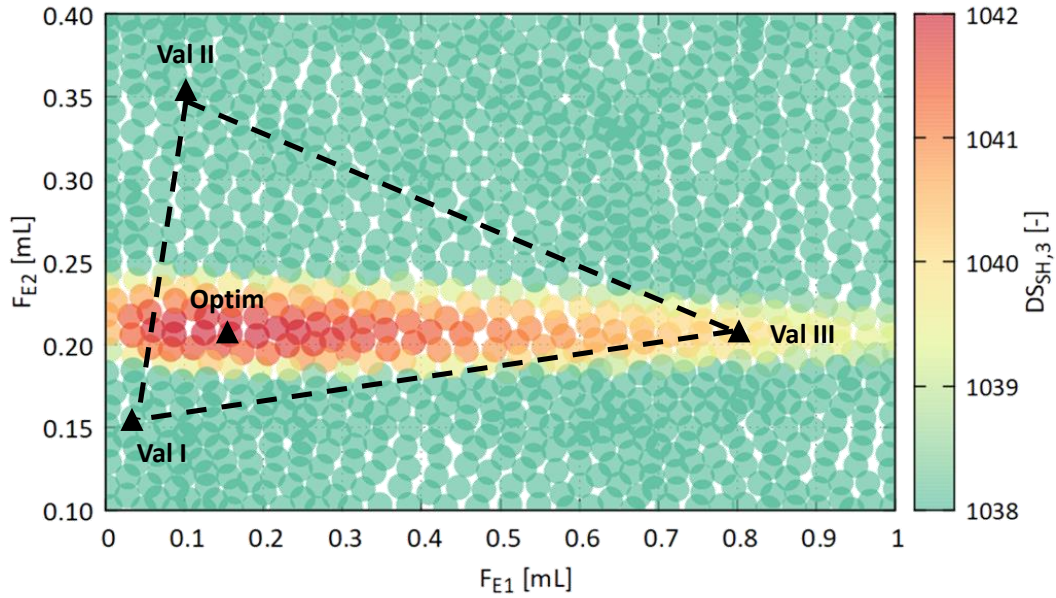

Figure 44: Results of the third mDoE performed for an enzymatic starch hydrolysis batch experiment. $DS_{SH,3}$ with w_{E1} = 10 and w_{E2} = 1000. V_{start} = 3.0 L, $c_{substrate,start}$ = 45 g L^{-1}, T = 60 °C, pH = 4.15 and N_{Stirr} = 300 rpm. Addition of 0.0-1.0 mL Termamyl SC (F_{E1}) and 0.1-0.4 mL Spirizyme Ultra (F_{E2}) after a processing time of 15 min. Set of parameters used for simulation: Par_{Optim}.

A weighting of $E1_1$ with 10 leads to a much clearer optimum of F_{E1} = 0.050-0.300 mL and F_{E2} = 0.220-0.230 mL.

To determine the absolute optimum, the now-determined $DS_{SH,3}$ was used for the optimisation with the OLFO controller. The optimisation part of the OLFO controller determined the highest $DS_{SH,3}$ with a value of 1042.115 for F_{E1} = 0.142 mL and F_{E2} = 0.208 mL. Sixty-two iterations were needed to determine the result.

Based on the results from the mDoE (Figure 44), three experiments were planned to validate the optimised process conditions determined by the optimisation part of the OLFO controller (Table 8).

Table 8: Starch hydrolysis batch experiments planned based on the mDoE result.

Experiment	$S_{t = 0\ min}$ [g L^{-1}]	F_{E1} [ml]	F_{E2} [ml]	$DS_{SH,3}$
Optimised (Optim)	45.00	0.142	0.208	1042.115
Validation I (Val I)	45.00	0.025	0.150	1006.094
Validation II (Val II)	45.00	0.100	0.350	1015.425
Validation III (Val III)	45.00	0.800	0.210	1039.991

Before the experiments (Optim, Val I, Val II, Val III) were carried out, they were pre-simulated with the new model for enzymatic hydrolysis processes. To verify whether a statement can be made after the execution of the experiments on whether the optimised experiment delivers the best results, the simulation courses of the validation experiments were compared with the simulated course of the optimised experiment (Figure 45).

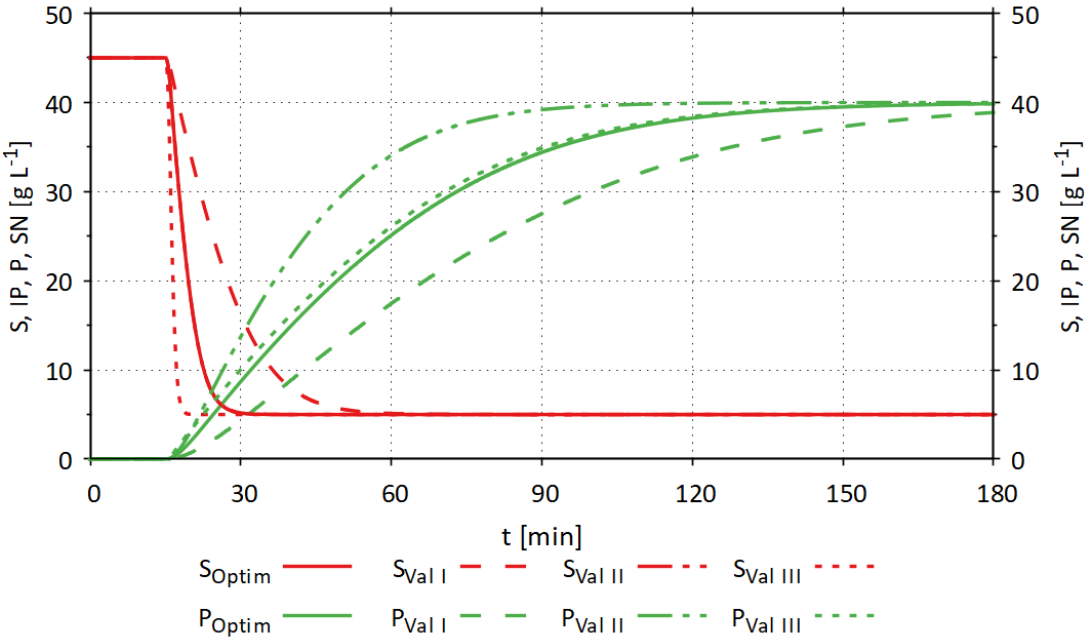

Figure 45: Simulation results of the validation (Val I, Val II, Val III) and optimised (Optim) starch hydrolysis batch experiments. V_{start} = 3.0 L, $c_{substrate,start}$ = 45 g L^{-1}, T = 60 °C, pH = 4.15 and N_{Stirr} = 300 rpm. Addition of 142 µL (Optim), 25 µL (Val I), 100 µL (Val II), 800 µL (Val III) Termamyl SC and 208 µL (Optim), 150 µL (Val I), 350 µL (Val II), 210 µL (Val III) Spirizyme Ultra after a processing time of 15 min. S: substrate (potato starch) concentration, P: product (glucose) concentration. Set of parameters used for simulation: Par_{Optim}.

In all planned experiments, the simulated substrate concentration started at a value of approx. 45 g L^{-1}. In the optimised experiment (Optim), the minimum simulated substrate concentration of approx. 5 g L^{-1} is reached after a processing time of 30 min, in the first validation experiment (Val I) after a processing time of 60 min, in the second validation experiment (Val II) after a processing time of 30 min and in the third validation experiment (Val III) after a processing time of 20 min.

In all experiments, the simulated product concentration started at a value of approx. 0.00 g L^{-1}. After a processing time of approx. 180 min, the simulated product concentration reached the maximum value of 39.85 g L^{-1} in the optimised experiment (Optim), 38.87 g L^{-1} in the first validation experiment (Val I), 39.99 g L^{-1} in the second validation experiment (Val II) and 39.86 g L^{-1} in the third validation experiment (Val III).

6.1.1 Experimental validation of the optimised starch hydrolysis batch process in a stirred tank reactor

The experiments shown in Table 9 were carried out to validate the optimised starch hydrolysis batch process.

Table 9: Starch hydrolysis batch experiments in a 6 L STR.

Experiment	$S_{t = 0\ min}$ [g L^{-1}]	F_{E1} [ml]	F_{E2} [ml]
Optimised (Optim)	45.00	0.142	0.208
Validation I (Val I)	45.00	0.025	0.150
Validation II (Val II)	45.00	0.100	0.350
Validation III (Val III)	45.00	0.800	0.210

Figure 46 presents the comparison of the experimental and simulated results of the optimised starch hydrolysis batch process. Here, 0.142 mL of Termamyl SC and 0.208 mL of Spirizyme Ultra were added to the reactor after a processing time of 15 min. The initial substrate concentration was adjusted to the experimentally determined data for the post-simulation with the model.

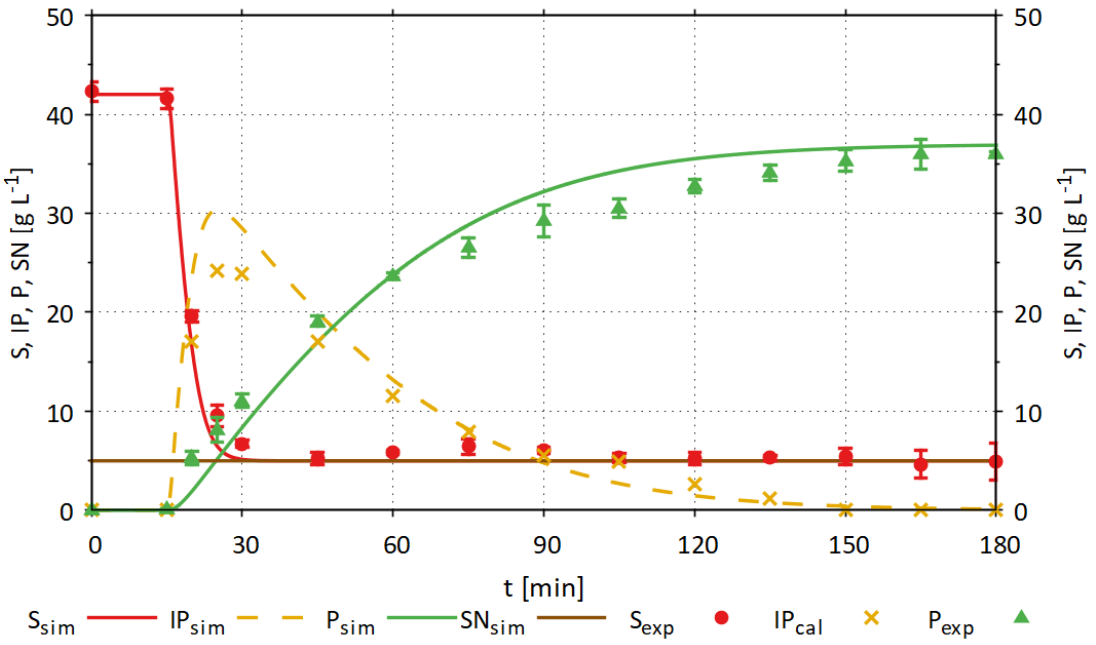

Figure 46: Comparison between simulation (index: sim) and experimental (index: exp) results of the optimised starch hydrolysis batch experiment (Optim), with $R^2_{substrate}$ = 0.989 and $R^2_{product}$ = 0.970. V_{start} = 3.0 L, $c_{substrate,start}$ = 42.29 g L^{-1}, T = 60 °C, pH = 4.15 and N_{Stirr} = 300 rpm. Addition of 0.142 mL Termamyl SC and 0.208 mL Spirizyme Ultra after a processing time of 15 min. S: substrate (potato starch) concentration, IP: intermediate product concentration, P: product (glucose) concentration, SN: concentration of the non-hydrolysable components of the substrate. Error bars represent the mean value ± of one standard deviation resulting from a double determination. Set of parameters used for simulation: Par_{Optim}.

The measured substrate concentration started at a value of 42.29 g L^{-1}. After a processing time of approx. 30 min, the measured substrate concentration decreased to a value of approx. 7 g L^{-1}. After a processing time of 180 min, the measured substrate concentration reached the minimum value of 4.90 g L^{-1}. The product concentration started at a value of approx. 0 g L^{-1}. After adding Termamyl SC and Spirizyme Ultra (t = 15 min) up to a processing time of 180 min, the measured product concentration increased to a maximum value of 36.02 g L^{-1}.

The substrate and product concentration curves simulated by the model reproduce the measured values with $R^2_{substrate}$ = 0.989 and $R^2_{product}$ = 0.970.

Figure 47 presents the comparison of the experimental and simulated results of the first validation starch hydrolysis batch process (Val I). Here, 0.025 mL of Termamyl SC and 0.150 mL Spirizyme Ultra were added to the reactor after a processing time of 15 min.

The initial substrate concentration was adjusted to the experimentally determined data for the post-simulation with the model.

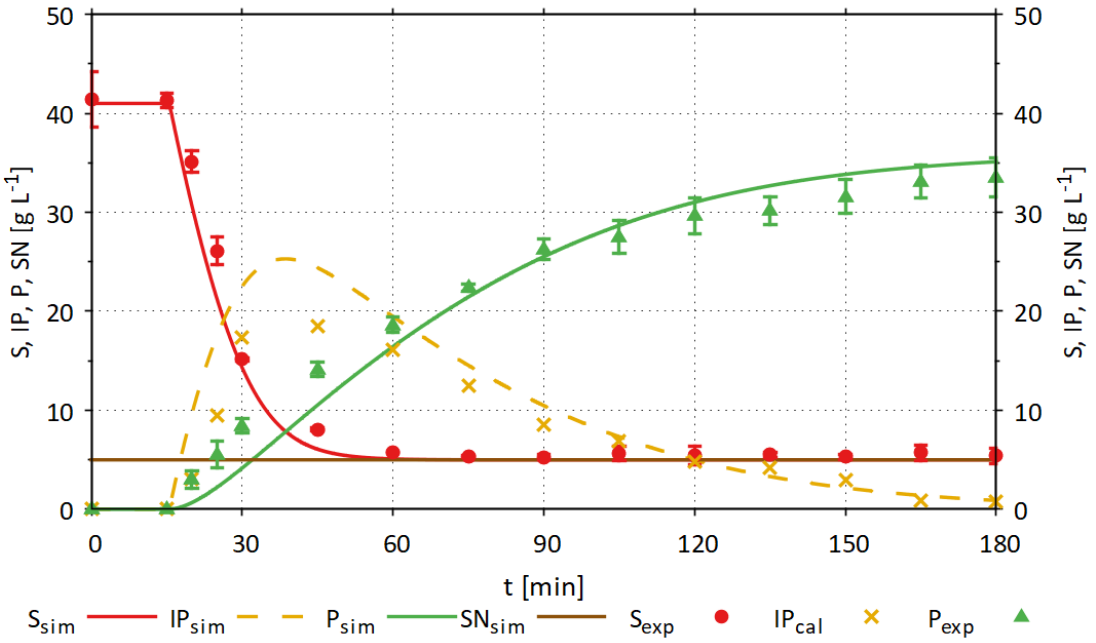

Figure 47: Comparison between simulation (index: sim) and experimental (index: exp) results of the first validation starch hydrolysis batch experiment (Val I), with $R^2_{substrate}$ = 0.982 and $R^2_{product}$ = 0.967. V_{start} = 3.0 L, $c_{substrate,start}$ = 41.40 g L^{-1}, T = 60 °C, pH = 4.15 and N_{Stirr} = 300 rpm. Addition of 0.025 mL Termamyl SC and 0.150 mL Spirizyme Ultra after a processing time of 15 min. S: substrate (potato starch) concentration, IP: intermediate product concentration, P: product (glucose) concentration, SN: concentration of the non-hydrolysable components of the substrate. Error bars represent the mean value ± of one standard deviation resulting from a double determination. Set of parameters used for simulation: Par_{Optim}.

The measured substrate concentration started at a value of 41.40 g L^{-1}. After a processing time of approx. 60 min, the measured substrate concentration decreased to a value of approx. 6 g L^{-1}. After a processing time of 180 min, the measured substrate concentration reached the minimum value of 5.40 g L^{-1}. The product concentration started at a value of approx. 0 g L^{-1}. After adding Termamyl SC and Spirizyme Ultra (t = 15 min) up to a processing time of 180 min, the product concentration increased to a maximum value of 33.49 g L^{-1}.

The substrate and product concentration curves simulated by the model reproduce the measured values with $R^2_{substrate}$ = 0.982 and $R^2_{product}$ = 0.967.

Figure 48 presents the comparison of the experimental and simulated results of the second validation starch hydrolysis batch process (Val II). Here, 0.100 mL of Termamyl SC

and 0.350 mL Spirizyme Ultra were added to the reactor after a processing time of 15 min. The initial substrate concentration was adjusted to the experimentally determined data for the post-simulation with the model.

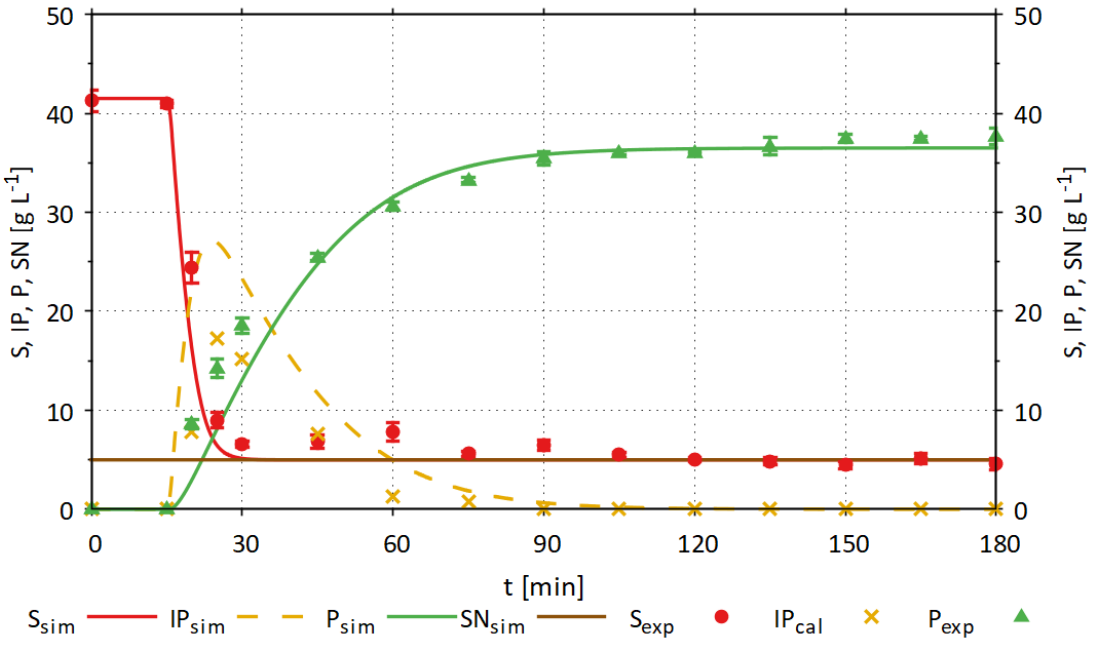

Figure 48: Comparison between simulation (index: sim) and experimental (index: exp) results of the second validation starch hydrolysis batch experiment (Val II), with $R^2_{substrate}$ = 0.960 and $R^2_{product}$ = 0.961. V_{start} = 3.0 L, $c_{substrate,start}$ = 41.26 g L^{-1}, T = 60 °C, pH = 4.15 and N_{Stirr} = 300 rpm. Addition of 0.100 mL Termamyl SC and 0.350 mL Spirizyme Ultra after a processing time of 15 min. S: substrate (potato starch) concentration, IP: intermediate product concentration, P: product (glucose) concentration, SN: concentration of the non-hydrolysable components of the substrate. Error bars represent the mean value ± of one standard deviation resulting from a double determination. Set of parameters used for simulation: Par_{Optim}.

The measured substrate concentration started at a value of 41.26 g L^{-1}. After a processing time of approx. 30 min, the measured substrate concentration decreased to a value of approx. 7 g L^{-1}. After a processing time of 180 min, the measured substrate concentration reached the minimum value of 4.56 g L^{-1}. The measured product concentration started at a value of approx. 0 g L^{-1}. After adding Termamyl SC and Spirizyme Ultra (t = 15 min) up to a processing time of 180 min, the measured product concentration increased to a maximum value of 37.68 g L^{-1}.

The substrate and product concentration curves simulated by the model reproduce the measured values with $R^2_{substrate}$ = 0.960 and $R^2_{product}$ = 0.961.

Figure 49 presents the comparison of the experimental and simulated results of the third validation starch hydrolysis batch process (Val III). Here, 0.800 mL of Termamyl SC and 0.210 mL Spirizyme Ultra were added to the reactor after a processing time of 15 min. The initial substrate concentration was adjusted to the experimentally determined data for the post-simulation with the model.

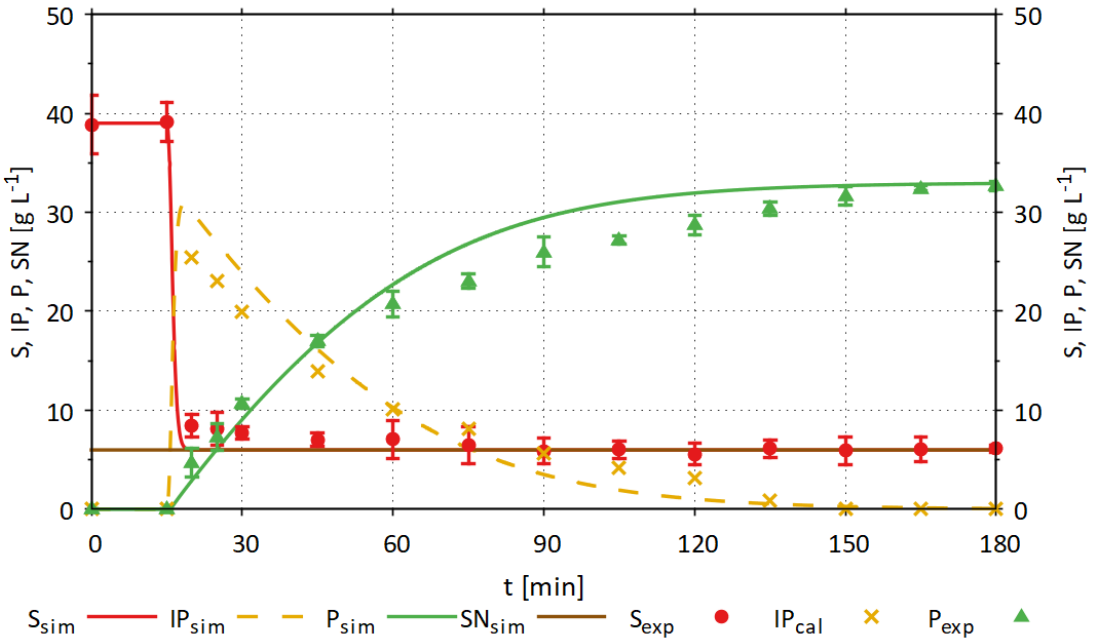

Figure 49: Comparison between simulation (index: sim) and experimental (index: exp) results of the third validation starch hydrolysis batch experiment (Val III), with $R^2_{substrate}$ = 0.991 and $R^2_{product}$ = 0.966. V_{start} = 3.0 L, $c_{substrate,start}$ = 38.86 g L^{-1}, T = 60 °C, pH = 4.15 and N_{Stirr} = 300 rpm. Addition of 0.800 mL Termamyl SC and 0.210 mL Spirizyme Ultra after a processing time of 15 min. S: substrate (potato starch) concentration, IP: intermediate product concentration, P: product (glucose) concentration, SN: concentration of the non-hydrolysable components of the substrate. Error bars represent the mean value ± of one standard deviation resulting from a double determination. Set of parameters used for simulation: Par_{Optim}.

The measured substrate concentration started at a value of 38.86 g L^{-1}. After a processing time of approx. 20 min, the measured substrate concentration decreased to a value of approx. 8 g L^{-1}. After 180 min, the measured substrate concentration reached the minimum value of 6.14 g L^{-1}. The measured product concentration started at a value of approx. 0 g L^{-1}. After adding Termamyl SC and Spirizyme Ultra (t = 15 min) up to a processing time of 180 min, the measured product concentration increased to the maximum value of 32.65 g L^{-1}.

The substrate and product concentration curves simulated by the model reproduce the measured values with $R^2_{substrate}$ = 0.991 and $R^2_{product}$ = 0.966.

Table 10 presents a comparison of the experimental results of the performed starch hydrolysis batch experiments.

Table 10: Summary of the starch hydrolysis batch experimental results.

Experiment	$S_{t = 0\ min}$ [g L^{-1}]	$S_{t = 180\ min}$ [g L^{-1}]	F_{E1} [ml]	F_{E2} [ml]	$IP_{cal,\ t = 180\ min}$ [g L^{-1}]	$P_{exp,\ t = 180\ min}$ [g L^{-1}]	$DS_{SH,3}$
Optim	42.29	4.90	0.142	0.208	0.00	36.02	904.64
Val I	41.40	5.40	0.025	0.150	0.82	33.49	809.48
Val II	41.26	4.56	0.100	0.350	0.00	37.68	974.19
Val III	38.86	6.14	0.800	0.210	0.00	32.65	802.00

After carrying out and evaluating all planned experiments, the experimental results of the optimised experiment for batch starch hydrolysis delivered the second highest $DS_{SH,3}$ with a value of 904.64. The highest experimental result for $DS_{SH,3}$ was achieved in the second validation experiment with a value of 974.19.

In the optimised experiment, the second highest product concentration of 36.02 g L^{-1} was obtained after 180 min. Here, 3.94 µL Termamyl SC and 5.78 µL Spirizyme Ultra were required to generate 1 g L^{-1} product. In the second validation experiment, where the highest product concentration of 37.68 g L^{-1} was achieved, 2.65 µL Termamyl SC and 9.29 µL Spirizyme Ultra were needed to generate 1 g L^{-1} product. 60% more Spirizyme Ultra was required to increase the product concentration by 1.66 g/L.

6.2 Model-based design and optimisation of a proteolysis batch process in a stirred tank reactor

At the beginning of the process optimisation, the general conditions of the proteolysis batch process were defined. The fixed settings for optimising the proteolysis batch process were V_{Start} = 3.0 L, S_{Start} = 50 g L^{-1}, T = 50 °C, pH = 7.50, N_{Stirr} = 300 rpm and t = 180 min. Organic sunflower seed meal (All Organic Treasures GmbH) was used as substrate.

The control variable to be optimised was the addition of the enzyme Flavourzyme (F_{E2}) after a processing time of 15 min. The limit for adding the enzyme was set to 0.0-5.0 mL. The model-based process optimisation aimed at producing the maximum amount of product with the lowest possible enzyme input.

For the verification of the DS_{PR} for proteolysis optimisation (Equation 34), a mDoE was carried out, and the response surface was analysed.

$$DS_{PR,1} = 150 \cdot P_1 - (25 \cdot 42.5 + 1 \cdot IP_1 + 500 \cdot E1_1 + 500 \cdot E2_1) \quad (34)$$

$DS_{PR,1}$ was calculated for 1000 equally distributed points in the DoE design space (F_{E2} = 0.0-5.0 mL). The result of the mDoE can be seen in Figure 50.

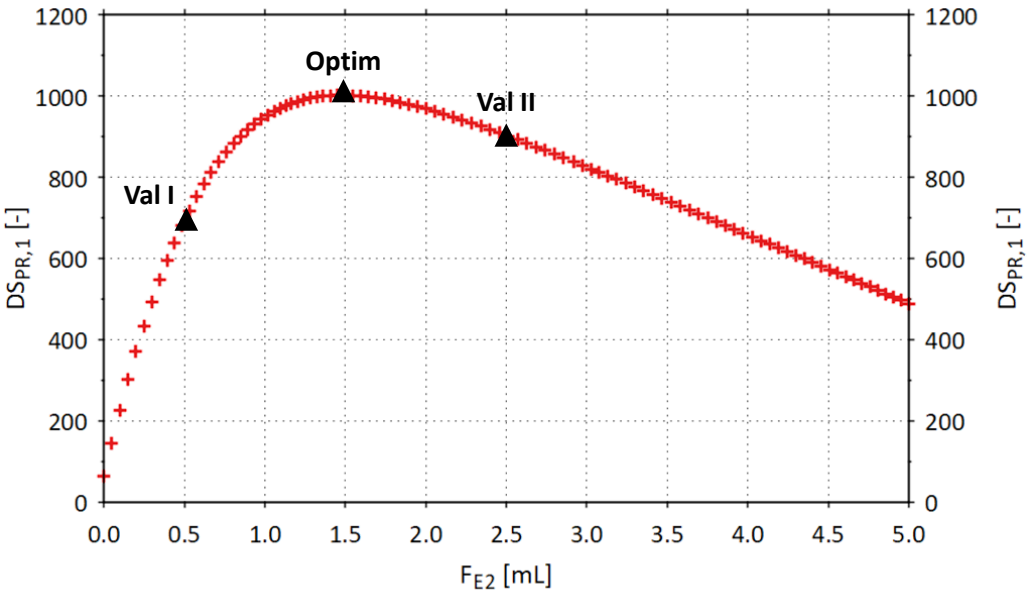

Figure 50: Results of mDoE performed for an enzymatic proteolysis batch experiment. V_{start} = 3.0 L, $c_{substrate,start}$ = 50 g L^{-1}, T = 50 °C, pH = 7.5 and NStirr = 300 rpm. Addition of 0.0-5.0 mL Flavourzyme (F_{E2}) after a processing time of 15 min. The total process time is 180 min. Set of parameters used for simulation: Par_{Optim}.

For F_{E2} = 0 mL, $DS_{PR,1}$ has the lowest value of approx. 30. If F_{E2} increases, $DS_{PR,1}$ increases until the maximum value of approx. 1000 is reached at F_{E2} = approx. 1.5 mL. With F_{E2} above 1.5 mL, $DS_{PR,1}$ decreases to a value of approx. 500 at F_{E2} = 5.0 mL.

To determine the absolute optimum, the determined $DS_{PR,1}$ (Equation 34) was used for the optimisation with the OLFO controller. The optimisation part of the OLFO controller determined the highest $DS_{PR,1}$ with 1001.69 for F_{E2} = 1.483 mL. Fifty-seven iterations were needed to determine the result.

Based on the result of the mDoE (Figure 50), two experiments were planned to validate the optimised experiment (Table 11).

Table 11: Proteolysis batch experiments planned based on mDoE result.

Experiment	**$S_{t = 0\ min}$ [g L^{-1}]**	**F_{E2} [ml]**	***$DS_{PR,1}$***
Optimised (Optim)	50.00	1.483	1001.69
Validation I (Val I)	50.00	0.500	693.19
Validation II (Val II)	50.00	2.500	902.24

Subsequently, the validation experiments were pre-simulated to see if a conclusion could be drawn about whether the optimised experiment was the best one based on the expected results. Figure 51 shows the pre-simulated results of the batch proteolysis experiment planned based on the result of the mDoE.

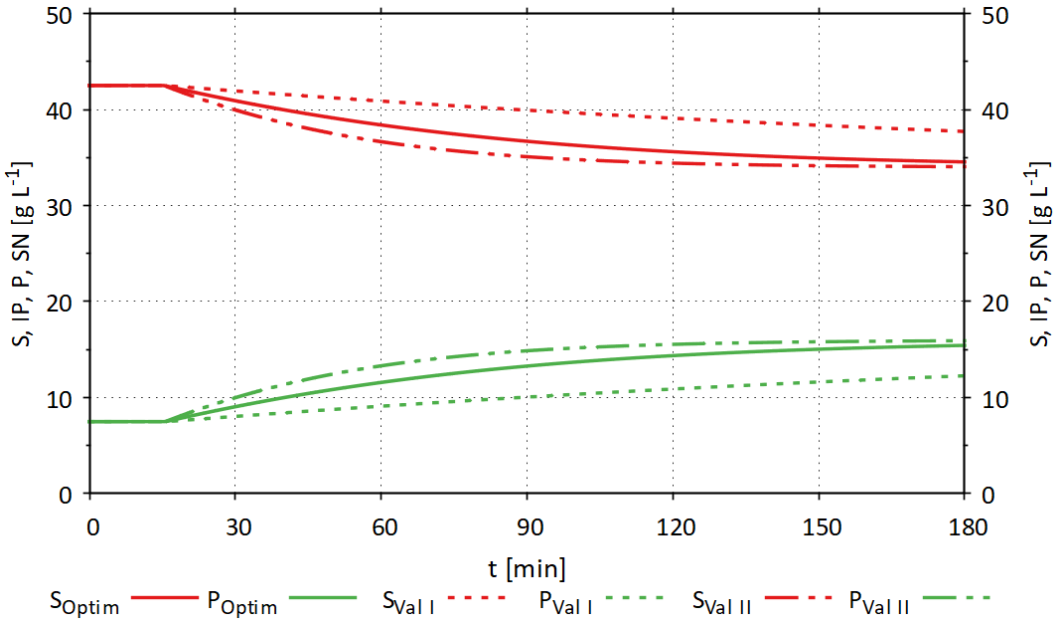

Figure 51: Simulation (index: sim) results of the optimised (Optim) and validation (Val I, Val II) proteolysis batch experiments, with V_{start} = 3.0 L, $c_{substrate,start}$ = 50 g L^{-1}, T = 50 °C, pH = 7.5 and N_{stirr} = 300 rpm. Addition of 1.483 mL (Optim), 0.500 mL (Val I) and 2.500 mL (Val II) Flavourzyme (E2) after a processing time of 15 min. S: substrate (protein) concentration, P: product (free amino acid) concentration. Set of parameters used for simulation: Par_{Optim}.

In all planned experiments, the simulated substrate concentration started at a value of approx. 42.5 g L^{-1}. After a processing time of approx. 180 min, the simulated substrate concentration reached the minimum value of 34.54 g L^{-1} in the optimised experiment (Optim), 37.71 g L^{-1} in the first validation experiment (Val I) and 34.04 g L^{-1} in the second validation experiment (Val II).

In all experiments, the simulated product concentration started at 7.50 g L^{-1}. After a processing time of approx. 180 min, the simulated product concentration reached the maximum value of 15.43 g L^{-1} in the optimised experiment (Optim), 12.27 g L^{-1} in the first validation experiment (Val I) and 15.92 g L^{-1} in the second validation experiment (Val II).

6.2.1 Experimental validation of the optimised proteolysis batch process in a stirred tank reactor

The experiments shown in Table 12 were carried out to validate the optimised proteolysis batch process.

Table 12: Proteolysis batch experiments in a 6 L STR.

Experiment	$S_{t = 0\ min}$ [g L^{-1}]	F_{E2} [ml]
Optimised (Optim)	50.00	1.483
Validation I (Val I)	50.00	0.500
Validation II (Val II)	50.00	2.500

Figure 52 compares the experimental results of the optimised (Optim) batch proteolysis experiment with the results simulated by the model. Here, 1.11 mL Flavourzyme was added to the STR after a processing time of 15 min.

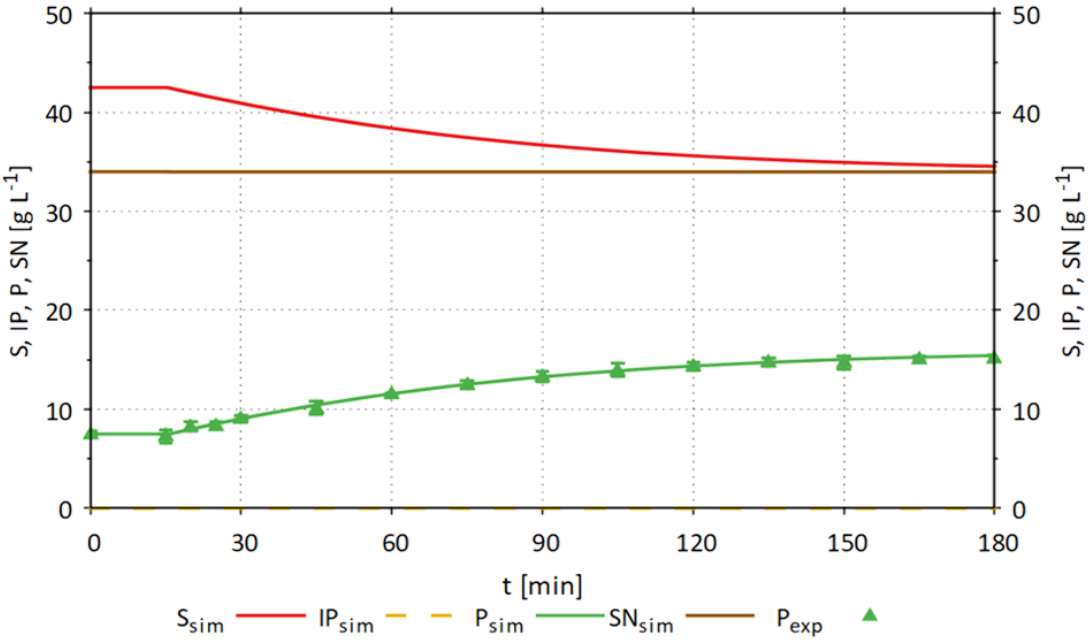

Figure 52: Comparison between simulation (index: sim) and experimental (index: exp) results of the optimised proteolysis batch experiment (Optim), with $R^2_{product}$ = 0.996. V_{start} = 3.0 L, $c_{substrate,start}$ = 50 g L^{-1}, T = 50 °C, pH = 7.5 and N_{stirr} = 300 rpm. Addition of 1.11 mL Flavourzyme (F_{E2}) after a processing time of 15 min. S: substrate (sunflower seed meal) concentration, IP: intermediate product concentration, P: product (free amino acid) concentration, SN: concentration of the non-hydrolysable components of the substrate. Error bars represent the mean value ± of one standard deviation resulting from a triple determination. Set of parameters used for simulation: Par_{Optim}.

The measured product concentration started at a value of 7.51 g L^{-1}. After a processing time of 180 min, the measured product concentration reached the maximum value of 15.15 g L^{-1}.

The curve of the product concentration simulated by the model reproduces the measured values with $R^2_{product}$ = 0.996.

Figure 53 compares the experimental results of the first validation (Val I) batch proteolysis experiment with the results simulated by the model. Here, 0.5 mL Flavourzyme was added to the STR after a processing time of 15 min.

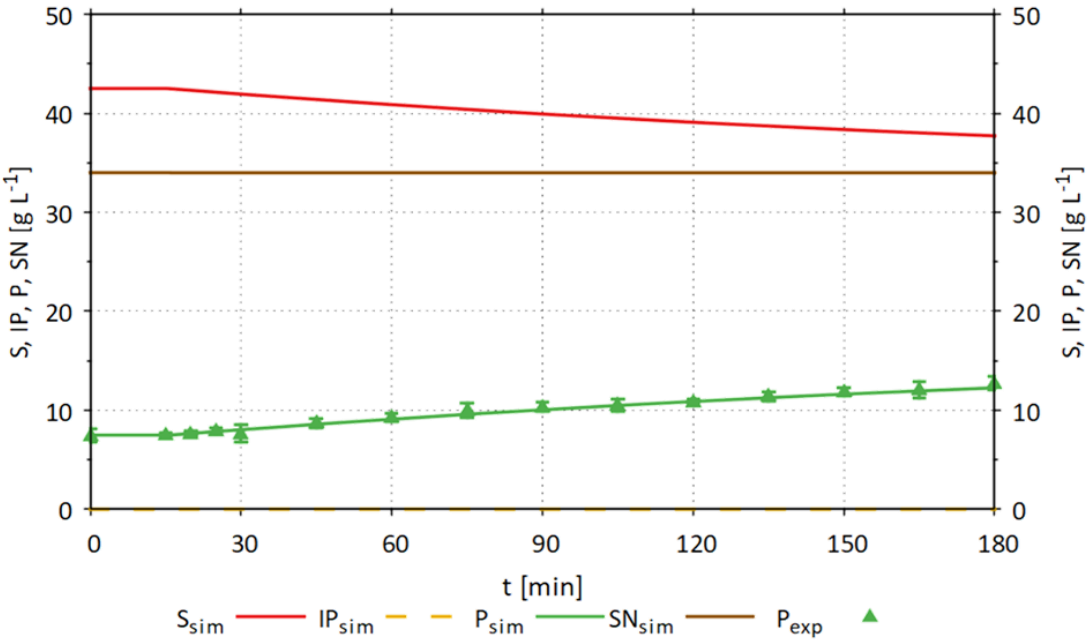

Figure 53: Comparison between simulation (index: sim) and experimental (index: exp) results of the first validation proteolysis batch experiment (Val I), with $R^2_{product}$ = 0.984. V_{start} = 3.0 L, $c_{substrate,start}$ = 50 g L^{-1}, T = 50 °C, pH = 7.5 and N_{stirr} = 300 rpm. Addition of 0.5 mL Flavourzyme (F_{E2}) after a processing time of 15 min. S: substrate (sunflower seed meal) concentration, IP: intermediate product concentration, P: product (free amino acid) concentration, SN: concentration of the non-hydrolysable components of the substrate. Error bars represent the mean value ± of one standard deviation resulting from a triple determination. Set of parameters used for simulation: Par_{Optim}.

The measured product concentration started at a value of 7.45 g L^{-1}. After a processing time of 180 min, the measured product concentration reached the maximum value of 12.74 g L^{-1}. The curve of the product concentration simulated by the model reproduces the measured values with $R^2_{product}$ = 0.984.

Figure 54 compares the experimental results of the second validation (Val II) batch proteolysis experiment with the results simulated by the model. Here, 2.5 mL Flavourzyme was added to the STR after a processing time of 15 min.

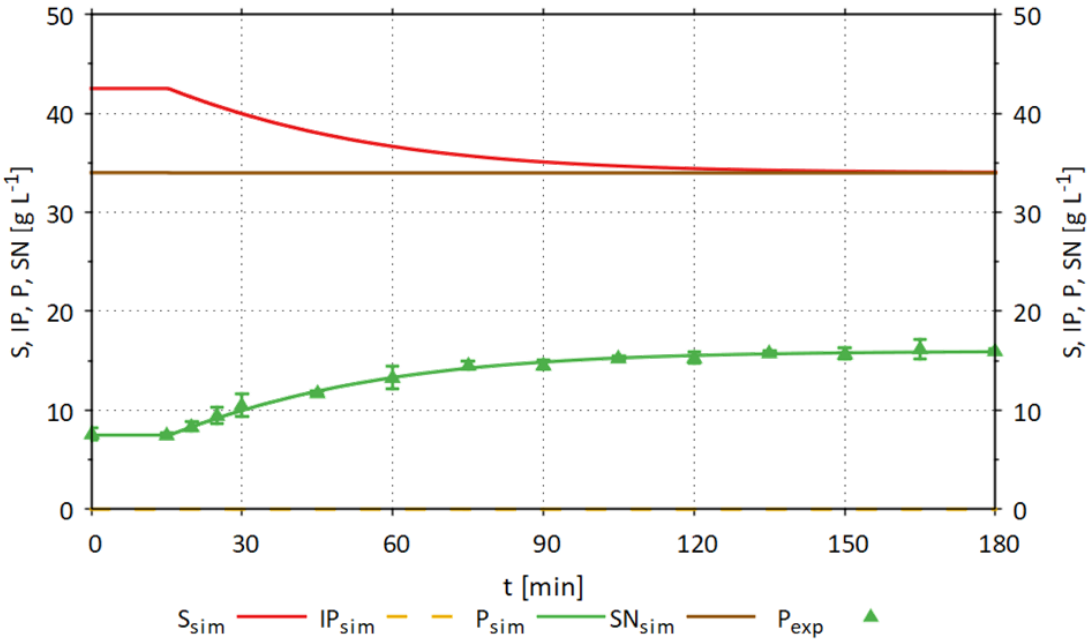

Figure 54: Comparison between simulation (index: sim) and experimental (index: exp) results of the second validation proteolysis batch experiment (Val II), with $R^2_{product}$ = 0.995. V_{start} = 3.0 L, $c_{substrate,start}$ = 50 g L^{-1}, T = 50 °C, pH = 7.5 and N_{stirr} = 300 rpm. Addition of 2.5 mL Flavourzyme (F_{E2}) after a processing time of 15 min. S: substrate (sunflower seed meal) concentration, IP: intermediate product concentration, P: product (free amino acid) concentration, SN: concentration of the non-hydrolysable components of the substrate. Error bars represent the mean value ± of one standard deviation resulting from a triple determination. Set of parameters used for simulation: Par_{Optim}.

The measured product concentration started at a value of 7.62 g L^{-1}. After a processing time of approx. 180 min, the measured product concentration reached the maximum value of 16.02 g L^{-1}. The curve of the product concentration simulated by the model reproduces the measured values with $R^2_{product}$ = 0.995.

In Table 13 the experimental results of the performed proteolysis batch experiments are summarised.

Table 13: Summary of the proteolysis batch experimental results.

Experiment	F_{E2} [ml]	$S_{t = 0\ min}$ [g L^{-1}]	$P_{exp,\ t = 0\ min}$ [g L^{-1}]	$P_{exp,\ t = 180\ min}$ [g L^{-1}]	$DS_{PR,1}$
Optim	1.483	42.49	7.51	15.15	961.31
Val I	0.500	42.55	7.45	12.74	761.63
Val II	2.500	42.38	7.62	16.02	915.42

After carrying out and evaluating all planned experiments, the experimental results of the optimised batch proteolysis experiment delivered the highest $DS_{PR,1}$ with a value of 961.31.

In the optimised experiment, the second highest product concentration of 15.15 g L^{-1} was obtained after 180 min. Here, 97,89 µL Flavourzyme was required to generate 1 g L^{-1} product. In the second validation experiment, where the highest product concentration of 16.02 g L^{-1} was achieved, 156.05 µL Flavourzyme was needed to generate 1 g L^{-1} product. 59.42% more Flavourzyme was required to increase the product concentration by 0.87 g L^{-1}.

6.3 Discussion

The model-based process design strategy, according to the OLFO principle, was successfully established and applied for enzymatic batch processes in a STR. Furthermore, through the combination with the mDoE strategy, the process conditions optimised by the OLFO could also be verified, and further experiments could be planned to validate the optimised experiment. Furthermore, the digital twin core model of the new standalone digital twin for enzymatic hydrolysis processes used for the optimisation could reproduce all the experiments carried out with an agreement of over 90%.

In the starch hydrolysis process, the enzyme used was reduced by more than 30% compared to the best validation experiment. In the proteolysis process, the amount of enzyme used was reduced by more than 50% compared to the best validation experiment.

Since the optimisation aimed to reduce the amount of enzyme used while maximising product formation, it can be said that the optimiser of the OLFO controller was able to determine the optimal process conditions. The developed *DS* can be extended to further improve the enzymatic hydrolysis batch processes. Here, for example, costs for energy or processing time could be considered.

Comparing the new strategies for model-based process design optimisation with the classical DoE method, an apparent reduction in the number of experiments required for optimisation can be seen.

With two variable parameters, four experiments must be carried out per DoE run for corner points of the DoE design space and two experiments for the centre point. To be able to determine the relatively small optimum that resulted from the starch hydrolysis process, at least 2-3 DoE runs would have been necessary. This would have resulted in about 12-18 experiments. Only six experiments were necessary with the process design optimisation strategies developed in this research work. The experimental effort could thus be reduced by more than 50%. Since the mDoE was only used to validate the result calculated by the OLFO controller, these experiments could also be eliminated, whereby only three experiments would have been necessary.

By using the new digital twin core model, the DoE design space can be narrowed down. This would have been difficult or even impossible with the classic DoE method.

7 Conclusion

Within the scope of this research work, a mechanistic model for enzymatic hydrolysis processes was developed. Michaelis-Menten kinetics were implemented to map the reaction rates. Double sigmoidal functions represent the influence of temperature and pH on enzyme activity and stability. The enzymatic hydrolysis processes of starch hydrolysis and proteolysis can be simulated with an agreement of over 90%.

Furthermore, a stand-alone digital twin for enzymatic hydrolysis processes in a 20 L STR was developed. Therefore, the model for the combined enzymatic starch hydrolysis and proteolysis was implemented into an existing stand-alone digital twin of a 20 L STR developed by the working group of Prof. Dr. Volker C. Hass at Furtwangen University (Appl et al., 2021; Gerlach et al., 2013; Gerlach et al., 2015; Hass et al., 2005a, 2005b; Hass, 2005; Hass et al., 2012; Hass, 2016; Hirschmann et al., 2018; Hirschmann, 2021; Isimite et al., 2018).

The new stand-alone digital twin can now map the nutrient media production through enzymatic hydrolysis, the cultivation of *S. cerevisiae*, the production of ethanol by *S. cerevisiae* and the whole-cell biocatalysis of ethyl-3-hydroxy-butyrate from the substrate ethyl acetoacetate in a 20 L STR under aerobic and anaerobic conditions.

Furthermore, the digital twin core model of the new stand-alone digital twin for enzymatic hydrolysis processes in a STR was coupled with new model-based process design strategies based on a combination of the OLFO and mDoE approaches and applied to enzymatic hydrolysis processes batch experiments in a STR. The new strategies improved starch hydrolysis and proteolysis batch processes in a STR and thus reduced enzyme consumption by more than 50% compared to the validation experiments.

In addition, it was investigated how the activity of the hydrolytic enzymes can be enhanced using high-pressure homogenisation. For Termamyl SC (α-amylase), an increase of approx. 7% in the 60 °C-activity was reached after high-pressure homogenisation at 1000 bar. An increase of approx. 5-12% in the 80 °C-activity was reached after high-pressure homogenisation at 1000-1500 bar. For Spirizyme Ultra (α-amylases and glucoamylases), an increase of approx. 1-4% in the 80 °C-activity was reached after high-pressure homogenisation at 1500-2000 bar. For EnerZyme P7 (endopeptidases), an increase of approx. 6% in the 25 °C-activity was reached after high-pressure homogenisation at

2000 bar. An increase of approx. 3-5% in the 50 °C-activity was reached after high-pressure homogenisation at 1500-2000 bar. For Flavourzyme (endopeptidases and exopeptidases), an increase of approx. 18-22% in the 25 °C-activity and approx. 13-20% in the 50 °C-activity was reached after high-pressure homogenisation at 500-1000 bar.

When investigating the enzyme activity after high-pressure homogenisation, the experimental results of all investigated enzyme preparations showed partially high standard deviations, which is why further investigations are necessary. A significantly higher enzyme activity could only be determined for high-pressure homogenisation of Flavourzyme at 1000 bar and 50 °C.

The model-based strategies and tools resulting from this work can find a wide range of industrial applications in the future. They can soon be used for the industrial production of organic nutrient media from regenerative substrates for the cultivation of a wide variety of microorganisms such as *S. cerevisiae* or *E. coli*. Furthermore, they provide the basis for reducing the costs of various enzymatic processes and thus improving their competitiveness compared to conventional chemical processes.

8 Outlook

The new model for enzymatic hydrolysis processes was designed to be as generic as possible. Thus, it can be quickly adapted to other enzymatic processes. The requirements for replacing the implemented Michaelis-Menten kinetics with other kinetics were created for this purpose.

The model for enzymatic hydrolysis processes was successfully integrated into stand-alone digital twins for an STR and a PBR. The new model could be integrated into other reactor concepts with various process setups (Section 1.3). This allows a comparison of which reactor is best suited for carrying out enzymatic hydrolysis processes. Furthermore, integration into more significant digital twin concepts, such as the "Biorefinery Black Forest" concept developed at Furtwangen University, is an attractive possibility. In this concept, the complete biotechnological processing of local renewable raw materials is considered, from producing nutrient media and cultivating microorganisms to producing products (e.g., ethanol, biogas).

Another possible application of the new stand-alone digital twin for enzymatic hydrolysis processes is its use for educational purposes. With this new tool, students can learn the basics of control engineering and bioprocess development in a very illustrative and hands-on way. However, due to the usually very high number of students in the courses, it is usually impossible for educational institutions to conduct such experiments on existing systems.

The digital twin core model of the new stand-alone digital twin for enzymatic hydrolysis processes in an STR was linked to new strategies for model-based process optimisation based on the OLFO and mDoE approaches. This made it possible to improve the enzymatic hydrolysis processes of starch hydrolysis and proteolysis with only a few experiments. Potato starch was used as substrate for starch hydrolysis, and sunflower seed meal was used as substrate in proteolysis. The strategies developed in this work could also be used to optimise these processes with other substrates (e.g., rice flour or soy protein powder). The developed model must only be adapted to the changed process properties using a few parameterisation experiments. This offers exciting possibilities for industrial application.

References

Adams MW and Kelly MR (eds) (1992) *Biocatalysis at extreme temperatures: Enzyme systems near and above 100 °C; developed from a symposium sponsored by the Division of Biochemical Technology at the 201st National Meeting of the American Chemical Society, Atlanta, Georgia, April 14 - 19, 1991*. Washington, DC: American Chemical Society.

Alford JS (2006) Bioprocess control: Advances and challenges. *Computers & Chemical Engineering* 30(10-12): 1464–1475.

Allen BR, Charles M and Coughlin RW (1979) Fluidized-bed immobilized-enzyme reactor for the hydrolysis of cornstarch to glucose. *Biotechnology & Bioengineering* 21(4): 689–706.

Allgöwer F and Zheng A (eds) (2000) *Nonlinear model predictive control*. Basel, Boston, Berlin: Birkhäuser Verlag.

Álvarez L, García J and Urrego D (2006) Control of a fedbatch bioprocess using nonlinear model predictive control. *IFAC Proceedings Volumes* 39(2): 347–352.

Anantharaman S, Padmarajaiah N, Al-Tayar NGS, et al. (2017) Ninhydrin-sodium molybdate chromogenic analytical probe for the assay of amino acids and proteins. *Spectrochimica Acta. Part A, Molecular and Biomolecular Spectroscopy* 173: 897–903.

Appl C, Baganz F and Hass VC (2021) Development of a digital twin for enzymatic hydrolysis processes. *Processes* 9(10): 1734.

Appl C, Fittkau C, Moser A, et al. (2019) *Adaptive, model-based control of Saccharomyces cerevisiae fed-batch cultivations*. ECCE 12 & ECAB 7. Florence, Italy.

Appl C, Moser A, Baganz F, et al. (2020) Digital twins for bioprocess control strategy development and realisation. *Advances in Biochemical Engineering/Biotechnology* 177: 63–94.

Arndt L (2022) *Internal communication (not publicly available)*.

Beaubier S, Framboisier X, Fournier F, et al. (2021) A new approach for modelling and optimizing batch enzymatic proteolysis. *Chemical Engineering Journal* 405: 126871.

Berg JM, Tymoczko JL, Gatto jr. GJ, et al. (eds) (2018) *Stryer Biochemie*. Berlin, Heidelberg: Springer Berlin Heidelberg.

Beschkov V, Marc A and Engasser JM (1984) A kinetic model for the hydrolysis and synthesis of maltose, isomaltose, and maltotriose by glucoamylase. *Biotechnology & Bioengineering* 26(1): 22–26.

Biegler LT (2021) A perspective on nonlinear model predictive control. *Korean Journal of Chemical Engineering* 38(7): 1317–1332.

Blesgen A and Hass VC (2010) Efficient biogas production through process simulation. *Energy & Fuels* 24(9): 4721–4727.

Brüning S (2016) Development of a generalized process model for optimization of biotechnological processes. PhD-Thesis, Jacobs University. Bremen.

Brüning S, Gerlach I, Pörtner R, et al. (2017) Modeling suspension cultures of microbial and mammalian cells with an adaptable six-compartment model. *Chemical Engineering & Technology* 40(5): 956–966.

Brunner M, Fricke J, Kroll P, et al. (2017) Investigation of the interactions of critical scale-up parameters (pH, pO2 and pCO2) on CHO batch performance and critical quality attributes. *Bioprocess and Biosystems Engineering* 40(2): 251–263.

Bück A, Casciatori FP, Thoméo JC, et al. (2015) Model-based control of enzyme yield in solid-state fermentation. *Procedia Engineering* 102: 362–371.

Buckow R, Heinz V and Knorr D (2005) Two fractional model for evaluating the activity of glucoamylase from aspergillus niger under combined pressure and temperature conditions. *Food and Bioproducts Processing* 83(3): 220–228.

Buckow R, Weiss U, Heinz V, et al. (2007) Stability and catalytic activity of alpha-amylase from barley malt at different pressure-temperature conditions. *Biotechnology and Bioengineering* 97(1): 1–11.

Bugg T (2012) *Introduction to enzyme and coenzyme chemistry*. Chichester, West Sussex: Wiley.

Cameron D, Clausen C and Morton W (2002) Dynamic simulators for operator training. In: Braunschweig B and Gani R (eds) *Software Architectures and Tools for Computer Aided Process Engineering:* Amsterdam: Elsevier, pp. 393–431.

Campbell NA and Reece JB (2005) *Biology*. San Francisco: Pearson Benjamin Cummings.

Chang L, Liu X and Henson MA (2016) Nonlinear model predictive control of fed-batch fermentations using dynamic flux balance models. *Journal of Process Control* 42: 137–149.

Chutipongtanate S, Watcharatanyatip K, Homvises T, et al. (2012) Systematic comparisons of various spectrophotometric and colorimetric methods to measure concentrations of protein, peptide and amino acid: detectable limits, linear dynamic ranges, interferences, practicality and unit costs. *Talanta* 98: 123–129.

Cordeiro CAM, Martins MLL and Luciano AB (2002) Production and properties of alpha-amylase from thermophilic Bacillus sp. *Brazilian Journal of Microbiology* 33(1).

Craven S, Whelan J and Glennon B (2014) Glucose concentration control of a fed-batch mammalian cell bioprocess using a nonlinear model predictive controller. *Journal of Process Control* 24(4): 344–357.

Dudley T, Villiers P de, Bouwer W, et al. (2008) The operator training simulator system for the pebble bed modular reactor (PBMR) plant. *Nuclear Engineering and Design* 238(11): 2908–2915.

Eisenmenger MJ and Reyes-De-Corcuera JI (2009) High pressure enhancement of enzymes: A review. *Enzyme and Microbial Technology* 45(5): 331–347.

El Saddik A (2018) Digital twins: The convergence of multimedia technologies. *IEEE MultiMedia* 25(2): 87–92.

ERBSLÖH Geisenheim GmbH EnerZyme® P7: Product description.

Eyring H and Magee JL (1942) Application of the theory of absolute reaction rates to bacterial luminescence. *Journal of Cellular and Comparative Physiology* 20(2): 169–177.

Fenila F and Shastri Y (2016) Optimal control of enzymatic hydrolysis of lignocellulosic biomass. *Resource-Efficient Technologies* 2: S96-S104.

Follonier S, Panke S and Zinn M (2012) Pressure to kill or pressure to boost: A review on the various effects and applications of hydrostatic pressure in bacterial biotechnology. *Applied Microbiology and Biotechnology* 93(5): 1805–1815.

Frahm B, Hass VC, Lane P, et al. (2003a) Fed-Batch-Kultivierung tierischer Zellen - Eine Herausforderung zur adaptiven, modellbasierten Steuerung. *Chemie Ingenieur Technik* 75(4): 457–460.

Frahm B, Lane P, Atzert H, et al. (2002) Adaptive, model-based control by the open-loop-feedback-optimal (OLFO) controller for the effective fed-batch cultivation of hybridoma cells. *Biotechnology Progress* 18(5): 1095–1103.

Frahm B, Lane P, Märkl H, et al. (2003b) Improvement of a mammalian cell culture process by adaptive, model-based dialysis fed-batch cultivation and suppression of apoptosis. *Bioprocess and Biosystems Engineering* 26(1): 1–10.

Galvanauskas V, Grigs O, Vanags J, et al. (2013) Model-based optimization and pO2 control of fed-batch Escherichia coli and Saccharomyces cerevisiae cultivation processes. *Engineering in Life Sciences* 13(2): 172–184.

Garcia-Palazon A, Suthanthangjai W, Kajda P, et al. (2004) The effects of high hydrostatic pressure on β-glucosidase, peroxidase and polyphenoloxidase in red raspberry (Rubus idaeus) and strawberry (Fragaria×ananassa). *Food Chemistry* 88(1): 7–10.

Gassenmeier V, Deppe S, Hernández Rodríguez T, et al. (2022) Model-assisted DoE applied to microalgae processes. *Current Research in Biotechnology* 4: 102–118.

Gbogouri GA, Linder M, Fanni J, et al. (2004) Influence of hydrolysis degree on the functional properties of salmon byproducts hydrolysates. *Journal of Food Science* 69(8): C615-C622.

Gerlach I, Hass VC, Brüning S, et al. (2013) Virtual bioreactor cultivation for operator training and simulation: application to ethanol and protein production. *Journal of Chemical Technology & Biotechnology* 88(12): 2159–2168.

Gerlach I, Hass VC and Mandenius C-F (2015) Conceptual design of an operator training simulator for a bio-ethanol plant. *Processes* 3(3): 664–683.

Giorgi FM, Ceraolo C and Mercatelli D (2022) The R language: An engine for bioinformatics and data science. *Life (Basel, Switzerland)* 12(5).

Glaessgen E and Stargel D (2012) The digital twin paradigm for future NASA and U.S. Air Force vehicles: 22267B.

Glauche F, Pilarek M, Bournazou MNC, et al. (2017) Design of experiments-based high-throughput strategy for development and optimization of efficient cell disruption protocols. *Engineering in Life Sciences* 17(11): 1166–1172.

Grieves M (2016) *Origins of the Digital Twin Concept: Working Paper*.

Guisan JM (2006) *Immobilization of enzymes and cells*. Totowa N.J.: Humana Press.

Gupta R, Beg QK and Lorenz P (2002) Bacterial alkaline proteases: molecular approaches and industrial applications. *Applied Microbiology and Biotechnology* 59(1): 15–32.

Haight RD and Morita RY (1962) Interaction between parameters of hydrostatic pressure and temperature on aspartase of Escherichia coli. *Journal of Bacteriology* (83): 112.

Hass VC (2005) Verbesserung der bioverfahrenstechnischen Ausbildung durch einen "Virtuellen Bioreaktor". *Chemie Ingenieur Technik* 77(1-2): 161–167.

Hass VC (2016) Operator training simulators for bioreactors. In: Mandenius C-F (ed) *Bioreactors: Design, operation and novel applications*. Weinheim, Germany: Wiley, pp. 453–486.

Hass VC, Knutzsch S, Gerlach I, et al. (2012) Towards the development of a training simulator for biorefineries. *Chemical Engineering Transactions*(29): 247–252.

Hass VC, Kuhnen F and Schoop K-M (2005a) An environment for the development of operator training systems (OTS) from chemical engineering models. *Computer Aided Chemical Engineering*(20): 289–293.

Hass VC, Kuhnen F and Schoop K-M (2005b) *Rapid design of interactive operator training simulators for training and education*. 7th World Congress of Chemical Engineering, WCCE 2005, 10th -14th July. Glasgow, Scotland.

Hass VC, Kuntzsch S, Schoop K-M, et al. (2014) Resource efficiency studies using a new operator training simulator for a bioethanol plant. In: *PRES 2014, 17th Conference on Process Integration, Modelling and Optimisation for Energy Saving and Pollution Reduction: PRES 2014, 23-27 August 2014, Prague, Czech Republic*. Milano: AIDIC Associazione Italiana di Ingegneria Chimica ČSCHI Česká Společnost Chemického Inženýrství, pp. 541–546.

Hass VC and Pörtner R (2011) *Praxis der Bioprozesstechnik: Mit virtuellem Praktikum*. Heidelberg: Spektrum Akad. Verl.

Hawley SA (1971) Reversible pressure-temperature denaturation of chymotrypsinogen. *Biochemistry* 10(13): 2436–2442.

He R, Chen G, Dong C, et al. (2019) Data-driven digital twin technology for optimized control in process systems. *ISA Transactions* 95: 221–234.

Heinz V, Buckow R and Knorr D (2005) Catalytic activity of beta-amylase from barley in different pressure/temperature domains. *Biotechnology Progress* 21(6): 1632–1638.

Hirschmann R (2021) Evaluating the potential of anaerobic production of ethyl(3)hydroxybutyrate for integration in biorefineries. PhD, University College London (UCL). London.

Hirschmann R, Reule W, Oppenländer T, et al. (2018) Integrating whole cell biocatalysis of aroma compounds into a novel biorefinery concept. *IntechOpen Book Chapter Template*.

Hodge DB, Karim MN, Schell DJ, et al. (2009) Model-based fed-batch for high-solids enzymatic cellulose hydrolysis. *Applied Biochemistry and Biotechnology* 152(1): 88–107.

Hodge JE (1953) Dehydrated foods, chemistry of browning reactions in model systems. *Journal of Agricultural and Food Chemistry* 1(15): 928–943.

Illanes A (2008) *Enzyme biocatalysis: Principles and applications*. Dordrecht: Springer.

Ingenieurbüro Dr.-Ing. Schoop GmbH (2018) *WinErs: Process control and automation system on PC under Windows*. Hamburg, Germany.

Isimite J, Baganz F and Hass VC (2018) Operator training simulators for biorefineries: current position and future directions. *Journal of Chemical Technology & Biotechnology* 93(6): 1529–1541.

Jaeger K-E, Liese A and Syldatk C (2018) *Einführung in die Enzymtechnologie*. Berlin, Heidelberg: Springer Berlin Heidelberg.

Jung S, Roussel-Philippe C, Briggs JL, et al. (2004) Limited hydrolysis of soy proteins with endo- and exoproteases. *Journal of the American Oil Chemists' Society* 81(10): 953.

Kamnerdpetch C, Weiss M, Kasper C, et al. (2007) An improvement of potato pulp protein hydrolyzation process by the combination of protease enzyme systems. *Enzyme and Microbial Technology* 40(4): 508–514.

Kaspar H, Dettmer K, Gronwald W, et al. (2009) Advances in amino acid analysis. *Analytical and Bioanalytical Chemistry* 393(2): 445–452.

Knez Z, Laudani CG, Habulin M, et al. (2007) Exploiting the pressure effect on lipase-catalyzed wax ester synthesis in dense carbon dioxide. *Biotechnology and Bioengineering* 97(6): 1366–1375.

Krause J and Merz J (2017) Comparison of enzymatic hydrolysis in a centrifugal partition chromatograph and stirred tank reactor. *Journal of Chromatography. A* 1504: 64–70.

Kuchemüller KB, Pörtner R and Möller J (2020) Efficient optimization of process strategies with model-assisted design of experiments. In: Pörtner R (ed) *Animal Cell Biotechnology: Methods and Protocols*. New York, NY: Springer US; Imprint Humana, pp. 235–249.

Kuhnen F (2008) Modellierungssystem eStIM - Kurzeinführung. Unpublished, Hochschule Bremen. Bremen.

Kumar P and Satyanarayana T (2009) Microbial glucoamylases: characteristics and applications. *Critical Reviews in Biotechnology* 29(3): 225–255.

Kuntzsch S (2014) Energy efficiency investigations with a new operator training simulator for biorefineries. PhD-Thesis, Jacobs University. Bremen.

Kusunoki K, Kawakami K, Shiraishi F, et al. (1982) A kinetic expression for hydrolysis of soluble starch by glucoamylase. *Biotechnology & Bioengineering* 24(2): 347–354.

Larroche C, Pandey A, Du G, et al. (eds) (2016) *Current developments in biotechnology and bioengineering: Bioprocesses, Bioreactors and Controls*. Saint Louis: Elsevier Science.

Lee C-G, Kim CH and Rhee SK (1992) A kinetic model and simulation of starch saccharification and simultaneous ethanol fermentation by amyloglucosidase and Zymomonas mobilis. *Bioprocess Engineering* 7(8): 335–341.

Li M (2015) Adaptive predictive control by open-loop-feedback-optimal controller for cultivation processes. Dissertation, Jacobs University. Bremen.

Liu M, Fang S, Dong H, et al. (2021) Review of digital twin about concepts, technologies, and industrial applications. *Journal of Manufacturing Systems* 58: 346–361.

Luttmann R, Munack A and Thoma M (1985) Mathematical modelling, parameter identification and adaptive control of single cell protein processes in tower loop bioreactors. In: Fiechter A, Aiba S, Bungoy HR, Cooney CL, Demain AL, Fukui S, et al. (eds)

Agricultural feedstock and waste treatment and engineering: Berlin, Heidelberg: Springer, pp. 95–205.

Maillard LC (1912) Formation of melanoidins in a methodical way. *Comptes Rendus*(154): 66–68.

Mandenius C-F and Brundin A (2008) Bioprocess optimization using design-of-experiments methodology. *Biotechnology Progress* 24(6): 1191–1203.

Manzon D, Claeys-Bruno M, Declomesnil S, et al. (2020) Quality by design: Comparison of design space construction methods in the case of design of experiments. *Chemometrics and Intelligent Laboratory Systems* 200: 104002.

MarketsandMarkets (2020) *Organic yeast market: Global forecast to 2025*.

Merz M, Eisele T, Berends P, et al. (2015) Flavourzyme, an enzyme preparation with industrial relevance: Automated nine-step purification and partial characterization of eight enzymes. *Journal of Agricultural and Food Chemistry* 63(23): 5682–5693.

Miller JF, Nelson CM, Ludlow JM, et al. (1989) High pressure-temperature bioreactor: assays of thermostable hydrogenase with fiber optics. *Biotechnology and Bioengineering* 34(7): 1015–1021.

Möller J, Hernández Rodríguez T, Müller J, et al. (2020) Model uncertainty-based evaluation of process strategies during scale-up of biopharmaceutical processes. *Computers & Chemical Engineering* 134: 106693.

Möller J, Kuchemüller KB, Steinmetz T, et al. (2019) Model-assisted design of experiments as a concept for knowledge-based bioprocess development. *Bioprocess and Biosystems Engineering* 42(5): 867–882.

Möller J and Pörtner R (2017) Model-based design of process strategies for cell culture bioprocesses: State of the art and new perspectives. In: Gowder SJT (ed) *New Insights into Cell Culture Technology:* InTech.

Moradi H, Saffar-Avval M and Bakhtiari-Nejad F (2011) Nonlinear multivariable control and performance analysis of an air-handling unit. *Energy and Buildings* 43(4): 805–813.

Morales-Rodríguez R, Capron M, Hussom JK, et al. (2010) Controlled fed-batch operation for improving cellulose hydrolysis in 2G bioethanol production. *20th European Symposium on Computer Aided Process Engineering – ESCAPE20*.

Morita RY and Haight RD (1962) Malic dehydrogenase activity at 101 °C under hydrostatic pressure. *Journal of Bacteriology* 83(6): 1341–1346.

Moser A, Appl C, Brüning S, et al. (2020) Mechanistic mathematical models as a basis for digital twins. *Advances in Biochemical Engineering/Biotechnology* 176: 133–180.

Moser A, Kuchemüller KB, Deppe S, et al. (2021) Model-assisted DoE software: optimization of growth and biocatalysis in Saccharomyces cerevisiae bioprocesses. *Bioprocess and Biosystems Engineering* 44(4): 683-700.

Murray JD (ed) (2004) *Mathematical biology: I. An introduction*. New York, NY: Springer-Verlag Berlin Heidelberg.

Narayanan H, Luna MF, Stosch M von, et al. (2020) Bioprocessing in the digital age: The role of process models. *Biotechnology Journal* 15(1): e1900172.

Nebesny E (1989) Kombinierte enzymatische Stärkehydrolyse. *Starch - Stärke* 41(7): 266–270.

Nelder JA and Mead R (1965) A simplex method for function minimization. *The Computer Journal* 7(4): 308–313.

Nienow AW (2014) Stirring and stirred-tank reactors. *Chemie Ingenieur Technik* 86(12): 2063–2074.

Noel M.-O. M, Athes V and Combes D (2000) Combined effects of pressure and temperature on enzyme stability. *High Pressure Research* 19(1-6): 317–322.

Novozymes (2002) Flavourzyme™: Product sheet.

Novozymes A/S (2004) Termamyl SC: Application sheet.

Novozymes A/S (2010) Novozymes Spirizyme® products for use in saccharification and fermentation: Application sheet.

Patle DS, Ahmad Z and Rangaiah GP (2014) Operator training simulators in the chemical industry: review, issues, and future directions. *Reviews in Chemical Engineering* 30(2).

Polaina J and MacCabe AP (2007) *Industrial enzymes: Structure, function, and applications*. Dordrecht: Springer.

Pörtner R, Platas-Barradas O, Gradkowski J, et al. (2011) "BioProzessTrainer" as training tool for design of experiments. *BMC Proceedings* 5 Suppl 8: P62.

Rao MB, Tanksale AM, Ghatge MS, et al. (1998) Molecular and biotechnological aspects of microbial proteases. *Microbiology and Molecular Biology Reviews* 62(3): 597–635.

R-Biopharm AG (2022) Enzytec™ Liquid D-Glucose - Food & Feed Analysis. Available at: https://food.r-biopharm.com/products/enzytec-liquid-d-glucose/ (accessed 18 March 2023).

Stosch M von, Hamelink J-M and Oliveira R (2016) Hybrid modeling as a QbD/PAT tool in process development: an industrial E. coli case study. *Bioprocess and Biosystems engineering* 39(5): 773–784.

Stosch M von and Willis MJ (2017) Intensified design of experiments for upstream bioreactors. *Engineering in Life Sciences* 17(11): 1173–1184.

Student (1908) The probable error of a mean. *Biometrika* 6(1): 1.

Sudhakaran VK, Deshpande BS, Shewale JG, et al. (1992) Production of 6-APA using a recirculated packed bed batch reactor. *Biotechnology Letters* 14(10): 913–918.

Summit M, Scott B, Nielson K, et al. (1998) Pressure enhances thermal stability of DNA polymerase from three thermophilic organisms. *Extremophiles* 2(3): 339–345.

Suzuki K (1960) Studies on the kinetics of protein denaturation under high pressure. *The Review of Physical Chemistry of Japan*(29).

Tao F, Zhang H, Liu A, et al. (2019) Digital Twin in Industry: State-of-the-Art. *IEEE Transactions on Industrial Informatics* 15(4): 2405–2415.

Tavano OL (2013) Protein hydrolysis using proteases: An important tool for food biotechnology. *Journal of Molecular Catalysis B: Enzymatic* 90: 1–11.

Tedjo W, Eshtiaghi MN and Knorr D (2000) Impact of supercritical carbon dioxide and high pressure on lipoxygenase and peroxidase activity. *Journal of Food Science* 65(8): 1284–1287.

Tribst AAL, Augusto PED and Cristianini M (2012) The effect of the high pressure homogenisation on the activity and stability of a commercial neutral protease from Bacillus subtilis. *International Journal of Food Science & Technology* 47(4): 716–722.

Vaccari M, Di Bacci Capaci R, Brunazzi E, et al. (2021) Optimally managing chemical plant operations: An example oriented by industry 4.0 paradigms. *Industrial & Engineering Chemistry Research* 60(21): 7853–7867.

Verhoff FH and Schlager ST (1981) Enzyme activity maintenance in packed-bed reactors via continuous enzyme addition. *Biotechnology & Bioengineering* 23(1): 41–60.

Villamide MJ and San Juan LD (1998) Effect of chemical composition of sunflower seed meal on its true metabolizable energy and amino acid digestibility. *Poultry Science* 77(12): 1884–1892.

Witte VC, Munack A and Märkl H (1996) *Mathematische Modellierung und adaptive Prozeßsteuerung der Kultivierung von Cyathus striatus*. Zugl.: Hamburg-Harburg, Techn. Univ., Arbeitsbereich Regelungstechnik und Systemdynamik [i.e. Arbeitsbereich Regelungstechnik] und Arbeitsbereich Bioprozess- und Bioverfahrenstechnik, Diss., 1996. Düsseldorf: VDI-Verl.

Zacher S and Reuter M (2017) *Regelungstechnik für Ingenieure*. Wiesbaden: Springer Fachmedien Wiesbaden.

Zhang C and Ji W (2019) Digital twin-driven carbon emission prediction and low-carbon control of intelligent manufacturing job-shop. *Procedia CIRP* 83: 624–629.

Zobel-Roos S, Schmidt A, Mestmäcker F, et al. (2019) Accelerating biologics manufacturing by modeling or: Is approval under the QbD and PAT approaches demanded by authorities acceptable without a digital-twin? *Processes* 7(2): 94.

Appendix

A List of publications

- Appl, Christian; Fittkau, Christian; Moser, André; Hass, Volker C. (2019): Adaptive, model-based control of Saccharomyces cerevisiae fed-batch cultivations. ECCE 12 & ECAB 5 - 12th European Congress of Chemical Engineering and 5th European of Applied Biotechnology. Florence, Italy, 2019.
- Appl, Christian; Moser, André; Baganz, Frank; Hass, Volker C. (2020): Digital twins for bioprocess control strategy development and realisation. In: Advances in Biochemical Engineering/Biotechnology 177, S. 63–94. DOI: 10.1007/10_2020_151.
- Moser, André; Appl, Christian; Brüning, Simone; Hass, Volker C. (2020): Mechanistic mathematical models as a basis for digital twins. In: Advances in Biochemical Engineering/Biotechnology 176, S. 133–180. DOI: 10.1007/10_2020_152.
- Appl, Christian; Fittkau, Christian; Moser, André; Hass, Volker C. (2021): Comparison of fixed feeding profiles, RQ feedback control and adaptive model-based control for aerobic Saccharomyces cerevisiae fed-batch cultivations. CHISA 2021 VIRTUALLY - 24th International Congress of Chemical and Process Engineering, 2021.
- Appl, Christian; Baganz, Frank; Hass, Volker C. (2021): Modelling of enzymatic hydrolysis processes for control strategy development. ESBES - 13th European Symposium on Biochemical Engineering Sciences. Virtually, 2021.
- Appl, Christian; Baganz, Frank; Hass, Volker C. (2021): Development of a digital twin for enzymatic hydrolysis processes. In: Processes 9 (10), S. 1734. DOI: 10.3390/pr9101734.
- Hass, Volker C.; Appl, Christian; Schoop-Zipfel, Jochen; Baganz, Frank (2022): Teaching control in biochemical engineering using a dynamic enzymatic hydrolysis process model and the control and automation software WinErs. CHISA - 26th International Congress of Chemical and Process Engineering. Prague, Czech Republic, 2022.

B States, variables and parameters of the model for enzymatic hydrolysis processes

The states, manipulated variables and parameters (Par_{Optim}) listed in the following tables were defined to create the digital twin core model for enzymatic hydrolysis processes.

Table B1: State variables of the model for enzymatic hydrolysis processes in a stirred tank reactor.

Abbreviation	Description	Lower bound	Upper bound	Unit
STR – Model				
V_B	Volume of the broth in the STR.	$1 \cdot 10^{-10}$	0.02	m^3
F_{in}	Total inflow to the STR.	0	$1.67 \cdot 10^{-6}$	m^3/s
Process 1 (P1) – Starch hydrolysis with α-amylase (E1) and glucoamylase (E2)				
$S_{1,P1}$	Concentration of total substrate (starch) in the STR.	0	500	kg/m^3
$SH_{1,P1}$	Concentration of hydrolysable substrate in the STR.	0	500	kg/m^3
$SN_{1,P1}$	Concentration of non-hydrolysable components of substrate in the STR.	0	500	kg/m^3
$E1_{1,P1}$	Concentration of E1 in the STR.	0	1000	kg/m^3
$E2_{1,P1}$	Concentration of E2 in the STR.	0	1000	kg/m^3
$IP_{1,P1}$	Concentration of intermediate product (oligosaccharide) in the STR.	0	500	kg/m^3
$P_{1,P1}$	Concentration of product (glucose) in the STR.	0	500	kg/m^3
$r_{SIP,E1,P1}$	Degradation rate of E1 (substrate to intermediate product).	0	100	1/s
$r_{IPP,E2,P1}$	Degradation rate of E2 (intermediate product to product).	0	100	1/s
$r_{IPS,E1,P1}$	Build-up rate of E1 (intermediate product from substrate).	0	100	1/s
$r_{PS,E1,P1}$	Build-up rate of E1 (product from substrate).	0	100	1/s
$r_{PIP,E2,P1}$	Build-up rate of E2 (product from intermediate product).	0	100	1/s
$r_{den,E1,P1}$	Denaturation rate of E1.	0	1	1/s

$r_{den,E2,P1}$	Denaturation rate of E2.	0	1	1/s
$f_{T,act,E1,P1}$	Factor for the temperature-dependent activity of E1.	0	1	-
$f_{T,act,E2,P1}$	Factor for the temperature-dependent activity of E2.	0	1	-
$f_{T,sta,E1,P1}$	Factor for temperature-dependent stability of E1.	0	1	-
$f_{T,sta,E2,P1}$	Factor for temperature-dependent stability of E2.	0	1	-
$f_{pH,act,E1,P1}$	Factor for the pH-dependent activity of E1.	0	1	-
$f_{pH,act,E2,P1}$	Factor for the pH-dependent activity of E2.	0	1	-
$f_{pH,sta,E1,P1}$	Factor for pH-dependent stability of E1.	0	1	-
$f_{pH,sta,E2,P1}$	Factor for pH-dependent stability of E2.	0	1	-

Process 2 (P2) – Proteolysis with endo- (E1) and exopeptidase (E2)

$S_{1,P2}$	Concentration of total substrate (protein) in the STR.	0	500	kg/m^3
$SH_{1,P2}$	Concentration of hydrolysable substrate in the STR.	0	500	kg/m^3
$SN_{1,P2}$	Concentration of non-hydrolysable components of substrate in the STR.	0	500	kg/m^3
$E1_{1,P2}$	Concentration of E1 in the STR.	0	1000	kg/m^3
$E2_{1,P2}$	Concentration of E2 in the STR.	0	1000	kg/m^3
$I_{P1,P2}$	Concentration of intermediate product (peptide) in the STR.	0	500	kg/m^3
$P_{1,P2}$	Concentration of product (free amino acids) in the STR.	0	500	kg/m^3
$r_{SIP,E1,P2}$	Degradation rate of E1 (substrate to intermediate product).	0	100	1/s
$r_{IPP,E2,P2}$	Degradation rate of E2 (intermediate product to product).	0	100	1/s
$r_{IPS,E1,P2}$	Build-up rate of E1 (intermediate product from substrate).	0	100	1/s
$r_{PS,E1,P2}$	Build-up rate of E1 (product from substrate).	0	100	1/s
$r_{PIP,E2,P2}$	Build-up rate of E2 (product from intermediate product).	0	100	1/s

$r_{den,E1,P2}$	Denaturation rate of E1.	0	1	1/s
$r_{den,E2,P2}$	Denaturation rate of E2.	0	1	1/s
$f_{T,act,E1,P2}$	Factor for the temperature-dependent activity of E1.	0	1	-
$f_{T,act,E2,P2}$	Factor for the temperature-dependent activity of E2.	0	1	-
$f_{T,sta,E1,P2}$	Factor for temperature-dependent stability of E1.	0	1	-
$f_{T,sta,E2,P2}$	Factor for temperature-dependent stability of E2.	0	1	-
$f_{pH,act,E1,P2}$	Factor for the pH-dependent activity of E1.	0	1	-
$f_{pH,act,E2,P2}$	Factor for the pH-dependent activity of E2.	0	1	-
$f_{pH,sta,E1,P2}$	Factor for pH-dependent stability of E1.	0	1	-
$f_{pH,sta,E2,P2}$	Factor for pH-dependent stability of E2.	0	1	-

Table B2: Manipulated variables of the model for enzymatic hydrolysis processes.

Abbreviation	Description	Lower bound	Upper bound	Unit
STR – Model				
T_B	Temperature (profile) of broth in the STR.	273.15	373.15	K
pH_B	Value (profile) of broth pH in the STR.	0	14	-
$F_{B,1}$	Outflow of broth from the STR.	0	$1.67 \cdot 10^{-6}$	m^3/s
Process 1 (P1) – Starch hydrolysis with α-amylase (E1) and glucoamylase (E2)				
$F_{S,0,P1}$	Inflow of substrate (protein) solution to the STR.	0	$1.67 \cdot 10^{-7}$	m^3/s
$F_{E1,0,P1}$	Inflow of E1 solution to the STR.	0	$1.67 \cdot 10^{-8}$	m^3/s
$F_{E2,0,P1}$	Inflow of E2 solution to the STR.	0	$1.67 \cdot 10^{-8}$	m^3/s
$SH_{0,P1}$	Concentration of hydrolysable substrate in the $F_{S,0,P1}$.	0	500	kg/m^3

$SN_{0,P1}$	Concentration of non-hydrolysable substrate in $F_{S,0,P1}$.	0	500	kg/m^3
$E1_{0,P1}$	Concentration of E1 in $F_{E1,0,P1}$.	0	1000	kg/m^3
$E2_{0,P1}$	Concentration of E2 in $F_{E2,0,P1}$.	0	1000	kg/m^3
$IP_{0,P1}$	Concentration of intermediate product (peptide) in $F_{S,0,P1}$.	0	500	kg/m^3
$P_{0,P1}$	Concentration of product (free amino acids) in $F_{S,0,P1}$.	0	500	kg/m^3
Process 2 (P2) – Proteolysis with endo- (E1) and exopeptidase (E2)				
$F_{S,0,P2}$	Inflow of substrate (protein) solution to the STR.	0	$1.67 \cdot 10^{-7}$	m³/s
$F_{E1,0,P2}$	Inflow of E1 solution to the STR.	0	$1.67 \cdot 10^{-8}$	m³/s
$F_{E2,0,P2}$	Inflow of E2 solution to the STR.	0	$1.67 \cdot 10^{-8}$	m³/s
$SH_{0,P2}$	Concentration of hydrolysable substrate in the $F_{S,0,P2}$.	0	500	kg/m^3
$SN_{0,P2}$	Concentration of non-hydrolysable substrate in $F_{S,0,P2}$.	0	500	kg/m^3
$E1_{0,P2}$	Concentration of E1 in $F_{E1,0,P2}$.	0	1000	kg/m^3
$E2_{0,P2}$	Concentration of E2 in $F_{E2,0,P2}$.	0	1000	kg/m^3
$IP_{0,P2}$	Concentration of intermediate product (peptide) in $F_{S,0,P2}$.	0	500	kg/m^3
$P_{0,P2}$	Concentration of product (free amino acids) in $F_{S,0,P2}$.	0	500	kg/m^3

Table B3: Set of parameters (Par_{Optim}) of the model for enzymatic hydrolysis processes.

Abbreviation	Description	Lower bound	Upper bound	Unit	Value
Process 1 (P1) – Starch hydrolysis with α-amylase (E1) and glucoamylase (E2)					
$r_{max,SIP,E1,P1}$	Maximal reaction rate of E1 (substrate to intermediate product).	0	100	1/s	8.64
$K_{M,SIP,E1,P1}$	Michaelis-Menten-constant for E1 (substrate to intermediate product).	0	10	kg/m^3 · s	25.60
$Y_{SIP,E1,P1}$	Yield factor during formation of intermediate product from substrate.	0	1	kg/kg	0.99

$r_{max,IPP,E2,P1}$	Maximal reaction rate of E2 (intermediate product to product).	0	100	1/s	0.82
$K_{M,IPP,E2,P1}$	Michaelis-Menten-constant for E2 (intermediate product to product).	0	10	$kg/m^3 \cdot s$	29.99
$Y_{IPP,E2,P1}$	Yield factor during formation of product from intermediate product.	0	1	kg/kg	1
$P_{IP,P1}$	Proportional factor for formation of intermediate product from substrate.	0	1	-	1
$P_{P,P1}$	Proportional factor for formation of product from intermediate product.	0	1	-	1
$f_{E2,FE1,P1}$	Factor for the proportion of E2 in $F_{E1,0,P1}$.	0	1	-	0
$f_{E1,FE2,P1}$	Factor for the proportion of E1 in $F_{E2,0,P1}$.	0	1	-	0.3
$r_{max,den,E1,P1}$	Maximal denaturation rate of E1.	0	1	1/s	$1e^{-5}$
$r_{max,den,E2,P1}$	Maximal denaturation rate of E2.	0	1	1/s	$1e^{-5}$
$Y_{LS,T,act,E1,P1}$	Lowest value on the left side of T-DSig for E1 activity.	0	5	-	0
$Y_{mid,T,act,E1,P1}$	Upper/lower limit between the left and the right inflexion points of T-DSig for E1 activity.	0	5	-	1
$Y_{RS,T,act,E1,P1}$	Highest value on the right side of T-DSig for E1 activity.	0	5	-	1
$K_{LS,T,act,E1,P1}$	Left slope of T-DSig for E1 activity.	0	10	-	0.111
$K_{RS,T,act,E1,P1}$	Right slope of T-DSig for E1 activity.	0	10	-	0.111
$r_{max,Tlow,act,E1,P1}$	Low temperature at which 50% of $r_{max,SIP,E1,P1}$ are achieved.	273.15	373.15	K	329
$r_{max,Thigh,act,E1,P1}$	High temperature at which 50% of $r_{max,SIP,E1,P1}$ are achieved.	273.15	373.15	K	329
$Y_{LS,T,act,E2,P1}$	Lowest value on the left side of T-DSig for E2 activity.	0	5		0
$Y_{mid,T,act,E2,P1}$	Upper/lower limit between the left and the right inflexion points of T-DSig for E2 activity.	0	5		1
$Y_{RS,T,act,E2,P1}$	Highest value on the right side of T-DSig for E2 activity.	0	5		1
$K_{LS,T,act,E2,P1}$	Left slope of T-DSig for E2 activity.	0	10		0.12
$K_{RS,T,act,E2,P1}$	Right slope of T-DSig for E2 activity.	0	10		0.12

$r_{max,Tlow,act,E2,P1}$	Low temperature at which 50% of $r_{max,IPP,E2,P1}$ are achieved.	273.15	373.15	K	318
$r_{max,Thigh,act,E2,P1}$	High temperature at which 50% of $r_{max,IPP,E2,P1}$ are achieved.	273.15	373.15	K	318
$Y_{LS,T,sta,E1,P1}$	Lowest value on the left side of T-DSig for E1 stability.	0	5	-	0.1
$Y_{mid,T,sta,E1,P1}$	Upper/lower limit between the left and the right inflexion points of T-DSig for E1 stability.	0	5	-	1
$Y_{RS,T,sta,E1,P1}$	Highest value on the right side of T-DSig for E1 stability.	0	5	-	1
$K_{LS,T,sta,E1,P1}$	Left slope of T-DSig for E1 stability.	0	10	-	0.2
$K_{RS,T,sta,E1,P1}$	Right slope of T-DSig for E1 stability.	0	10	-	0.2
$r_{max,Tcrit,sta,E1,P1}$	Critical temperature at which the denaturation rate is already 50% of $r_{max,den,E1,P1}$.	273.15	373.15	K	393
$Y_{LS,T,sta,E2,P1}$	Lowest value on the left side of T-DSig for E2 stability.	0	5	-	0.1
$Y_{mid,T,sta,E2,P1}$	Upper/lower limit between the left and the right inflexion points of T-DSig for E2 stability.	0	5	-	1
$Y_{RS,T,sta,E2,P1}$	Highest value on the right side of T-DSig for E2 stability.	0	5	-	1
$K_{LS,T,sta,E2,P1}$	Left slope of T-DSig for E2 stability.	0	10	-	0.2
$K_{RS,T,sta,E2,P1}$	Right slope of T-DSig for E2 stability.	0	10	-	0.2
$r_{max,Tcrit,sta,E2,P1}$	Critical temperature at which the denaturation rate is already 50% of $r_{max,den,E2,P1}$.	273.15	373.15	K	393
$Y_{LS,pH,act,E1,P1}$	Lowest value on the left side of pH-DSig for E1 activity.	0	5	-	0
$Y_{mid,pH,act,E1,P1}$	Upper/lower limit between the left and the right inflexion points of pH-DSig for E1 activity.	0	5	-	1.45
$Y_{RS,pH,act,E1,P1}$	Highest value on the right side of pH-DSig for E1 activity.	0	5	-	0
$K_{LS,pH,act,E1,P1}$	Left slope of pH-DSig for E1 activity.	0	10	-	2.5
$K_{RS,pH,act,E1,P1}$	Right slope of pH-DSig for E1 activity.	0	10	-	1.5
$r_{max,pHlow,act,E1,P1}$	Low pH value at which 50% of $r_{max,SIP,E1,P1}$ are achieved.	0	14	-	4.3
$r_{max,pHhigh,act,E1,P1}$	High pH value at which 50% of $r_{max,SIP,E1,P1}$ are achieved.	0	14	-	6

$Y_{LS,pH,act,E2,P1}$	Lowest value on the left side of pH-DSig for E2 activity.	0	5	-	0
$Y_{mid,pH,act,E2,P1}$	Upper/lower limit between the left and the right inflexion points of pH-DSig for E2 activity.	0	5	-	1
$Y_{RS,pH,act,E2,P1}$	Highest value on the right side of pH-DSig for E2 activity.	0	5	-	0
$K_{LS,pH,act,E2,P1}$	Left slope of pH-DSig for E2 activity.	0	10	-	3
$K_{RS,pH,act,E2,P1}$	Right slope of pH-DSig for E2 activity.	0	10	-	3
$r_{max,pHlow,act,E2,P1}$	Low pH at which 50% of $r_{max,IPP,E2,P1}$ are achieved.	0	14	-	4
$r_{max,pHhigh,act,E2,P1}$	High pH at which 50% of $r_{max,IPP,E2,P1}$ are achieved.	0	14	-	8.5
$Y_{LS,pH,sta,E1,P1}$	Lowest value on the left side of pH-DSig for E1 stability.	0	5	-	1
$Y_{mid,pH,sta,E1,P1}$	Upper/lower limit between the left and the right inflexion points of pH-DSig for E1 stability.	0	5	-	0.1
$Y_{RS,pH,sta,E1,P1}$	Highest value on the right side of pH-DSig for E1 stability.	0	5	-	1
$K_{LS,pH,sta,E1,P1}$	Left slope of pH-DSig for E1 stability.	0	10	-	3
$K_{RS,pH,sta,E1,P1}$	Right slope of pH-DSig for E1 stability.	0	10	-	3
$r_{max,pHlow,sta,E1,P1}$	Low pH, at which the denaturation rate is already 50% of $r_{max,den,E1,P1}$.	0	14	-	1.5
$r_{max,pHhigh,sta,E1,P1}$	High pH, at which the denaturation rate is already 50% of $r_{max,den,E1,P1}$.	0	14	-	11
$Y_{LS,pH,sta,E2,P1}$	Lowest value on the left side of pH-DSig for E2 stability.	0	5	-	1
$Y_{mid,pH,sta,E2,P1}$	Upper/lower limit between the left and the right inflexion points of pH-DSig for E2 stability.	0	5	-	0.1
$Y_{RS,pH,sta,E2,P1}$	Highest value on the right side of pH-DSig for E2 stability.	0	5	-	1
$K_{LS,pH,sta,E2,P1}$	Left slope of pH-DSig for E2 stability.	0	10	-	3
$K_{RS,pH,sta,E2,P1}$	Right slope of pH-DSig for E2 stability.	0	10	-	3
$r_{max,pHlow,sta,E2,P1}$	Low pH, at which the denaturation rate is already 50% of $r_{max,den,E2,P1}$.	0	14	-	1.5
$r_{max,pHlow,sta,E2,P1}$	High pH, at which the denaturation rate is already 50% of $r_{max,den,E2,P1}$.	0	14	-	12

Process 2 (P2) – Proteolysis with endo- (E1) and exopeptidase (E2)					
$r_{max,SIP,E1,P2}$	Maximal reaction rate of E1 (substrate to intermediate product).	0	100	1/s	0.57
$K_{M,SIP,E1,P2}$	Michaelis-Menten-constant for E1 (substrate to intermediate product).	0	10	$kg/m^3 \cdot s$	22.55
$Y_{SIP,E1,P2}$	Yield factor during formation of intermediate product from substrate.	0	1	kg/kg	0.95
$r_{max,IPP,E2,P2}$	Maximal reaction rate of E2 (intermediate product to product).	0	100	1/s	0.67
$K_{M,IPP,E2,P2}$	Michaelis-Menten-constant for E2 (intermediate product to product).	0	10	$kg/m^3 \cdot s$	1.57
$Y_{IPP,E2,P2}$	Yield factor during formation of product from intermediate product.	0	1	kg/kg	1
$P_{IP,P2}$	Proportional factor for formation of intermediate product from substrate.	0	1	-	1
$P_{P,P2}$	Proportional factor for formation of product from intermediate product.	0	1	-	1
$f_{E2,FE1,P2}$	Factor for proportion of E2 in $F_{E1,0,P2}$.	0	1	-	0
$f_{E1,FE2,P2}$	Factor for proportion of E1 in $F_{E2,0,P2}$.	0	1	-	0.5
$r_{max,den,E1,P2}$	Maximal denaturation rate of E1.	0	1	1/s	$1e^{-5}$
$r_{max,den,E2,P2}$	Maximal denaturation rate of E2.	0	1	1/s	$1e^{-5}$
$Y_{LS,T,act,E1,P2}$	Lowest value on the left side of T-DSig for E1 activity.	0	5	-	0
$Y_{mid,T,act,E1,P2}$	Upper/lower limit between the left and the right inflexion points of T-DSig for E1 activity.	0	5	-	1.52
$Y_{RS,T,act,E1,P2}$	Highest value on the right side of T-DSig for E1 activity.	0	5	-	0
$K_{LS,T,act,E1,P2}$	Left slope of T-DSig for E1 activity.	0	10	-	0.09
$K_{RS,T,act,E1,P2}$	Right slope of T-DSig for E1 activity.	0	10	-	0.2
$r_{max,Tlow,act,E1,P2}$	Low temperature at which 50% of $r_{max,SIP,E1,P2}$ are achieved.	273.15	373.15	K	316
$r_{max,Thigh,act,E1,P2}$	High temperature at which 50% of $r_{max,SIP,E1,P2}$ are achieved.	273.15	373.15	K	338

$Y_{LS,T,act,E2,P2}$	Lowest value on the left side of T-DSig for E2 activity.	0	5	-	0
$Y_{mid,T,act,E2,P2}$	Upper/lower limit between the left and the right inflexion points of T-DSig for E2 activity.	0	5	-	1.12
$Y_{RS,T,act,E2,P2}$	Highest value on the right side of T-DSig for E2 activity.	0	5	-	0
$K_{LS,T,act,E2,P2}$	Left slope of T-DSig for E2 activity.	0	10	-	0.13
$K_{RS,T,act,E2,P2}$	Right slope of T-DSig for E2 activity.	0	10	-	0.2
$r_{max,Tlow,act,E2,P2}$	Low temperature at which 50% of $r_{max,IPP,E2,P2}$ are achieved.	273.15	373.15	K	301
$r_{max,Thigh,act,E2,P2}$	High temperature at which 50% of $r_{max,IPP,E2,P2}$ are achieved.	273.15	373.15	K	337
$Y_{LS,T,sta,E1,P2}$	Lowest value on the left side of T-DSig for E1 stability.	0	5	-	0.1
$Y_{mid,T,sta,E1,P2}$	Upper/lower limit between the left and the right inflexion points of T-DSig for E1 stability.	0	5	-	1
$Y_{RS,T,sta,E1,P2}$	Highest value on the right side of T-DSig for E1 stability.	0	5	-	1
$K_{LS,T,sta,E1,P2}$	Left slope of T-DSig for E1 stability.	0	10	-	0.2
$K_{RS,T,sta,E1,P2}$	Right slope of T-DSig for E1 stability.	0	10	-	0.2
$r_{max,Tcrit,sta,E1,P2}$	Critical temperature at which the denaturation rate is already 50% of $r_{max,den,E1,P2}$.	273.15	373.15	K	345
$Y_{LS,T,sta,E2,P2}$	Lowest value on the left side of T-DSig for stability of E2.	0	5	-	0.1
$Y_{mid,T,sta,E2,P2}$	Upper/lower limit between the left and the right inflexion points of T-DSig for E2 stability.	0	5	-	1
$Y_{RS,T,sta,E2,P2}$	Highest value on the right side of T-DSig for E2 stability.	0	5	-	1
$K_{LS,T,sta,E2,P2}$	Left slope of T-DSig for E2 stability.	0	10	-	0.2
$K_{RS,T,sta,E2,P2}$	Right slope of T-DSig for E2 stability.	0	10	-	0.2
$r_{max,Tcrit,sta,E2,P2}$	Critical temperature at which the denaturation rate is already 50% of $r_{max,den,E2,P2}$.	273.15	373.15	K	345
$Y_{LS,pH,act,E1,P2}$	Lowest value on the left side of pH-DSig for E1 activity.	0	5	-	0

$Y_{mid,pH,act,E1,P2}$	Upper/lower limit between the left and the right inflexion points of pH-DSig for E1 activity.	0	5	-	1.1
$Y_{RS,pH,act,E1,P2}$	Highest value on the right side of pH-DSig for E1 activity.	0	5	-	0
$K_{LS,pH,act,E1,P2}$	Left slope of pH-DSig for E1 activity.	0	10	-	2.5
$K_{RS,pH,act,E1,P2}$	Right slope of pH-DSig for E1 activity.	0	10	-	2
$r_{max,pHlow,act,E1,P2}$	Low pH at which 50% of $r_{max,SIP,E1,P2}$ are achieved.	0	14	-	5.8
$r_{max,pHhigh,act,E1,P2}$	High pH at which 50% of $r_{max,SIP,E1,P2}$ are achieved.	0	14	-	8.6
$Y_{LS,pH,act,E2,P2}$	Lowest value on the left side of pH-DSig for E2 activity.	0	5	-	0
$Y_{mid,pH,act,E2,P2}$	Upper/lower limit between the left and the right inflexion points of pH-DSig for E2 activity.	0	5	-	1.8
$Y_{RS,pH,act,E2,P2}$	Highest value on the right side of pH-DSig for E2 activity.	0	5	-	0
$K_{LS,pH,act,E2,P2}$	Left slope of pH-DSig for E2 activity.	0	10	-	1.2
$K_{RS,pH,act,E2,P2}$	Right slope of pH-DSig for E2 activity.	0	10	-	1
$r_{max,pHlow,act,E2,P2}$	Low pH at which 50% of $r_{max,IPP,E2,P2}$ are achieved.	0	14	-	6.4
$r_{max,pHhigh,act,E2,P2}$	High pH at which 50% of $r_{max,IPP,E2,P2}$ are achieved.	0	14	-	8.4
$Y_{LS,pH,sta,E1,P2}$	Lowest value on the left side of pH-DSig for E1 stability.	0	5	-	1
$Y_{mid,pH,sta,E1,P2}$	Upper/lower limit between the left and the right inflexion points of pH-DSig for E1 stability.	0	5	-	0.1
$Y_{RS,pH,sta,E1,P2}$	Highest value on the right side of pH-DSig for E1 stability.	0	5	-	1
$K_{LS,pH,sta,E1,P2}$	Left slope of pH-DSig for E1 stability.	0	10	-	3
$K_{RS,pH,sta,E1,P2}$	Right slope of pH-DSig for E1 stability.	0	10	-	3
$r_{max,pHlow,sta,E1,P2}$	Low pH, at which the denaturation rate is already 50% of $r_{max,den,E1,P2}$.	0	14	-	3
$r_{max,pHhigh,sta,E1,P2}$	High pH, at which the denaturation rate is already 50% of $r_{max,den,E1,P2}$.	0	14	-	11
$Y_{LS,pH,sta,E2,P2}$	Lowest value on the left side of pH-DSig for E2 stability.	0	5	-	1

$Y_{mid,pH,sta,E2,P2}$	Upper/lower limit between the left and the right inflexion points of pH-DSig for E2 stability.	0	5	-	0.1
$Y_{RS,pH,sta,E2,P2}$	Highest value on the right side of pH-DSig for E2 stability.	0	5	-	1
$K_{LS,pH,sta,E2,P2}$	Left slope of pH-DSig for E2 stability.	0	10	-	3
$K_{RS,pH,sta,E2,P2}$	Right slope of pH-DSig for E2 stability.	0	10	-	3
$r_{max,pHlow,sta,E2,P2}$	Low pH, at which the denaturation rate is already 50% of $r_{max,den,E2,P2}$.	0	14	-	2
$r_{max,pHlow,sta,E2,P2}$	High pH, at which the denaturation rate is already 50% of $r_{max,den,E2,P2}$.	0	14	-	12